ELECTRICAL CHARACTERISTICS OF ALUMINUM AIR BATTERY UNDER OPEN-CIRCUIT AND CLOSED-CIRCUIT CONDITIONS

CHEAH ZHEN KE

A project report submitted in partial fulfilment of the requirements for the award of Bachelor of Engineering (Honours) Mechanical Engineering

Lee Kong Chian Faculty of Engineering and Science Universiti Tunku Abdul Rahman

April 2020

DECLARATION

I hereby declare that this project report is based on my original work except for citations and quotations which have been duly acknowledged. I also declare that it has not been previously and concurrently submitted for any other degree or award at UTAR or other institutions.

Signature   :

Name   :   Cheah Zhen Ke

ID No.   :   1504459

Date   :   21/4/2020
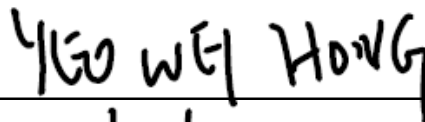
APPROVAL FOR SUBMISSION

I certify that this project report entitled **"ELECTRICAL CHARACTERISTICS OF ALUMINUM AIR BATTERY UNDER OPEN-CIRCUIT AND CLOSED-CIRCUIT CONDITIONS"** was prepared by **CHEAH ZHEN KE** has met the required standard for submission in partial fulfilment of the requirements for the award of Bachelor of Engineering (Honours) Mechanical Engineering at Universiti Tunku Abdul Rahman.
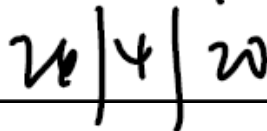
Approved by,

Signature   :

Supervisor   :   YEO WEI HONG

Date   :   26/4/20

ACKNOWLEDGEMENTS

I would like to thank everyone who has supported me on this research journey. I would like to express my gratitude to my research supervisor, Dr. Yeo Wei Hong for his invaluable advice, guidance and his enormous patience throughout the development of the research.

In addition, I would also like to express my gratitude to my loving parents that supported me financially and gave me strong mental encouragement to do my best for the project. I am thankful to my friends who brainstormed with me and taught me the procedures to conduct proper research and experiments.

Lastly, I appreciate the help from UTAR staff that had provided me key equipment and supplies for my research.

ABSTRACT

Aluminium-air battery has great potential as it is capable of achieving high theoretical energy density of 8100 Wh kg^{-1}, and high theoretical cell voltage of 2.7 V. However, the aluminium anode is vulnerable to self-corrosion and surface passivation issues, causing the practical aluminium-air battery to yield energy density at only 1300 Wh kg^{-1}. The practical cell voltage ranges from 1.22 V – 1.46 V for aluminium-air battery in 4M NaOH electrolyte. Therefore, the open-circuit condition such as self-corrosion, surface passivation behaviours, and open-circuit voltage are studied. The closed-circuit condition that includes discharge characteristics is investigated. This research is to study the self-corrosion and surface passivation behaviours of pure aluminium and alloy 6063 in alkaline electrolyte using SEM-EDX, XRD analysis, and their corresponding open-circuit voltage using potentiostat. Besides that, the effects of graphite felt and graphite powder as catalysts on the discharge characteristic of aluminium-air battery is investigated using potentiostat. The electrolyte for the aluminium-air battery is 4M KOH solution. It is found that alloy 6063 as anode has better electrical characteristics that can achieve 10.3% higher open-circuit voltage, better discharge characteristics on average, and 54 % better capacity as compared to pure aluminium. However, the self-corrosion in alloy 6063 is 60 % faster than pure aluminium based on Tafel plot. The graphite felt is a better catalyst than graphite powder, it has significantly improved the initial discharge voltage by 35 % and 41 %, as well as the final discharge voltage by 65 % and 69 % for pure aluminium and alloy 6063 respectively.

TABLE OF CONTENTS

CHAPTER

LIST OF TABLES

LIST OF FIGURES

LIST OF SYMBOLS / ABBREVIATIONS

E_{corr}	corrosion potential, V
I_{corr}	corrosion current, A
η	overpotential, V
E	actual potential, V
E_{eq}	reaction equilibrium potential, V
Q	coulombs, C
n	the number of electrons involved in electrochemical reaction
F	Faraday constant, 96487 coulombs
W	weight of the electroactive species
M	molecular weight, u
t	time, s
$E.W.$	equivalent weight
$C.R.$	corrosion rate
ρ	metal density, g/cm^3
A	area, cm^2
$Wt\ \%$	weight percent
$At\ \%$	atom percent

AC	alternate current
BSE	back-scattered electrons
CC-CV	constant current-constant voltage
CL	cathode-luminescence
DC	direct current
EDX	energy-dispersive x-ray spectroscopy
EIS	electrochemical impedance spectroscopy
ESR	equivalent series resistance
ICDD	International Centre for Diffraction Data
OCP	open-current potential
OCV	open-circuit voltage
ORR	oxygen reduction reaction
OER	oxygen evolution reaction

PDF-2	powder diffraction file
PTFE	polytetrafluoroethylene
SEM	scanning electron microscopy
SE	secondary electrons
SHE	standard hydrogen electrode
XRD	X-ray powder diffraction crystallography

LIST OF APPENDICES

CHAPTER 1

INTRODUCTION

1.1 General Introduction

The automobile industry today is marching towards a technology advancement by transitioning from the carbon-releasing fossil fuel era into the zero-emission electric era. Under natural circumstances, fossil fuels release carbon at low rate as they are dormant under the Earth crust, and carbon dioxide (CO_2) is emitted through volcanic activity and organisms' respiration. However, transportation vehicles play a significant role in removing the carbon from the fossil fuels and releasing them into the atmosphere as CO_2 and eventually causes global environmental pollution problems such as the greenhouse effect. The U.S. Department of Energy (2019) states that in terms of energy efficiency, electric vehicles are about 60 % efficient when using its electrical energy to power up the engine, while conventional gasoline vehicles only used up to 20 % of the energy stored in fossil fuel to power up the engine. In response to these issues, electric vehicles have been introduced and considered as an alternative to the conventional fossil-fuelled vehicle.

The key challenge to electric vehicle development is the power source. It demands efficient, reliable, and safe energy storage technologies with adequate reproducibility so that it becomes viable for commercialisation. Currently, the promising candidates are hydrogen-fuel battery and lithium-ion battery. Hydrogen-fuel battery has potential to be developed as clean power battery, but it is relatively expensive. Lithium-ion battery is one of the most commonly used battery and have dominated the market due to their high volumetric and gravimetric capacity as well as good energy efficiency. This technology is even adopted by the electric car pioneer company, Tesla. Yet, the shortcomings of lithium-ion battery is its low energy density at approximately 100~200 Wh kg^{-1} and short cruising range (Liu et al., 2017). Thus, a better energy storage technology is desired to further improve the power capacity of electric vehicles.

The emergence of metal-air battery had people believing that it could be the successor of the current lithium-ion energy storage technology due to its

high energy density and capacity, as well as the simplicity in fabrication. As compared to lithium-ion, metal-air battery provides a significant advantage in which the storage of cathode reactants is not required as they are widely present in the atmosphere. This allows a significant volume reduction in metal-air battery, while obtaining the same energy capacity as lithium-ion battery.

Table 1.1 summarises the electrical performances of various metal-air batteries made out of metal that are abundantly found in the market. The anode potentials are with referenced to standard hydrogen electrodes (SHE). The cell voltage is calculated and tested with an oxygen cathode.

Table 1.1: Performance of Metal-air batteries (Li and Bjerrum, 2002).

Batteries	Theoretical Voltage (V)	Theoretical specific capacity (Ah Kg^{-1})	Theoretical energy density (kWh kg^{-1})	Practical operating voltage (V)
Li-air	3.4	1170	13.0	2.4
Zn-air	1.6	658	1.3	1.0 – 1.2
Mg-air	3.1	920	6.8	1.2 – 1.4
Na-air	2.3	687	1.6	2.3
Al-air	2.7	1030	8.1	1.2 1.6

From Table 1.1, lithium-air battery has theoretical energy density at 13000 Wh kg^{-1} and theoretical specific capacity of 1170 Ah kg^{-1}. Despite having the best theoretical capabilities, Liu *et al.* (2017) concludes that rechargeable Li-air batteries have to overcome many hurdles such as insufficient understanding of catalytic mechanism, instability of lithium in humid environments, the porous carbon cathodes that can be blocked by discharge products, the formation of side product, which are lithium alkyl carbonates and Li_2CO_3 during the cycle, and low electrochemical efficiency caused by high charging overpotential. These issues have affected the rechargeability and cycle life of lithium-air batteries. Additionally, lithium-air batteries mainly utilise non-aqueous electrolyte, such as flammable organic solvents that can be a safety hazard. The challenges mentioned above prove that Li-air is hardly feasible.

Therefore, an alternative metal anode with better potential is suggested, thus introducing the aluminium-air battery. Aluminium-air battery will be the topic of this study and will be discussed in utmost detail.

1.2   Importance of the Study

The findings of this study will propel the metal-air battery technology in the energy storage sector and benefit the society in many aspects. According to Energy Access Outlook (2017), 14 % of the global population that accounts to 1.1 billion people live without any electricity supply. By developing an energy storing method that can hold a tremendous amount of energy in addition to having a long shelf life, it is sure to revolutionise the current societies and industries. We can provide electricity to rural regions that are away from the electricity grid. Electrical energy generated can be stored efficiently with minimal energy lost. This technology is also potent in solving the energy lost issue in electric power transmission by transporting electrical energy in high-performing batteries.

Aluminium-air battery is believed to be the next generation of energy storage technology that can replace Li-ion battery. The realisation of this technology is certain to make this world a better and greener place. It would be a catalyst in the development of electric vehicles. This study may provide readers with fundamental knowledge, working principles, challenges and recent research progress of aluminium-air battery. This may lay the foundation for the commercial grade aluminium alloy 6063 to be utilised as the anode to develop a practically high-performing aluminium-air battery

1.3   Problem Statement

Based on Liu *et al.* (2017), the main issues that aluminium-air battery come across are the self-corrosion induced by low hydrogen evolution overpotential, surface passivation due to the formation of inactive product, ineffective catalyst, and sluggish oxygen reaction at cathode. At the anode, self-corrosion behaviour will greatly reduce the shelf life of the battery, and surface passivation will cause the battery to wear out prematurely as an unreactive oxide layer is formed on anode surface. Nevertheless, ineffective catalysts are unable to bring out the potential of aluminium-air battery. Therefore, different types of anode are tested to determine its self-corrosion and surface passivation behaviours. Different catalysts are experimented to find an effective catalyst for aluminium-air battery. The sluggish oxygen reaction at cathode is improved with an improvised design.

1.4   Aims and Objectives

This study aims to investigate the electrical characteristics of aluminium-air battery constructed using different anode materials and catalysts under open-circuit and closed-circuit conditions. The open-circuit condition includes the battery open-circuit voltage and anode self-corrosion and surface passivation behaviours, while closed-circuit tests are to probe into the discharge characteristics of the battery. This study also aims to experiment with an improvised design of aluminium-air battery. The specific objectives of this study are as follow:

1. To study the self-corrosion and surface passivation behaviours of pure aluminium and alloy 6063 in alkaline electrolyte.
2. To study the open-circuit voltage of aluminium-air battery with pure aluminium and alloy 6063 as anode.
3. To investigate the effects of graphite felt and graphite powder as catalysts on the discharge characteristic of aluminium-air battery.
4. To design and experiment on an improvised double cathode aluminium-air battery to determine its viability.

1.5   Scope and Limitation of the Study

The scope of the study covers the essential components that are required to build an aluminium-air battery, which are the aluminium anode, electrolyte, air positive cathode, catalytic layer, and so on. Each of the components have their own specific researches that can be found on the internet. The pros and cons of the relevant materials are investigated. The improvised or patented designs of aluminium-air battery that can improve the performance and alleviate the issues are also studied. The study also includes the comprehension of evaluation techniques and tools that can assess the performance and characteristics of aluminium-air battery.

Other than that, the limitation faced in this project is the unfortunate covid-19 outbreak that leads to University close, thus the experiment progress is strongly affected. Besides that, advanced studies regarding electrocatalyst are not included in project scope as they are very wide-scaled and have high complexity that involve lattice structure, surface energy, composite structures,

and even nanotechnologies. There is also limited access to the thesis, journals and research articles.

The experimental scopes of this project are as follows:

i.   The anode materials experimented in this project are pure aluminium and aluminium alloy 6063.

ii.   The catalysts tested in this project are graphite felt and graphite powder.

iii. The electrolyte used is 4M potassium hydroxide, KOH solution.

iv.   Open-circuit and closed-circuit tests are performed using potentiostat.

v.   Anode samples analysis is completed using scanning electron microscope (SEM), energy dispersive X-ray spectroscopy (EDX), and X-ray powder diffraction crystallography (XRD).

vi.   Corrosion rate is analysed with Tafel plot by IVMAN software.

1.6   Contribution of the Study

The research and development on aluminium-air battery is still at its infancy as there are still a lot of untouched topics. This study has contributed to existing literature by determining the capability of commercial grade aluminium alloy 6063 as anode for the aluminium-air battery. This study could contribute an in-depth understanding on the working principle of aluminium-air battery, detailed procedures to build aluminium-air battery, and the relevant evaluation tool. This study reveals the corrosion behaviour of pure aluminium and alloy 6063 in 4M KOH solution that were widely used as the electrolyte by taking SEM images of the corroded pure aluminium and alloy 6063. This study can spark the interest in the society and draw their attention towards aluminium-air battery and propel the development of aluminium-air battery. This study can educate the basics of aluminium-air battery to those who are unfamiliar with aluminium-air battery.

1.7 Outline of the Report

The report consists of 5 chapters that illustrate the flow of work done in this project from introduction to the conclusion. The contents presented in each chapter are different. Readers are recommended to read continuously without jumping from chapter to chapter to fully comprehend the project details and outputs.

CHAPTER 1 decides the direction of the project by discussing the importance of the study, problem statement, aims and objectives, scope and limitations of the study, and contribution of the study.

CHAPTER 2 covers the literature reviews that are relevant to this study. This chapter will explain the fundamentals and potential of aluminium-air battery, as well as the recent development progress regarding aluminium-air battery. Some frequently-used evaluation techniques and tools for battery are also studied.

CHAPTER 3 contains the methodology for this study. The methods and procedures for the experiments are described in detail.

CHAPTER 4 compiles and analyses the results that were obtained from the experiment in this study. Discussions of the result are also included in this chapter.

CHAPTER 5 summarises the study and concludes the findings of the study. This chapter also provides recommendations for future work.

CHAPTER 2

LITERATURE REVIEW

2.1 Introduction to Aluminium-air Battery

Aluminium-air battery have sparked the interest of many researchers due to a number of reasons. Besides possessing low atomic mass, aluminium has high negative standard potential and is capable of transferring three electrons per atom. These characteristics lead to high theoretical voltage of 2.7 V, high theoretical energy density of 8100 Wh kg^{-1} and high theoretical specific capacity of 2980 Ah kg^{-1}, which are only second to that of lithium-air (Liu et al., 2017).

According to Thomas National Accelerator Facility (2020), oxygen ranked first as being the most abundant element in the world, while aluminium ranked third. This shows that the essential raw materials for aluminium-air battery are easily accessible. The by-product of aluminium-air battery, aluminium hydroxide, $Al(OH)_3$ is a primary component of bauxite, which can be used to fabricate alumina in the Bayer process. Then, the resulting alumina can be used for the production of aluminium metal. It demonstrates that aluminium-air battery has appreciable recyclability. Aluminium-air battery is primary battery, it is non-rechargeable in general. The aluminium anode will be consumed by its chemical reaction with oxygen to form aluminium hydroxide, provided that a complete circuit with electrolyte is prepared. The battery can no longer produce electricity once all the aluminium anode has been consumed. However, mechanically recharging aluminium-air battery is made possible by replacing new aluminium anodes, while the aluminium hydroxide can be reprocessed to produce aluminium metal.

If the application of aluminium-air battery into electric vehicles is realised, automakers will have to devise a way of replacing the anode plates and the automobile industry is sure to experience a paradigm shift. It is believed that this development of event is highly possible because in 2014, Edelstein mentioned that the company Phinergy had already accomplished the application of 55-pound aluminium-air battery pack in a converted Citroen C1 minicar that can lasts 2000 km range before the replacement of aluminium anodes is necessary.

2.2   Aluminium Recyclability

Aside from its attractive electrical performance attributes, recyclability of aluminium-air battery is also one of the deciding assets that outshine other metal-air battery (Li and Bjerrum, 2002). To understand the recyclability of aluminium-air battery, the aluminium production process was studied. According to The International Aluminium Institute (2018), there are 3 main stages in extracting the aluminium, which are the bauxite mining, Bayer process that produce alumina, and Hall-Herout process that perform alumina electrolysis.

Bauxite is the primary ore of aluminium that can be found in earth crust. Bauxite is a rock composed of a mixture of aluminium oxide, aluminium hydroxide, and other impurities such as quartz, iron oxide, magnetite, and etc. After the bauxite mining process, the Bayer process begins by adding hot solution of sodium hydroxide into the bauxite so that the aluminium is precipitated in the form of aluminium hydroxide, $Al(OH)_3$. The final stage of the Bayer process is known as calcination, where the aluminium hydroxide is heated to about 1000 ℃ to produce aluminium oxide, also known as alumina. The subsequent aluminium extraction stage is the Hall-Heroult process. Alumina is immersed into molten solution of cryolite (Na_3AlF_6) and electric current is passed through so that the aluminium and oxygen in alumina are segregated by electrolysis. The resulting product of aluminium after Hall-Heroult process has a purity of 99.6-99.8 % pure (Yang and Knickle, 2003). However, if a higher purity aluminium is desired, electrolytic refining can be done to achieve purity of 99.995 %. The flowchart of aluminium production is shown in Figure 2.1.
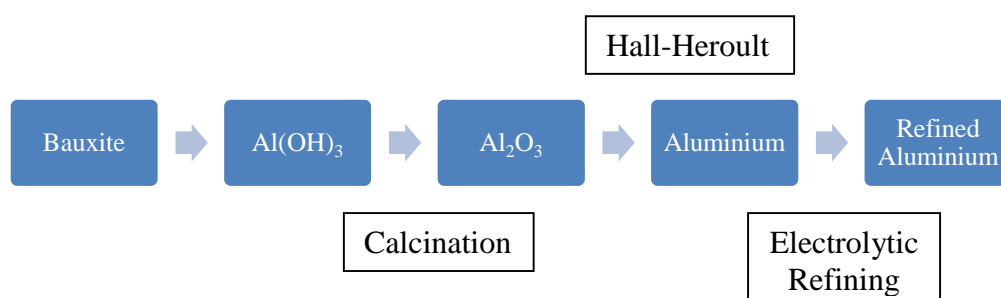
Figure 2.1: Aluminium formation process.

Referring to Figure 2.1, aluminium hydroxide can undergo calcination to form aluminium oxide, Al_2O_3, and eventually goes through Hall-Heroult

process to form aluminium. Since the operation of aluminium-air battery consumes the aluminium anode and produces aluminium hydroxide, $Al(OH)_3$, a recycling loop can be formed as shown in Figure 2.2. The cycle suggests that the energy source of aluminium-air battery comes from electricity consumed in the aluminium reprocessing, instead of the charging of the battery from the electric grid.
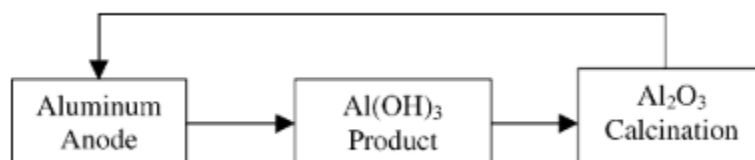
Figure 2.2: Aluminium-air battery recycling process.

2.3 Advantages over Existing Battery

There are four commonly used rechargeable batteries in the market, which are the Lithium-ion (Li-ion) battery, Nickel-cadmium (Ni-Cd) battery, Nickel-Metal Hydride (Ni-MH) battery, and Lead-Acid battery. Lithium-ion battery can be found in a wide variety of portable appliances, such as mobile phones, smart devices, electric vehicles, and etc. According to Emmanuel (2018), lithium-ion batteries often have little or no memory effect, high energy density, and low self-discharge as compared to other battery types. Next, Nickel-cadmium battery is good for storage as the voltage are maintained when not in operation. However, Ni-Cd faces "memory" effect, such that the future capacity of the battery will be lowered when a partially charged battery is recharged.

Another rechargeable battery is Nickel-Metal Hydride battery that has similar anode chemical reaction with Ni-Cd battery. Unlike Ni-Cd battery that uses cadmium, Ni-MH uses a hydrogen-absorbing alloy as the negative electrode and is not prone to the "memory" effect. On the other hand, Shapley (2012) states that lead acid battery is capable of providing high current and their cost is relatively low. Lead-acid batteries are made up of sponge metallic lead anode, lead-dioxide cathode, with sulphuric acid solution as electrolyte. The materials involved are heavy metal elements that can be hazardous to the environment when improperly disposed. Despite having low energy to volume and energy to weight ratios, lead acid battery has a relatively large power to

weight ratio. It can supply huge surge currents when needed, making it favourable in high current application such as powering automobile starter motors.

Table 2.1 depicts the practical attributes of Lithium-ion battery, Nickel-cadmium battery, Nickel-Metal hydride battery, Lead acid battery and the theoretical properties of Aluminium-air batteries. Since aluminium-air battery is currently under development, the in-depth characteristics have yet to be discovered. It shall be noted that the characteristics mentioned below are in general and the specific properties are subjected to variations due to design specification, operating temperature, and other factors.

Table 2.1: Aluminium-air battery (Theoretical) vs. Commonly used Batteries (Practical) (Emmanuel, 2018)(Lawson, n.d.).

	Li-ion	Ni-Cd	Ni-MH	Lead acid	Al-air
Specific Energy (Wh kg^{-1})	100-265	40-60	60-120	35-40	8100
Energy Density (Wh L^{-1})	250-693	50-150	140-300	80-90	N/A
Specific Power (W kg^{-1})	250-340	150	250-1000	180	200
Charge/discharge efficiency	80%-90%	70%-90%	66%-92%	50-95%	N/A
Self-discharge rate	0.34-2.5% /month	10% /month	1.3-2.9% /month at 20 ℃	3-20% /month	N/A
Cycle life (cycles)	400-1200	2000	180-2000	350	N/A
Nominal cell voltage	3.6 – 3.85 V	1.2 V	1.2 V	2.1 V	2.7 V

The actual specific energy of aluminium-air battery is 1300 Wh/kg (Yang and Knickle, 2003) and the practical cell voltage ranges from 1.22 V – 1.46 V for aluminium-air battery in 4M NaOH electrolyte (Goel et al., 2020). Considering the theoretical specific energy of 8100 Wh/kg and the actual specific energy of 1300 Wh/kg, it can be realised that there is still a vast room for improvement for aluminium-air battery. Regardless of its growth potential, the current aluminium-air battery technology that can provide 1300 Wh/kg is

already leading in the chart among the existing state-of-the-art batteries in the market in terms of specific energy capacity. The contemporary widely used Li-ion battery possesses 265 Wh/kg specific energy capacity, which is only 20% the capacity of aluminium-air battery. Yang and Knickle (2003) also agreed that aluminium-air battery is more suited as candidate to replace internal combustion engines than lead/acid or NiMH battery in the future after considering their purchase price, travel range, fuel cost, and life-cycle cost..

2.4   Working Principles

The working principle of aluminium-air battery derives from the electrochemical reaction between the aluminium and oxygen. The aluminium is stored in the anode and oxygen is usually taken from the ambient air. Figure 2.3 presents the fundamental structure of Al-air battery, which consists of an aluminium anode, air cathode, and a compatible electrolyte, typically potassium hydroxide (KOH) and sodium hydroxide (NaOH) solutions. The aluminium anode undergo oxidation to release electrons, while the air cathode undergoes reduction by accepting electrons.
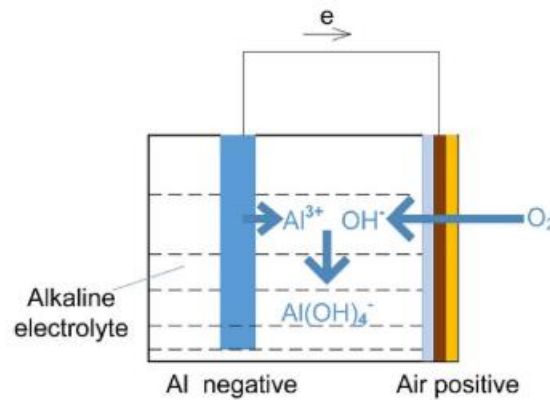
Figure 2.3: Illustration of Operating Aluminium-air Battery (Hu et al., 2019).

As shown in Figure 2.3, the air positive cathode is composed of 4 layers, which are the current collector, catalyst layer, gas diffusion layer, and oxygen permeable membrane. Generally, metal mesh that have good electrical conductivity, mechanical properties, and stability in electrolyte are selected as the current collector. Catalyst layer plays a significant role in improving the oxygen reduction reaction kinetics efficiency, which in turn improves the electrode performance. Typically, gas diffusion layer and oxygen permeable

membrane are associated into a single layer that allows and promotes oxygen flow while preventing leakage of electrolyte.
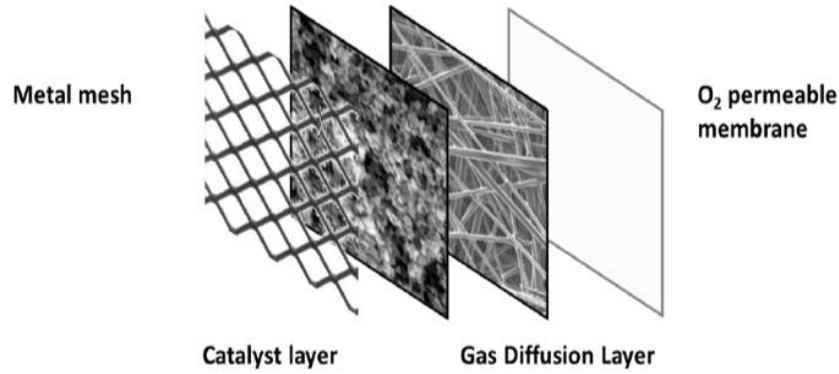
Figure 2.4: Air cathode Standard Architecture (Martinez *et al.*, 2017).

Table 2.2 depicts the electrode processes of aluminium-air battery and their respective potential difference with reference to the Standard Hydrogen Electrode (SHE). It can be observed that the corrosion reaction is in fact a parasitic corrosion reaction that releases hydrogen gas.

Table 2.2: Chemical equation of Aluminium-air battery in Alkaline Electrolyte (Hu et al., 2019).

Reaction Name	Chemical Equation of reactions	Voltage
Cathode (air) reaction	$O_2 + 2H_2O + 4e^- \rightarrow 4OH^-$	$E^o = +0.4$ V
Anode (aluminium) reaction	$Al + 4OH^- \rightarrow Al(OH)_4^- + 3e^-$	$E^o = -2.35$ V
Total reaction	$4Al + 3O_2 + 6H_2O + 4OH^- \rightarrow Al(OH)_4^-$	$E = 2.75$ V
Corrosion reaction	$2Al + 6H_2O + 2OH^- \rightarrow 2Al(OH)_4^- + 3H_2$	-
Dissolution reaction	$Al_2O_3 + 2OH^- + 3H_2O \rightarrow 2Al(OH)_4^-$	-

Aluminium-air battery is a type of galvanic cell because it is driven by spontaneous chemical reaction and converts chemical energy into electrical energy. The electrochemical reaction occurs readily as soon as the electrode is in contact with the electrolyte in a connected circuit. Therefore, aluminium anode should be connected to negative terminal while cathode should be connected to positive terminal in a circuit when operating as a battery.

2.5 Challenges of Aluminium-air Battery

The exposure of aluminium surface to air and aqueous solutions will cause surface passivation that produce a thermodynamically favourable protective oxide film. As a result, the electron conducting process is weakened as the oxide film halts the ion exchanges between aluminum anode and electrolyte. Pino *et al.* (2015) concludes that this surface passivation also causes positive shifting of the corrosion potential of the aluminium electrode and a considerable slow-down of aluminium activation. Furthermore, the self-corrosion mechanism that produces hydrogen gas as shown in Figure 2.5 is unfavourable to the capacity and cycle time of the aluminium-air battery and can diminish the discharge efficiency. It can be seen that the aluminium hydroxide formed on the surface is preventing the exposure of aluminium anode to the electrolyte.
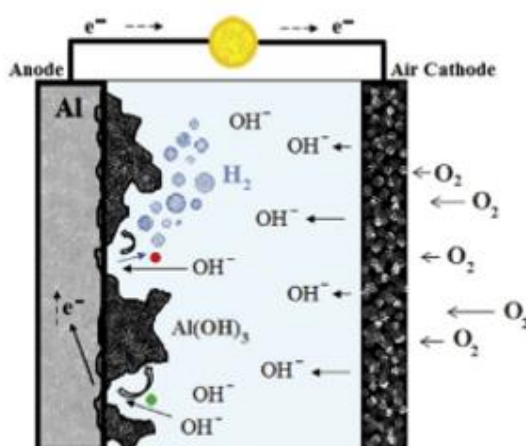
Figure 2.5: Representation of Aluminium anode Self-corrosion and Oxidation processes (Pino et al., 2015).

Hydrogen evolution overpotential is one of the significant factors that affect the performance of aluminium-air battery. It is responsible for the self-corrosion that occurs at the aluminium anode. Investigation on the corrosion rate of the aluminium anode is generally conducted by capturing the amount of hydrogen gas released, where more hydrogen released indicates that there is a high rate of self-corrosion. Hydrogen evolution overpotential indicates the energy level to activate the hydrogen evolution reaction. Consequently, high hydrogen evolution overpotential is demanded in aluminium-air battery to impede the hydrogen evolution reaction that is parasitic and harmful.

Overpotential is the differences of a thermodynamically determined equilibrium potential and the actual potential in working condition as given in the equation below (Papalambros and Wilde, 2018):

$$\eta = E - E_{eq} \tag{2.1}$$

where

η = overpotential, V

E = resultant potential, V

E_{eq} = reaction equilibrium potential, V

2.6 Anode Material

2.6.1 Pure Aluminium

Pure aluminium is first considered as the anode of Al-air battery. However, Hu *et al.* (2019) said that the lack of hydrogen-inhibiting elements in pure aluminium results in uncontrolled parasitic reaction and tends to be unstable in terms of heat dissipation. The electrolyte temperature when associated with pure aluminium often skyrockets as shown in Figure 2.6. Therefore, the authors concluded that pure aluminium anode is not optimal for practical application after considering its uncontrolled heat dissipating behaviour that can be dangerous.
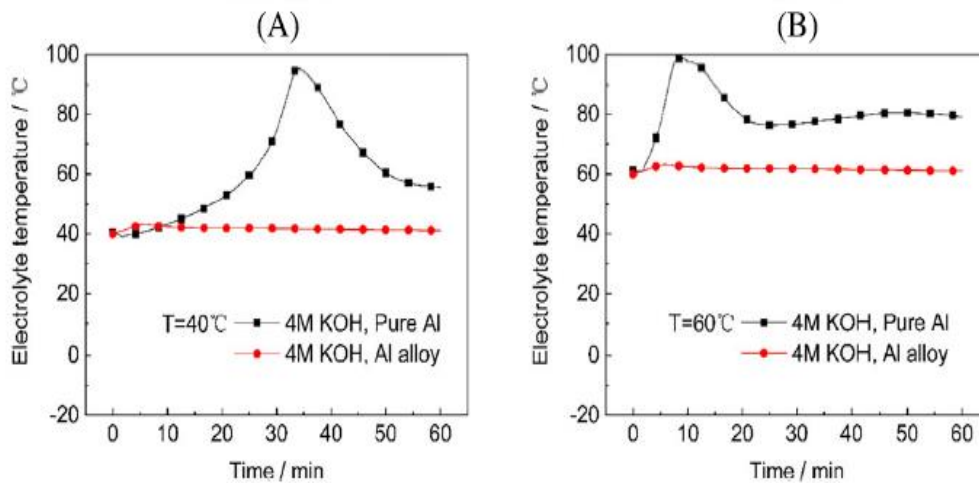
Figure 2.6: Trend of Electrolyte Temperature with Time pure aluminium and its alloys (Hu et al., 2019).

In order to investigate whether high purity aluminium anode is desired in terms of cost-efficiency, Cho *et al.* (2015) investigated the relationship between the behaviour of impurities in aluminum anode and battery performance and concluded that the battery performance of 2N5 grade aluminium with 99.5% purity is lower than 4N grade Al with 99.99% purity at stand-by and low-power discharge. The complex film formed in 2N5 grade aluminium disappears at higher power discharge voltage, causing the discharge current density of 2N5 grade aluminium and 4N grade aluminium to have similar value. Since Yang and Knickle (2003) mentioned that the energy required to fabricate 99.995% grade aluminium is double the amount of energy spend to fabricate 99.9% grade aluminium, it can be concluded that using high purity 4N grade aluminium is not cost-efficient, and thus the cheaper 2N5 grade aluminium is preferred.

2.6.2   Aluminium Alloys

Aluminium alloys are widely experimented to seek out the best performing alloy as anode for aluminium-air battery. There are many researches that focus on investigating the performance of different aluminium alloys to discover the most suitable anode for aluminium-air battery. According to Liu *et al.* (2017), the alloying element, zinc and indium can enhance the hydrogen evolution overpotential and reduce hydrogen evolution, but the latter could result in a positive shift of anode potential. The authors also mentioned that gallium can limit aluminium surface passivation in chloride solutions. It is clear that doping the aluminium can affect the performance of aluminium-air battery. However, the drawback of adding excessive kinds of elements is detrimental to the recovery of aluminium, thus bringing negative impacts to its recyclability. Thus, the amount of alloying element added to aluminium should be minimised.

Sun *et al.* (2015) investigated the aluminium-air battery that utilises Al-Ga, Al-Sn, and Al-Sn as their electrodes, along with the control set of pure aluminium electrode. The author concluded that Al-0.1wt% Ga results in the highest hydrogen gas evolution among pure aluminium, Al-In, and Al-Sn, which shows that Al-Ga promotes the undesired self-corrosion. On the other hand, Al-In and Al-Sn can increase the hydrogen evolution potential and eventually reduce the corrosion rate.

2.6.3 Carbon-treated Aluminium Anode

Pino *et al.* (2016)introduced a simple and affordable technique to improve saline based aluminium-air battery that uses sodium chloride electrolyte. The authors realised that aluminate gel tends to deposit around the aluminium anode in neutral electrolyte, thus prohibiting the active contact area between electrode and electrolyte as shown in Figure 2.7. The battery prematurely wears out when all active areas are covered by aluminium hydroxide gel.
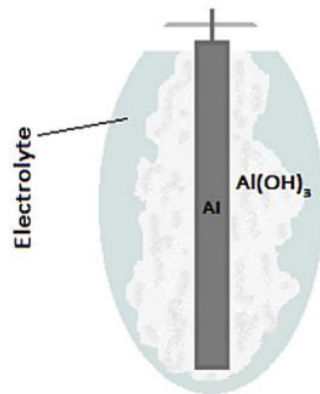
Figure 2.7: Formation of Aluminate at Aluminium anode (Pino et al., 2016).

In order to get the aluminate off the aluminate anode, carbonaceous materials are applied onto the surface of the anode. The material reduces the adherence of aluminate on the electrode and allows precipitation of the aluminate to flake off as depicted in Figure 2.8. The author concluded that this carbon coating technique is capable of increasing the shelf life of aluminium anode up to 3 times longer than non-coated anode.
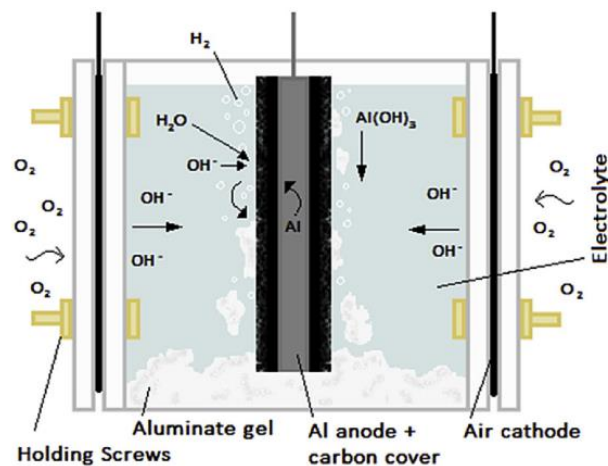
Figure 2.8: Operation of Carbon-treated Aluminium-air battery in Neutral Electrolyte (Pino et al., 2016).

2.7   Electrolyte

The electrolyte functions as a medium for ions to travel, thus completing the circuit and allowing electrochemical reactions to occur. Aqueous electrolyte that includes alkaline, neutral and acidic electrolyte often have low oxygen solubility. Alkaline electrolyte ranges from pH 8-14, neutral electrolyte ranges from pH 7, while acidic electrolyte ranges from pH 1-6.

2.7.1   Alkaline Electrolyte

Generally, alkaline electrolyte is used because it can produce a high current and cell voltage at approximately 2 V in practical cases. Candidates that are often implemented in aluminium-air battery are sodium hydroxide (NaOH) and potassium hydroxide (KOH) solutions. The latter is generally preferred because it is better than NaOH in terms of viscosity, ionic conductivity, and oxygen diffusion rate (Liu et al., 2017).

Potassium hydroxide, KOH solution is selected as the electrolyte due to its higher oxygen solubility than sodium hydroxide, NaOH solution. Figure 2.9 demonstrates the result of OCV of different electrolytes at different temperatures. Despite having comparable performance at low temperature around 0 ℃ and 20 ℃, KOH solution won the competition at around 40 ℃ and 60 ℃ which resulted in a higher open-circuit voltage.
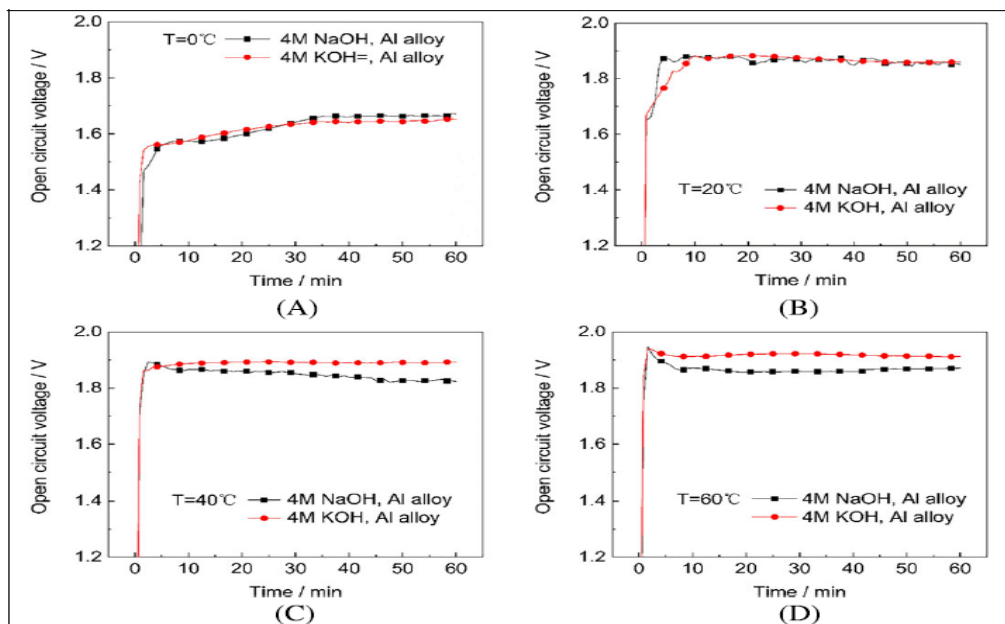
Figure 2.9: Open-circuit Voltage of KOH and NaOH at different Ambient Temperature (Hu et al., 2019).

However, self-corrosion of aluminium anode is promoted in alkaline environment and hydrogen gas is constantly released. This causes the aluminium anode to be consumed even when the battery is not in use, and eventually shorten the battery life. Alkaline electrolyte is generally selected to make aluminium-air battery with good electrical performance.

2.7.2 Neutral pH Electrolyte

Neutral pH electrolyte is also known as the salt-water electrolyte. It is famous for its low self-corrosion rate as compared to alkaline electrolyte, however at the expense of low cell voltage at approximately 1.1 V. Most studies regarding neutral electrolyte revolves around sodium chloride (NaCl). As mentioned in Section 2.6.3, the product, aluminium hydroxide is partially soluble in neutral electrolyte and will form a layer of inactive gel around aluminium anode due to high adherence of the gel onto aluminium. The layer of gel can cover all the active area at anode and prevent the electrochemical reaction to occur and the battery will no longer be functional. Neutral pH electrolyte is generally considered when developing a long shelf-life aluminium-air battery.

2.7.3 Acidic Electrolyte

Acidic electrolyte is not used in aluminium-air battery because aluminium can corrode drastically in an acidic environment.

2.7.4 Corrosion Inhibitor

Aside from alloying the aluminium anode, electrolytes are sometimes mixed with corrosion inhibitors to deal with the self-corrosion issue. Lunarska and Chernyayeva (2006) found that the corrosion rate of aluminium in NaOH solution can be reduced with the addition of potassium permanganate, $KMnO_4$.

Liu *et al.* (2016) has proven that corrosion of AA5052 can be effectively suppressed when the electrolyte contains a small amount of CMC and ZnO. Sun and Lu (2015) also studied the effect of additive inhibitors on the aluminium corrosion behaviour. In their study, 4M sodium hydroxide with ZnO additives corrodes the Al-In at a reduced rate which suggests that zinc in the electrolyte can increase the hydrogen evolution overpotential. From their perspective, the presence of zinc can change the anode reaction to develop porous film that still

can allow ion movement. The effect of adding sodium stannate (Na_2SnO_3) into 4M sodium hydroxide were also studied by the authors, which leads to a conclusion that the existence of tin can improve the aluminium dissolution, besides decreasing self-corrosion rate. Figure 2.10 exhibits the effect of additive corrosion inhibitor on the evolution of hydrogen gas. It can be noticed that the hydrogen evolved has significantly reduced after adding the corrosion inhibitors, which indicates that the self-corrosion behaviour has been reduced.
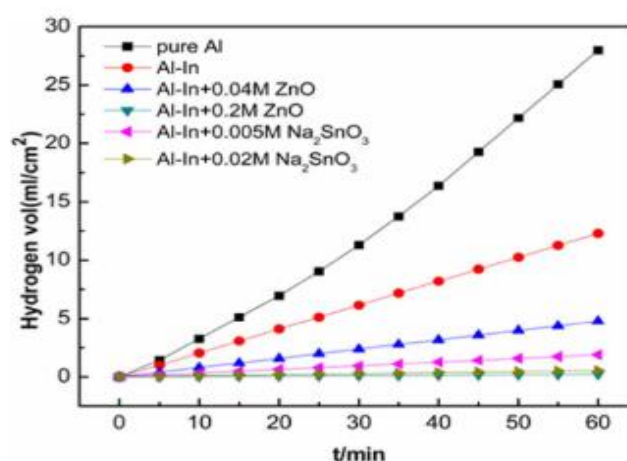
Figure 2.10: Volume of Hydrogen gas released by different samples in Aluminium-air battery with 4M NaOH solution. (Sun and Lu, 2015).

2.8 Air Positive Cathode

2.8.1 Chemical Reaction at Cathode

Oxygen reduction reaction (ORR) occurs at the air cathode as the central cathodic reaction in aluminium-air battery. In alkaline electrolyte, oxygen undergoes reduction through 2 types of pathways (Neburchilov and Zhang, 2016). Understanding these pathways is essential, especially in neutral electrolyte because oxygen reduction produces hydroxyl ions OH^- that can contribute to alkaline properties and increases the pH value. ORR reacts differently in acidic electrolyte, but it is not discussed here because acidic electrolyte is not used in aluminium-air battery.

In alkaline electrolyte, the first pathway is the direct 4-electron pathway as shown in equation (2.2). The second pathway is the successive 2-electron pathway that produces intermediate peroxide, HO_2^- before the hydroxyl ions are formed. Equation (2.3), (2.4), and (2.5) are the reactions of successive 2-electron pathways. Figure 2.11 schematically illustrates the ORR pathways.

$$O_2 + 2H_2O + 4e^- \rightarrow 4OH^- \tag{2.2}$$

$$O_2 + 2H_2O + 2e^- \rightarrow HO_2^- + OH^- \tag{2.3}$$

$$HO_2^- + 2H_2O + 2e^- \rightarrow 3OH^- \tag{2.4}$$

$$2HO_2^- \rightarrow 2OH^- + O_2 \tag{2.5}$$
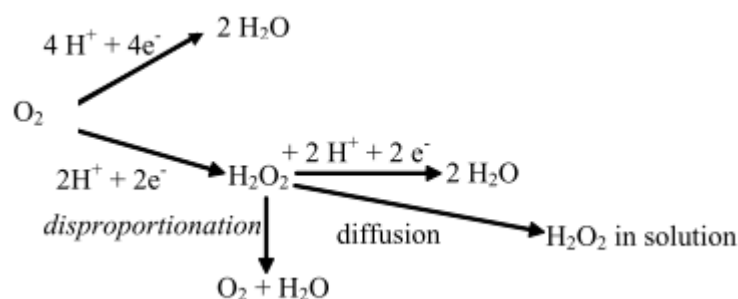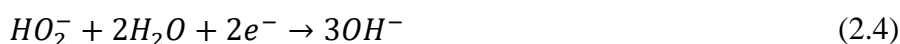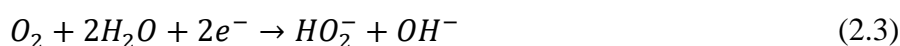
Figure 2.11: Possible pathways of ORR (Neburchilov and Zhang, 2016).

2.8.2 Complication Encountered in Air Cathode

There are several problems that aluminium-air battery often encounters at the air positive cathode. One of them is the precipitation of carbonate. According to Soler *et al.* (2005), the exposure of aluminium-air battery to the atmosphere will cause a reaction between the electrolyte and the carbon dioxide in the air and produce carbonate precipitate. This contaminant is harmful towards the electrical conductivity performance of the electrode. This suggests that the air composition that passes through is desired to have low carbon dioxide concentration and high oxygen concentration to provide conducive environment for cathode reaction. The subsequent issue will occur if the gas diffusion layer is not optimised. As a result, electrolyte tends to sip into the tiny opening of air cathode, causing difficulty in the diffusion of oxygen into the air cathode layers.

Electrolyte might also dry out during the operation before the aluminium anode is fully consumed. Therefore, Avoundjian, Galvan and Gomez (2017) proposed an architecture of aluminium-air battery based on paper. The usage of paper to contain electrolyte is beneficial as the capillary action can be achieved. The paper is designed to have an extended section so that it can be put into the electrolyte reservoir. Hence, electrolyte is passively supplied to the paper without any external effort. From the authors' point of view, the porosity of paper can ease and control the movement of ions and electrons in electrolyte.

Finally, the most discussed issue in air cathode is the sluggish oxygen reactions that can significantly impede the performance of aluminium-air battery. This inefficient cathode reaction is targeted to be improved by using catalysts to reduce the oxygen reduction reaction overpotential and oxygen evolution reaction overpotential. The studies regarding electrocatalyst are rather wide-scaled and complex that involve lattice structure, surface energy, nanotechnology, composite structures.

2.9   Evaluation Methods of Aluminium-air Battery

The performances of aluminium-air battery are often characterised in power density and energy density. Power density is also known as specific power, it represents the power generated per unit weight, having a unit of W/kg. On the other hand, energy density represents the total energy accessible that has a unit of Wh/kg. Several evaluation tools and techniques are utilised to assess the performance and characteristics of aluminium-air battery prototype.

2.9.1   Pourbaix Diagram (Potential/pH diagram)

Pourbaix diagram is commonly used to study the thermodynamic properties of pure aluminium when it reacts with water in simple solutions. The x-axis of the diagram is the pH value of the solution while the y-axis represents the potential of metal, in this case, aluminium. Figure 2.12 shows the Pourbaix diagram of aluminium.
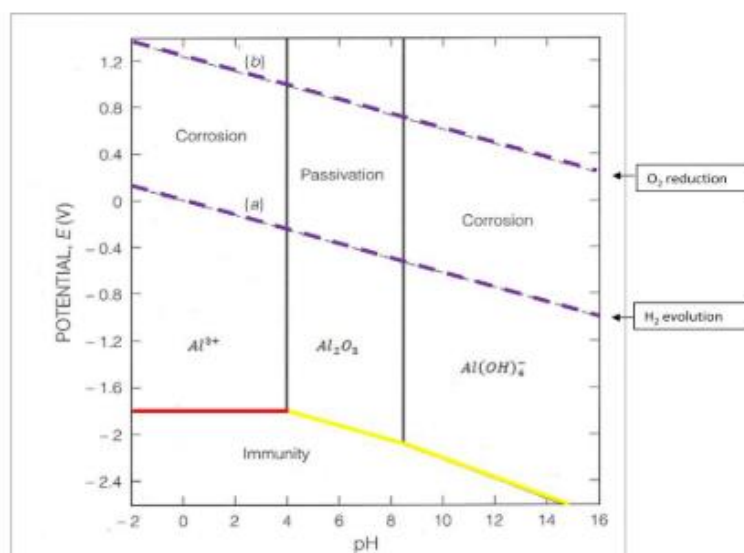
Figure 2.12: Pourbaix diagram – Pure Aluminium (Nestoridi, 2008).

By observing Figure 2.12, three distinct regions that include the immunity region, corrosion region, and passivation region can be found. These regions indicate the condition at which the aluminium anode will corrode, become passive, or immune to corrosion. The dotted line represents the corresponding oxygen or hydrogen evolution for metal in their given environment. When the metal is in contact with the environment above the oxygen reduction line, oxygen tends to evolve as a result of water dissociation. When it is below the hydrogen evolution line, water dissociates and hydrogen gas is evolved instead of oxygen.

It is not thermodynamically favourable for corrosion to occur in the immunity region, which means that aluminium is immune from corrosion attack. The passive region is the region where the aluminium forms an adherent oxide film that barricades the contact between the metal and the environment. This diagram supports the formation of non-reactive gel at the aluminium anode when neutral electrolyte is used in aluminium-air battery as stated in section 2.7.2. Pourbaix diagram suggests that it is always thermodynamically favourable for aluminium metal to corrode on open-circuit because the immunity region is at negative potential value. The corrosion region shows the condition at which aluminium is stable as ionic product and vulnerable to corrosion attack.

Pourbaix diagram implies that aluminium anode in aluminium-air battery will undergo self-corrosion albeit there is no potential difference. Pourbaix diagram also supports the hydrogen evolution phenomena given that the aluminium anode is in the condition below the hydrogen evolution line.

2.9.2   Potentiodynamic Polarisation Curves - Tafel plots

According to Martinez *et al.* (2017), data regarding the pitting vulnerability, corrosion rate, passivity, and cathode behaviour of electrochemical systems can be identified using the Tafel plots. Tafel plot is known as the Potentiodynamic polarisation curves that can obtain the overpotential value of electrochemical reactions.

The corrosion potential (E_{corr}) is the open-circuit potential of metal in a given liquid environment and it can be identified with the horizontal section in Tafel plot. The corrosion current (I_{corr}) is determined to calculate the corrosion

rate and it can be identified at the crossing point between the tangent of anodic and cathodic slopes. Besides that, the voltage response towards current and the behaviour of oxidation reaction can be identified from the anodic slopes. This technique is used by Sun and Lu (2015) to easily identify the corrosion potential of pure aluminium and Al-In. The authors noticed the fluctuation at the Al-In anodic slope between -1.3 V and -0.7 V and suggests that the oxidation occurs on indium and the aluminium alternately.
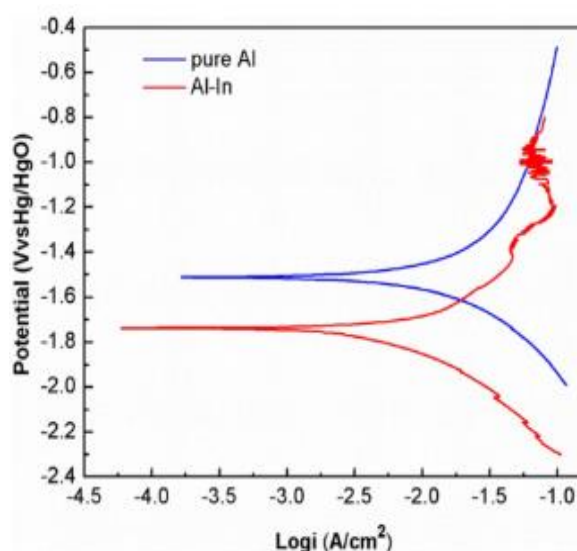
Figure 2.13: Application of Tafel plot in experiment (Sun and Lu, 2015).

Tafel plots are also utilised by Xia *et al.* (2020) to determine the electron transfer rate in ORR process, which can deduce the performance of catalytic activity. In the study, Tafel plot obtained from Linear Sweep Voltammetry (LSV) curves provides the slope values of $Co-MnO_2/C$ catalysts and MnO_2/C catalysts as shown in Figure 2.14. By analysing these data yields a conclusion that 40% $Co-MnO_2/C$ catalyst is the best performing catalyst among all the other candidates by having the least steep slope value. According to Gulati, S. (2019), Tafel slope value is an indicator to the efficiency of an electrode to produce current correspondingly to the change in applied voltage, where a low slope value signify that less overpotential is needed to achieve high current.
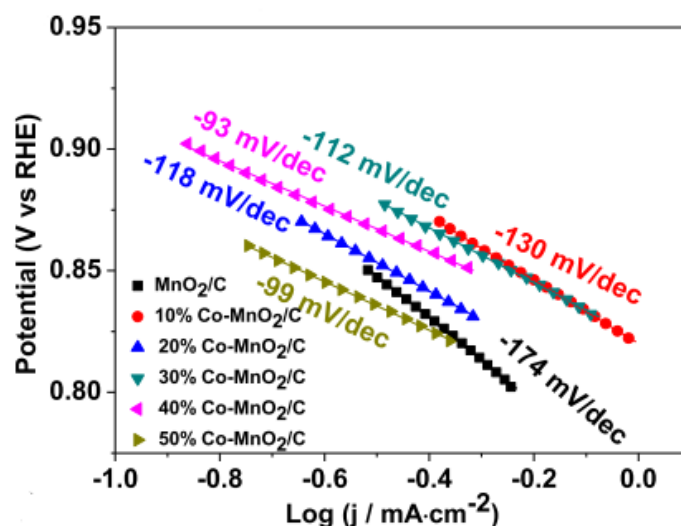
Figure 2.14: Tafel plot of MnO_2/C catalyst and different mole percent of Co-MnO_2/C catalysts in ORR process (Xia et al., 2020).

2.9.3 Scanning Electron Microscopy

Aluminium anode surface is often analysed using Scanning Electron Microscopy (SEM) to understand the ongoing process in anode. SEM is an electron microscope that can observe images in nano-scale, and can reveal details that are less than 1 nm. In SEM, concentrated beam of electrons are fired towards the sample, and the resultant signal emitted from the interaction between the electrons and the atoms in the specimen are obtained and processed to generate a detailed image with high resolution. Different scanning process are available because a variety of signal are produced from the interaction, such as back-scattered electrons (BSE), secondary electrons (SE), cathode-luminescence (CL), and etc. The image produced using SEM can accurately provide information of the surface composition and morphology in the sample.

SEM were utilised in many researches regarding aluminium-air battery, including Pino *et al.* (2015), Jingling *et al.* (2015), and Sun and Lu (2015) to investigate the surface of the anode after discharge. Generally, the pitting, pores, material surface composition and corrosion morphology are observed to deduce the effect of corrosion inhibitors on the aluminium anode.

2.9.4   Energy Dispersive X-ray Spectroscopy

The atomic structure of each element is one-of-a-kind and therefore result in specific peaks on electromagnetic emission spectrum. By utilising the principle above, energy-dispersive X-ray spectroscopy is capable of measuring the composition of the specimen. X-rays beam is directed to sample to displace an inner shell electron by excitation, causing an electron hole that eventually be filled up by an outer shell electron. This mechanism that involves higher energy outer shell and lower energy inner cell will emit X-ray, which is then captured by energy-dispersive spectrometer. Analysing the energy of the emitted X-ray and matching it with the unique electromagnetic emission peak can identify the composition of the specimen. This technique is also recognised as EDX, EDXS, EDAX or XEDS.

Nestoridi (2008) utilised EDX to determine the material composition in the area of EDX2 as circled in SEM image in Figure 2.15 to identify the cause of white dot in the aluminium anode surface. The corresponding EDX result is depicted in Figure 2.16, showing that the area is consists of 59.23% of tin. It can be implied that the white dot indicates the presence of Sn particles.
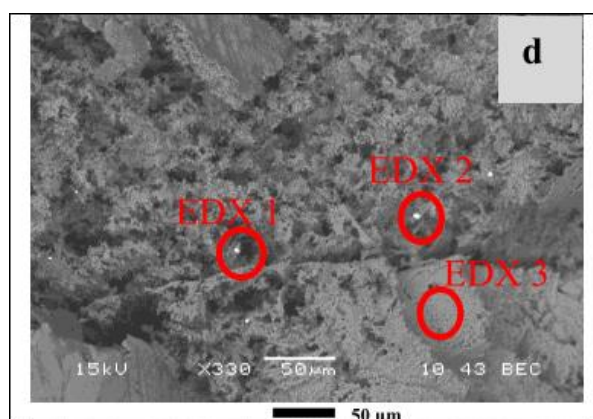
Figure 2.15: SEM image of Aluminium anode surface.
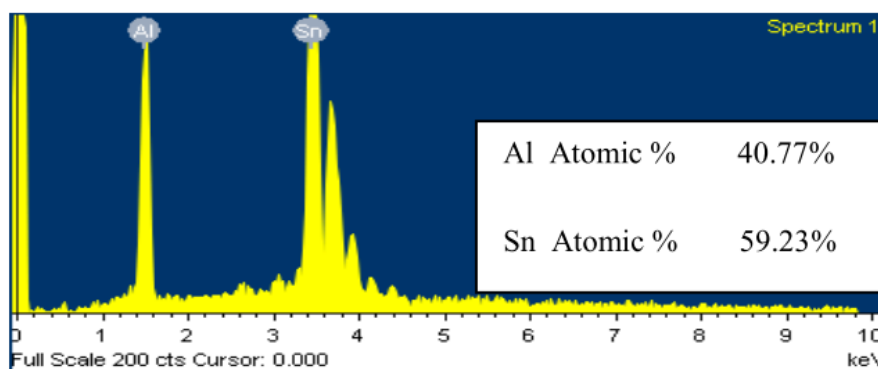
Figure 2.16: EDX result of red circled EDX2 area in Figure 2.15.

2.9.5   Electrochemical Impedance Spectroscopy

Electrochemical impedance spectroscopy (EIS) is a measurement of impedance that resulted from the solution resistance and capacitance on the electrode. AC signal over a range of frequency is applied to the sample to determine its dissipation behaviour, frequency response, energy storage, and other electrical properties. The advantage of EIS measurement is that the information obtained is more detailed than conventional DC technique and single frequency method. Multiple electrochemical reactions that simultaneously occur in the sample may be identified using EIS. EIS is also convenient in experimenting the behaviour of passive film diffusion. However, the downside of EIS is that the measurement will take a considerable amount of time, it usually takes several hours to complete. Unstable system shall be avoided in EIS measurement as the result will be inaccurate and meaningless. Bode plot or Nyquist plot will be generated as the result of EIS measurement.

In the case of assessing aluminium-air battery, Nyquist plot is analysed to evaluate the stability of the battery and to model the equivalent circuit modelling. The purpose of generating an equivalent circuit is beneficial in making electrical assumptions and calculations to the electrochemical battery, the Equivalent Series Resistance (ESR) of a battery that represents the system loss can be analysed with EIS. This is a rather complicated task because the equivalent circuits are generated based on the patterns in the EIS, such as the capacitive loop and inductive loop. An example of Nyquist plot and its respective equivalent circuit model is shown in Figure 2.17. This process is also called impedance modelling. Sun and Lu (2015) has employed the EIS measurement to create the equivalent circuit of aluminium-air battery composed of Al-In in 4M NaOH solutions as shown in Figure 2.18.
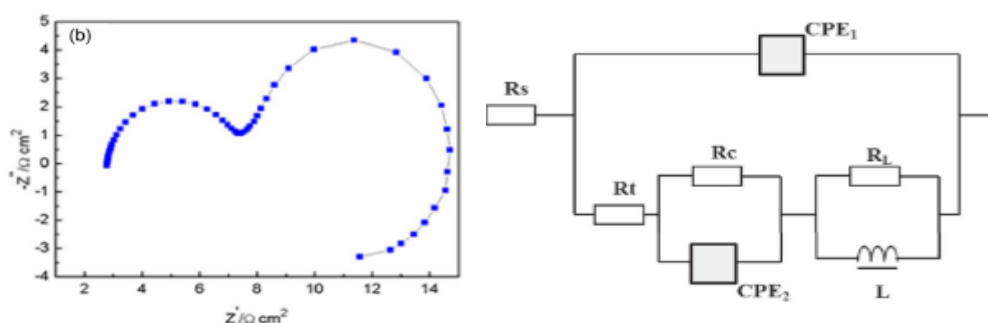
Figure 2.17: Equivalent Circuit Modelling based on Nyquist plot.
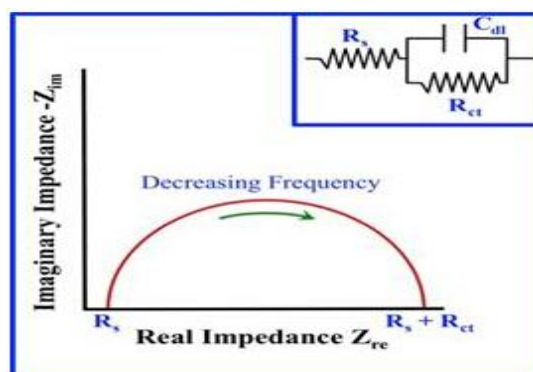
Figure 2.18: Nyquist plot of Al-In in 4M NaOH solution (Left) and its Equivalent Circuit (Right).

2.9.6   X-Ray Powder Diffraction Crystallography

Similar to EDX, X-ray powder Diffraction crystallography (XRD) also uses x-ray technology. XRD is a rapid and non-destructive way to identify the phase, crystal imperfections, and grain size of crystalline materials. The MnO_2 catalyst for aluminium-air battery are characterized by Sun *et al.* (2016) using XRD.

According to Microscopy Australia (2014), XRD works by directing x-rays toward the sample and the interaction of the incident rays with sample produces constructive interference and a diffracted ray when the Bragg's Law conditions are met. These diffracted X-rays are then detected, processed and counted. Since the sample is randomly oriented, scanning range should include all possible diffraction directions of the crystal lattice. The diffraction peaks in the XRD graph are subsequently converted into d-spacings and compared with a reference database because each mineral has their unique d-spacings. The database is compiled in Powder Diffraction File (PDF-2) and constantly being updated by International Centre for Diffraction Data (ICDD). Typically, XRD samples are in the form of finely divided powders, but it can also investigate solid materials given that the surface is flat enough.

Through the use of XRD, Fan *et al.* (2015) had investigated the effect of crystal orientation of the aluminium anode on alkaline-based aluminium-air battery. Figure 2.19 displays the XRD reference file that the authors used to identify the crystal orientation of aluminium. The authors concluded that the (100) plane possesses the highest capacity density and the lowest corrosion rate among the other (110), (111), and polycrystalline structures.
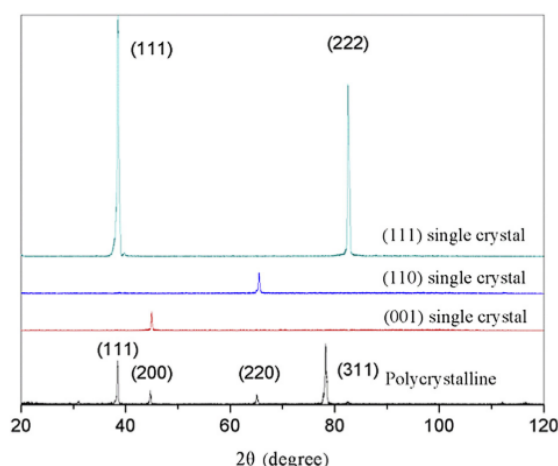
Figure 2.19: XRD patterns of different crystal orientation in aluminium (Fan et al., 2015).

2.10   Other Evaluation Techniques for Battery

There are several aspects of battery that have to be examined. Cyclic voltammetry is a type of technique that can be used to identify the potential window of battery, which is the charge cut-off voltage and discharge cut-off voltage. In some cases, cyclic voltammetry is also used to identify new electrolytes. Charge-discharge technique is also used to measure the cycle-life in the case of secondary battery. One of the variants for this technique is the constant current-constant voltage (CC-CV). Charge cut-off voltage is supplied to battery, followed by trickle charging to ensure the battery is fully charged. The aluminium anode and air cathode of the battery can be monitored using auxiliary voltage measurements.

By utilising these techniques, the relationship between capacity and cycle number can be determined to assess the battery cycle-life. Capacity is defined as a measurement of charge that have Ampere-hour (Ah) units. For instance, a powerbank that has 10,000 mAh or 10 Ah is expected to supply current at 10A and last for one hour. Coulomb efficiency that quantifies the ratio of input charge to output charge is also determined in the experiments.

2.11   Summary

Aluminium-air battery has high theoretical voltage of 2.7 V, high theoretical energy density of 8100 Wh kg^{-1} and high theoretical specific capacity of 2980 Ah kg^{-1}. Aluminium is the third most abundant element on planet Earth, which makes it easily accessible. The recyclability of aluminium-air battery between the aluminium anode and the resulting product, aluminium hydroxide is beneficial and sustainable. The characteristics of existing battery in the market are studied and compared with the aluminium-air battery. Aluminium-air battery has the highest energy capacity, such that the Li-ion battery that has the best performance in specific energy capacity, only possesses 265 Wh/kg, which is 20% of the expected capacity of aluminium-air battery.

The working principle of aluminium-air battery is explained and the chemical reactions involved are discussed. The general issue that aluminium-air battery encounter is the formation of protective oxide film that reduces the conductivity of electrode. The anode self-corrosion due to low hydrogen evolution overpotential that occurs readily also decreases the battery life. Aluminium-air battery constructed with pure aluminium and different types of aluminium alloys are discussed.

In most cases, alkaline or neutral electrolyte is used instead of acidic electrolyte because acid can cause serious corrosion on the metal. Alkaline electrolyte has better cell voltage while the self-corrosion issue in neutral electrolyte is less serious. Corrosion inhibitor can be added into the electrolyte to alleviate self-corrosion. The oxygen reduction reaction at air cathode undergoes direct 4 electron path and successive 2 electron pathway. Pourbaix diagram, Tafel plots, SEM, EDX, XRD, and EIS are frequently utilised to evaluate the characteristics of aluminium-air battery.

CHAPTER 3

METHODOLOGY AND WORK PLAN

3.1   Aluminium-air Battery Model Architecture

The basic design of aluminium-air battery would require aluminium anode as the fuel, electrolyte to carry electrical charges, and the air positive cathode which is made from catalytic layer, current collector, and breathable waterproof membrane. In order to assemble these components into a functional aluminium-air battery, supplementary components such as acrylic boards, separator, wires, and binding clips are used. Aluminium-air battery is designed using Solidworks as shown in Figure 3.1. All the components are rectangular except for current collector. The current collector section is extended to allow easy wire connection using crocodile clips.
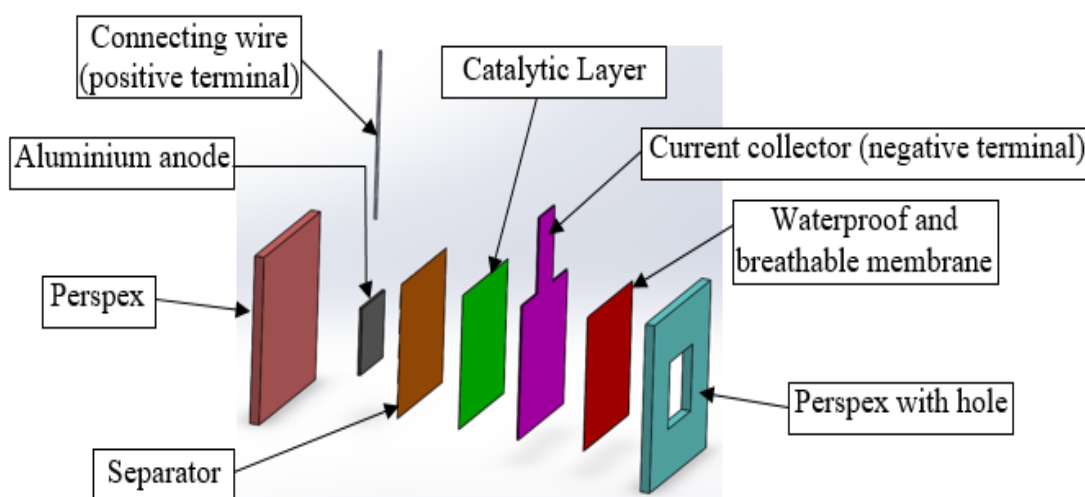
Figure 3.1: Architecture of Aluminium-air Battery.

As stated in section 2.4, aluminium-air battery is galvanic cell, thus aluminium anode should be connected to negative terminal and cathode should be connected to positive terminal in a circuit when operating as a battery. However, Smart Manager software only recognises the 'discharge' status when the input current is negative. Hence, the wire connection to the potentiostat is reversed in response as illustrated in Figure 3.2. The plus and minus sign in Figure 3.2 indicates the wire connection to the potentiostat. The negative current

input produces a current flow from the air cathode to aluminium anode, which makes the aluminium anode to become negative terminal and cathode to become positive terminal during the discharge process. The voltage measured in the experiment is referenced to standard hydrogen electrode (SHE).
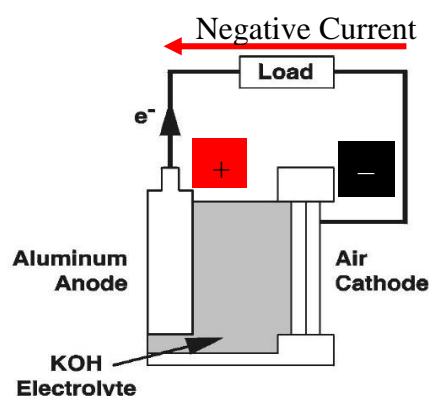
Figure 3.2: Illustration of Wire Connection to the Potentiostat (Sleight, 2011).

Figure 3.3 shows the assembled version of aluminium-air battery where the four corners of the acrylic board are clamped using binder clips.
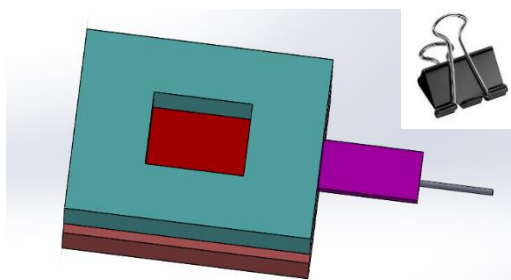
Figure 3.3: Conceptual design of Aluminium-air Battery.

3.2 Required Material List and Procurement Plan

During the procurement stage, materials such as PTFE sheet and stainless steel mesh are purchased from two different vendors with different specifications. This is to ensure that a more suitable component can be used to build the aluminium-air battery, as well as to serve as a backup plan in case one of the components cannot be used to build a functional aluminium-air battery. Stainless steel mesh is used as current collector to withstand the alkaline electrolyte that can corrode the mesh. Table 3.1 and Table 3.2 summarises the shopping list cost of the required materials to build the battery respectively.

Table 3.1: Required Materials to Build Aluminium-air Battery.

Functional Units	Material	Quantity
Aluminium Anode	Pure aluminium, alloy 6063	-
Acrylic Board	Perspex	2
Waterproof & breathable membrane	PTFE sheet	1
Current collector	Stainless steel mesh	1
Catalytic Layer	Carbon paper, Graphite felt, Graphite powder	1
Separator	Polypropylene chemical absorbent paper	1
Electrolyte	Potassium hydroxide (KOH) solution	1
Clamping tool	Binder clip	6

Table 3.2: Cost of each Material and its Specification.

Material	Price	Remarks
Aluminium alloy 6063	-	6 cm $\times$ 6 cm
Pure aluminium	-	6 cm $\times$ 6 cm
Perspex	RM 22.80	A4, 3 mm thick
PTFE sheet	RM 19.80	20 cm $\times$ 20 cm, 1 mm
	RM 18.00	20 cm $\times$ 20 cm, 0.25 mm
Steel mesh	RM 11.70	Stainless steel, Fine
	RM 12.50	Stainless steel, Coarse
Carbon Paper	RM 1.00	1 sheet
Graphite powder	RM 5.00	1 small bottle
Graphite felt	-	-
Kim's Wipe	-	From Lab
Polypropylene chemical absorbent paper	-	Sample from dealer
Potassium Hydroxide (KOH) solution	-	4M KOH
Binder clip	-	-
Total Cost = RM85.80		

3.2.1 Material Specification for Separator

The separator's function is to inhibit the contact between aluminium anode and air cathode to prevent short-circuit. The separator material is chosen from a company named Crisben. It is made out of 100% polypropylene chemical absorbent paper as shown in Figure 3.4. Its dimpled pattern allows it to quickly soak up liquid. This material is capable of absorbing liquids up to 12.5 times of its own weight. Besides that, it is also very durable as it can resist tearing and

friction and no lint fall even after reaching absorption saturation. Lastly, polypropylene's chemical resistant property allows it to absorb most liquids including acids and caustics without being corroded or deteriorated. A sample of the absorbent paper has been retrieved from the dealer.

Figure 3.4: Crisben Chemical Absorbent Paper.

3.3 Constructing the Aluminium-air Battery Prototype

The construction of the prototype is divided into two stages, where the first stage is done at mechanical workshop to machine the Perspex into desirable shape, while the second stage is completed at chemical laboratory to acquire the electrolyte with correct concentration.

3.3.1 Mechanical Workshop Steps

Pure aluminium sheets and aluminium alloy 6063 are cut into 6cm × 6cm. Perspex is cautiously cut into 2 pieces of 10cm × 10cm square units because it is brittle and can break easily. One of the Perspex is then machined to have a 6cm × 6cm hole in the middle as shown in Figure 3.5. Meanwhile, the chemical absorbent paper, PTFE sheet, and steel mesh is cut into 10cm × 10cm square.
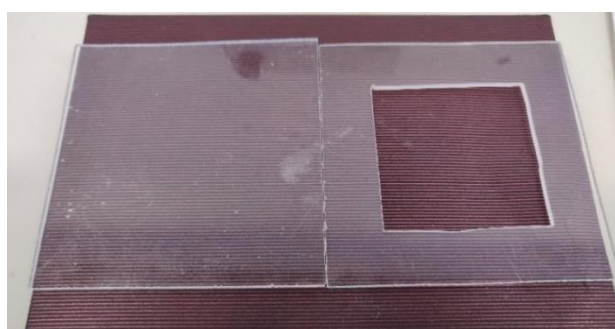
Figure 3.5: Machined Perspex.

3.3.2   Chemical Laboratory Steps

Potassium hydroxide solution (KOH) is prepared. 200 ml of distilled water is mixed with 11.17g of KOH pellets to produce 200ml of 4M KOH solutions as shown in Figure 3.6. The pellets are added slowly into the distilled water as the reaction is exothermic and tends to generate a great amount of heat that might break the beaker. A vigorous exothermic reaction is dangerous and shall be avoided.
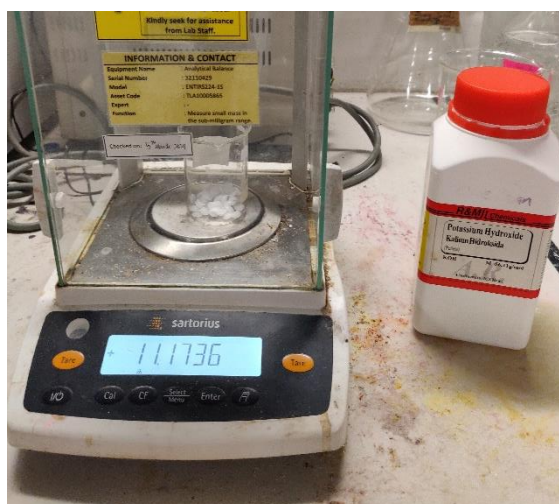
Figure 3.6: KOH solution Preparation.

3.3.3   Setup of Apparatus

Supplementary materials and apparatus required throughout the experiments are:

1) Multimeter
2) Sandpaper
3) Potassium hydroxide pellets
4) Copper wire
5) Dropper
6) Scissors
7) Ruler
8) Duct Tape
9) Electric scaling machine
10) Kim's Wipe
11) 100 ml Beaker
12) 15 ml Measuring cylinder
13) Spatula

Detailed procedures for aluminium-air battery preparation are:

1) Oxide layer on anode is removed using sandpaper.

2) Copper wire is connected to the aluminium anode.

3) 8ml of 4M KOH solution is added to the separator using dropper.

4) The components are stacked in the order of Perspex, aluminium anode, separator, catalytic layer, current collector, waterproof & breathable membrane, Perspex with hole.

5) The stacked components are clamped with binder clips.

6) The positive terminal of potentiostat is connected to the anode, and the negative terminal is connected to the cathode.

The components are assembled according to the conceptual design in Figure 3.1. The assembled prototype is presented in Figure 3.7.
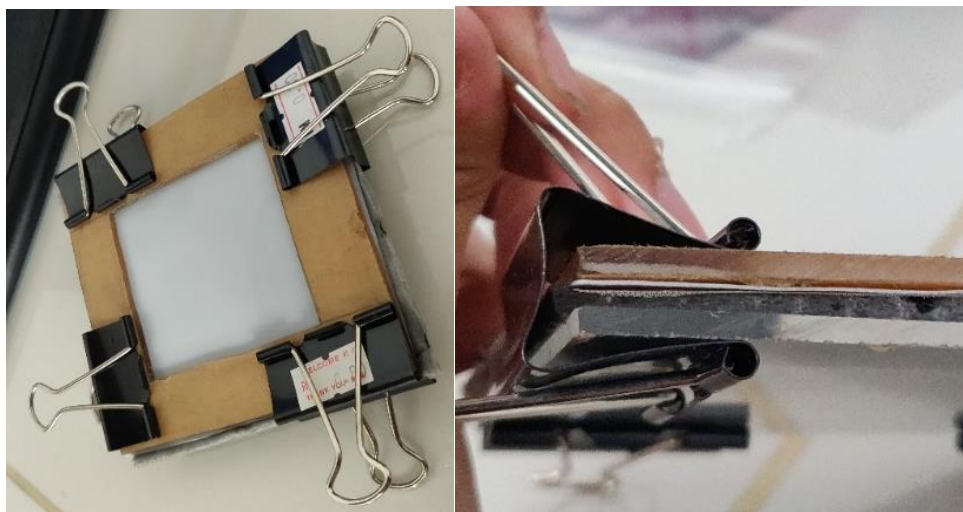
Figure 3.7: Aluminium-air Battery Prototype.

3.4 Preliminary Experiment on Prototype

A simple pre-test is conducted on the prototype to select the most suitable materials among the purchased materials to construct the prototype that can yield the highest open-circuit voltage. In the pre-test, the aluminium-air battery prototype is constructed with different components. The constant variables in the experiment is the amount of 4M KOH electrolyte which is set at 8ml, chemical absorbent paper as separator, and aluminium alloy 6063 as anode. The air cathode materials involved in this pre-testing are the carbon paper, 1mm and

0.25mm PTFE film, as well as the fine steel mesh and coarse steel mesh. Multiple combinations of the stated materials to build air cathode are sorted in Table 3.3. The resultant open-circuit voltage is measured using a multimeter as shown in Figure 3.8. The prototype in the figure is built with fine steel mesh, carbon paper, and without the PTFE sheet.

The results are recorded and discussed in section 4.1. The pre-test concluded that the aluminium-air battery produced the highest open-circuit voltage with only coarse steel mesh as air cathode, which makes it as the standard air cathode design.

Figure 3.8: Open-circuit voltage of Prototype Constructed with Fine Steel Mesh and Carbon Paper as Air Positive Cathode.

Table 3.3: Result table for Preliminary Test.

	PTFE sheet (0.25mm)	PTFE sheet (1mm)	PTFE sheet (0.25mm), carbon paper	PTFE sheet (1mm), carbon paper
Fine steel mesh				
Coarse steel mesh				
	Only steel mesh		With carbon paper	
Fine steel mesh				
Coarse steel mesh				

3.5   **Open-circuit Voltage Analysis**

With the aid of potentiostat and ZIVELAB Smart Manager software, this experiment is conducted to acquire open-circuit voltage graphs of aluminium-air battery built with different anode materials, which are pure aluminium and alloy 6063. The software is operated with the steps listed in Figure 3.9, Figure 3.10, Figure 3.11, Figure 3.12, Figure 3.13, Figure 3.14, and Figure 3.15 below:

1) "SMART Manager – Controls and realtime viewer" is opened.

Figure 3.9: SMART Manager Software.

2) "Experiment" >> "Sequence File Editor" >> "New" are clicked.
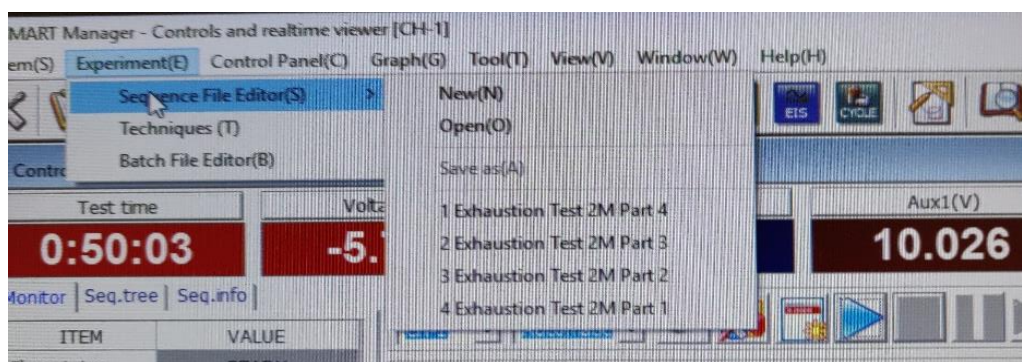
Figure 3.10: Sequence File Editor.

3) A new window 'SM sequence' has popped up. "Add" is clicked.
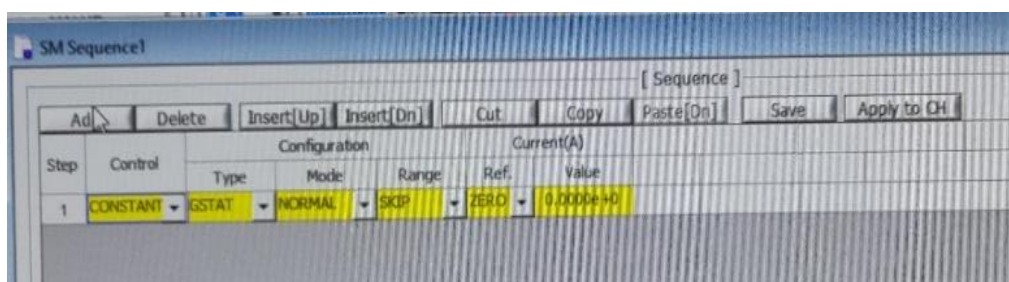
Figure 3.11: Sequence Editor Window.

4) The configuration type is changed to "C-RATE".
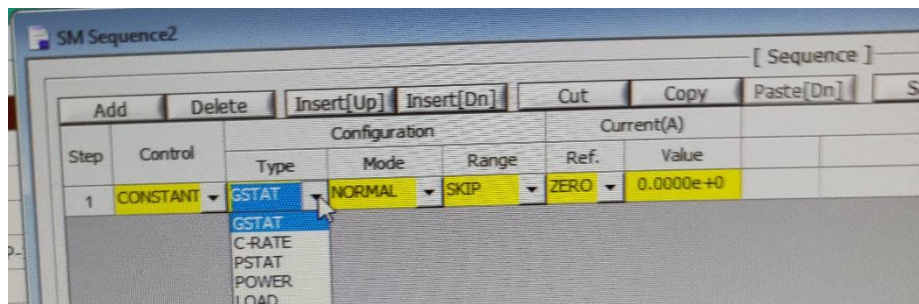
Figure 3.12: Configuration of Sequence Type.

5) The C-rate value is changed to '0' to simulate open-circuit condition.
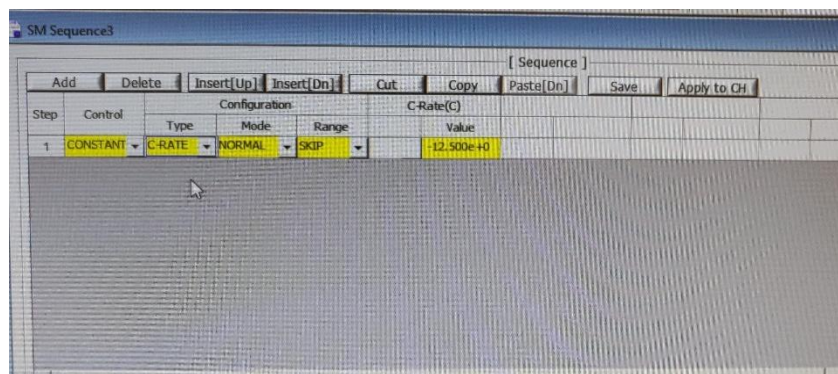
Figure 3.13: Configuration of C-Rate value.

6) The Cut-off condition is configured and "Apply to CH" is clicked.
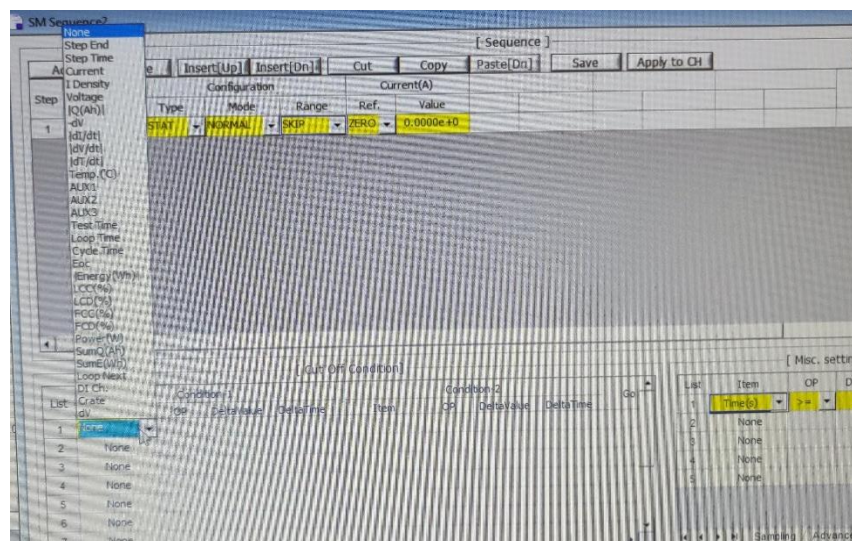
Figure 3.14: Configuration of Cut-off condition.

7) Waited for 2 hours to allow the aluminium-air battery to discharge.

Figure 3.15: Result generation process.

8) Step 2-7 are repeated with different setups and the results are compared.

3.6 Effects of Different Catalysts and Anode Materials

In these experiments, pure aluminium and alloy 6063 are tested with different types of catalytic layer and the resultant discharge characteristics are recorded and analysed. The catalytic layer for the experiment includes graphite felt and graphite powder. The implementation of graphite felt is fairly easy as it is a solid layer that can be added to the aluminium-air battery directly by placing it between separator and steel mesh. However, graphite powder has to be sprinkled evenly and adequately on the separator. The layer of graphite powder should cover the whole reactive area.

Their respective performances are investigated with the aid of a potentiostat by conducting a series of tests. The tests include the constant current discharge test, Tafel test, and the capacity test. All the required tests are sorted and organised in Table 3.4 to easily keep track of the experiment progress. A control set without catalytic layer is also tested. Observe any physical changes in the anode and cathode, as well as the formation of gas bubbles from anode.

Table 3.4: Tests required for Experiment part A.

Anode Material	Types of catalyst	Constant current discharge	Tafel plot	Capacity test
Pure Aluminium	No catalyst			✗
	Graphite felt			✗
	Graphite powder		✗	✗
Aluminium alloy 6063	No catalyst		✗	✗
	Graphite felt			✗
	Graphite powder		✗	✗

Initially, this experiment utilised chemical absorbent paper as separator. Halfway through the experiment, it is discovered that the chemical absorbent paper is inferior to the Kim's Wipe as discussed in section 4.2. Therefore, all the experiments are conducted using Kim's Wipe as the separator.

3.6.1   Constant Current Discharge Test

This test is conducted by discharging the battery at 10 mA for 1 hour to obtain the discharge curve of the battery. The procedures for operating ZIVELAB Smart Manager are identical to the open-circuit voltage test at section 3.5. However, the C-rate value is changed to -10mA. The entered value is in negative sign, which means it would be in discharge state. Figure 3.16 shows the window to adjust the input the discharge current.
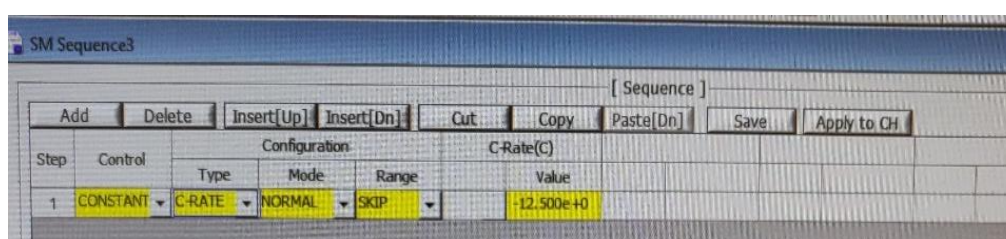
Figure 3.16: Configuration of current discharge value.

3.6.2   Tafel Plot

3.6.2.1 Experimental Procedure

Tafel plot of the battery can be obtained using a technique provided in ZIVELAB Smart Manager software. As mentioned in section 2.9.2, Tafel plot is used by Sun and Lu (2015), and Xia *et al.* (2020) to determine the open-circuit voltage and corrosion rate. The initial potential of the Tafel scan is -0.25 V and

the final potential is 0.25V. The scan rate is set at 0.001 V/s, and consequently the test is expected to take 500s to complete, which is approximately 8 minutes.

Through the use of Tafel Analysis feature in IVMAN software, E_{corr} and I_{corr} can be estimated. The intersection point of anodic slope tangent line, cathodic slope tangent line, and the E_{corr} horizontal line is the estimated value for I_{corr}. The feature is accessed by the means as depicted in Figure 3.17 and Figure 3.18 below:

1) "Experiment" >> "Techniques" are clicked.
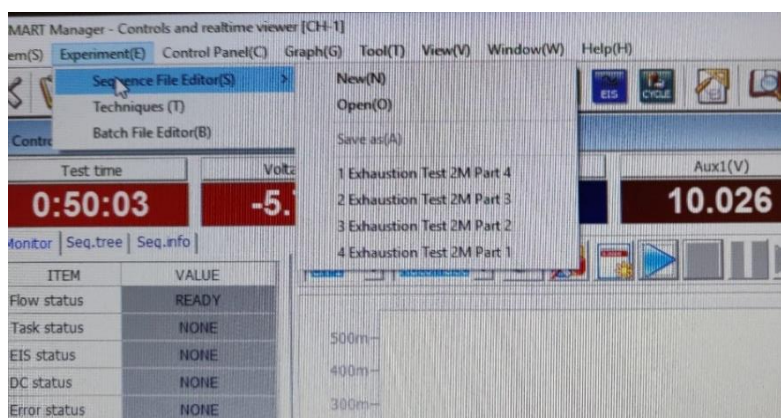
Figure 3.17: Smart Manager Techniques.

2) "Corrosion package (COR)" is expanded, then "Tafel" >> "Apply to CH" are clicked
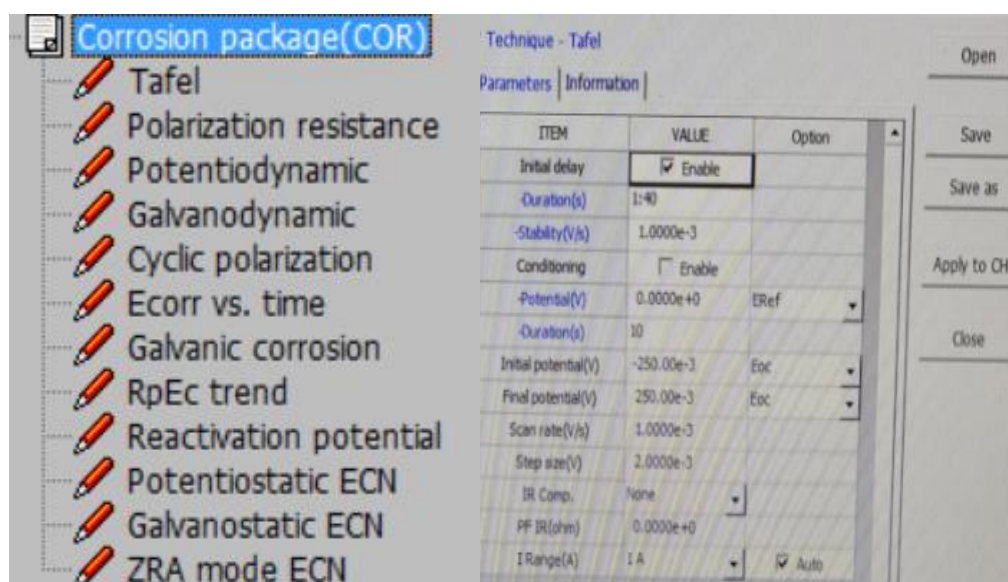
Figure 3.18: Configuration of Tafel plot.

3.6.2.2　Calculation

The obtained corrosion current from Tafel plot is used to calculate corrosion rate. Figure 4.1 demonstrates the information that can be obtained from a Tafel plot. The Tafel plots before and after installing the graphite felt are compared to investigate the effect of graphite felt catalyst.
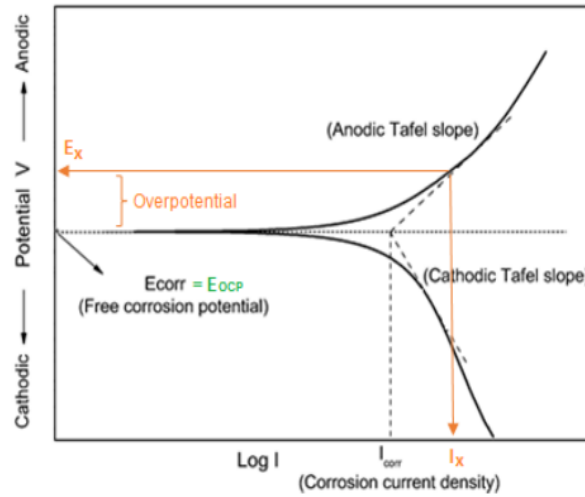
Figure 4.1: General Tafel plot.

To calculate corrosion rate, it starts with Faraday's Law of electrolysis that relate current flow to mass (Electrical4u, 2019).

$$Q = \frac{nFW}{M} \qquad (4.1)$$

where

Q = coulombs, C

n = the number of electrons involved in the electrochemical reaction

F = Faraday constant, 96487 coulombs

W = the weight of the electroactive species, u

M = the molecular weight, u

From (4.1),

$$W = \frac{QM}{nF} \qquad (4.2)$$

Given that equivalent weight, $E.W. = \frac{M}{n}$,

$$W = \frac{Q \times E.W.}{F} \qquad (4.3)$$

Given that $Q = it$ according to Faraday's Law,

$$W = \frac{it \times E.W.}{F} \qquad (4.4)$$

where

i = corrosion current, A

t = time, s

From (4.4),

$$\frac{W}{t} = \frac{i \times E.W.}{F} \qquad (4.5)$$

where

$W/t = (C.R.)$ = corrosion rate, g/s

The corrosion rate is expressed as penetration rate by dividing (4.5) by the anode reactive area (A) and anode density (ρ),

$$C.R.\,(cm/s) = \frac{i \times E.W.}{\rho A F} \qquad (4.6)$$

The units for corrosion rate is converted from cm/s to $mm/year$ for easier comparison, yielding:

$$C.R.\,(mm/year) = 0.003272 \, \frac{i_{corr} \times E.W.}{\rho A} \qquad (4.7)$$

The corrosion rate can also be expressed in terms of mass loss rate.

$$C.R. (mg/dm^2 day) = \frac{0.0895 \, i_{corr} \, E.W}{A} \qquad (4.8)$$

The parameters required for (4.7) and (4.8) are listed below,

where

i_{corr} = corrosion current density, μA

$E.W.$ = equivalent weight, u

ρ = metal density, g/cm^3

A = reactive area, cm^2

Equation (4.7) is used to calculate the penetration rate directly from I_{corr}.

3.6.3   Capacity Test with Reduced Anode Size

This test is to evaluate the capacity of the battery by allowing it to fully discharge at constant current, to the extent where the voltage hits zero. The preceding test with 6 cm $\times$ 6 cm anode size is too large and it is very time consuming for it to fully discharge. Therefore, a reduced anode size is used for this test. Similar to Pan *et al.* (2019), the dimension of 1.5 cm $\times$ 1.5 cm and constant discharge current of 10 mA are selected. Aluminium anode is covered using duct tape, leaving behind a 1.5 cm $\times$ 1.5 cm opening as shown in Figure 3.19. The procedures for operating ZIVELAB Smart Manager are identical to the constant current discharge test at section 3.6.1.
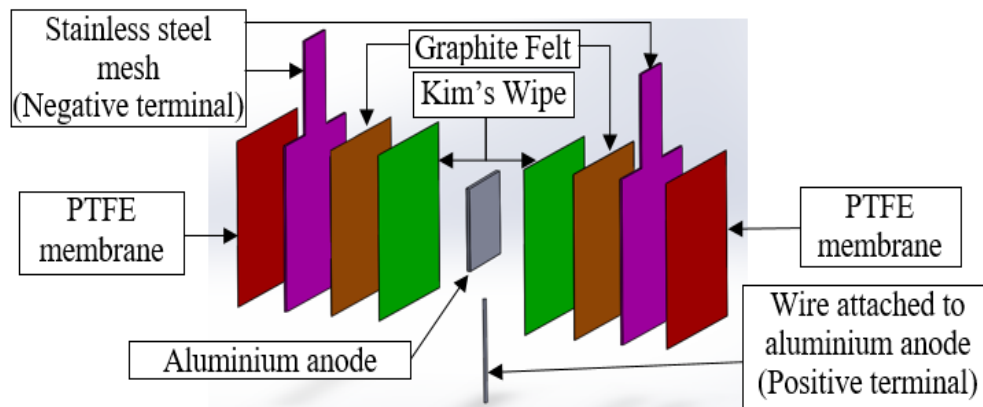
Figure 3.19: 1.5 cm $\times$ 1.5 cm Aluminium Anode Setup.

3.7   **Double Cathode Aluminium-air Battery**

The reaction at air cathode is the one of the determining factors for the performance of aluminium-air batteries. Therefore, a direct yet simple approach to improve the air cathode efficiency is by increasing the reactive area. It can be accomplished by implementing double cathode design as graphically illustrated in Figure 3.20 to attain more surface exposure to ambient.

Figure 3.20: Double cathode aluminium-air battery design.

The constructed model of double cathode aluminium-air battery is shown in Figure 3.21 and Figure 3.22. Instead of Perspex, breathable PTFE sheet is used to sandwich the battery components. The catalytic layer used in this experiment is graphite felt because it is a more effective catalyst as discussed in section 4.4.1.4. The arrangement of components in Figure 3.22 starting from the left is PTFE sheet, steel mesh, graphite felt, 2 pieces of Kim's Wipe, aluminium anode, 2 pieces Kim's Wipe, graphite felt, steel mesh, and finally PTFE sheet.

This experiment is conducted twice, where the first is done using pure aluminium, and the second is completed using alloy 6063. The amount of 4M KOH solution added is 4ml each side. The current discharge rate is set at 10mA. The double cathode aluminium-air battery discharge performance is then compared with the conventional single cathode aluminium-air battery. The mass of aluminium anode is measured before and after the experiment to determine the associated weight loss.

Connect to negative terminal

Connect to positive terminal
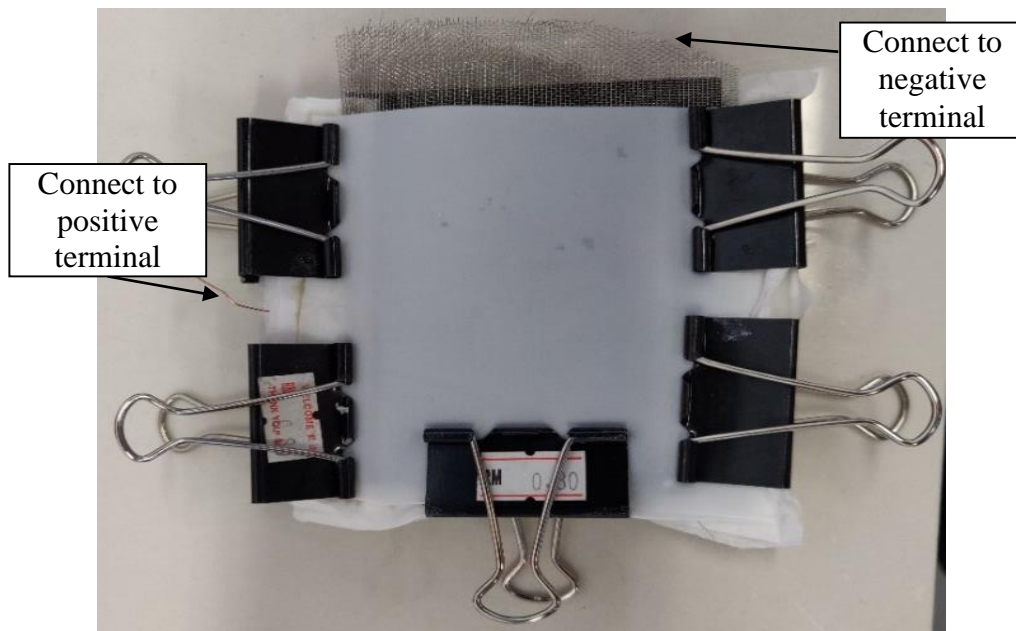
Figure 3.21: Assembled Double Cathode Aluminium-air Battery.

Figure 3.22: Double Cathode Aluminium-air Battery.

3.8   Anode Analysis in Alkaline Environment

In order to investigate the anode in alkaline environment, XRD and SEM-EDX are utilised to observe pure aluminium and alloy 6063 in 4M KOH solution.

3.8.1   Anode Samples Preparation

Three samples from each anode material are examined, where the first sample will be the original anode, followed by the anode after two hours of alkaline solution exposure, and the third sample will be exposed to alkaline environment for two weeks.

The first set of samples are prepared by scraping the surface of pure aluminium and alloy 6063 using sandpaper to remove the oxide layer. To prepare the second and third sample, four chemical absorbent papers are added with 15ml of 4M KOH solution each. Two of the chemical absorbent paper are put in contact with pure aluminium, and the other two is put together with alloy 6063. These samples are isolated in sealed plastic bag. The dimension of chemical absorbent paper should be large enough to cover one surface side of the anode.

The second set of samples are ready when the aluminium anodes are exposed to alkaline solution for two hours. These samples are cautiously cleaned with distilled water and isolated from the electrolyte to prevent further self-corrosion. After two weeks, the third set of samples are completed and the chemical absorbent paper is removed from the sealed plastic bag.

3.8.2   XRD Specifications

The anode materials are separated from the sealed plastic bag. Gloves are worn to protect the hand from alkaline solution. The materials are cut into roughly 2 cm $\times$ 2 cm to be fitted into the XRD solid specimen holder. The solid sample is carefully placed on Plasticine at the same level with the specimen holder as shown in Figure 3.23. Among all the samples, pure aluminium that is left to corrode for 2 weeks exhibits an adhesive toothpaste form unlike other solid samples. Hence, this sample is left to dry and fitted to the powder specimen holder as depicted in Figure 3.23(c).
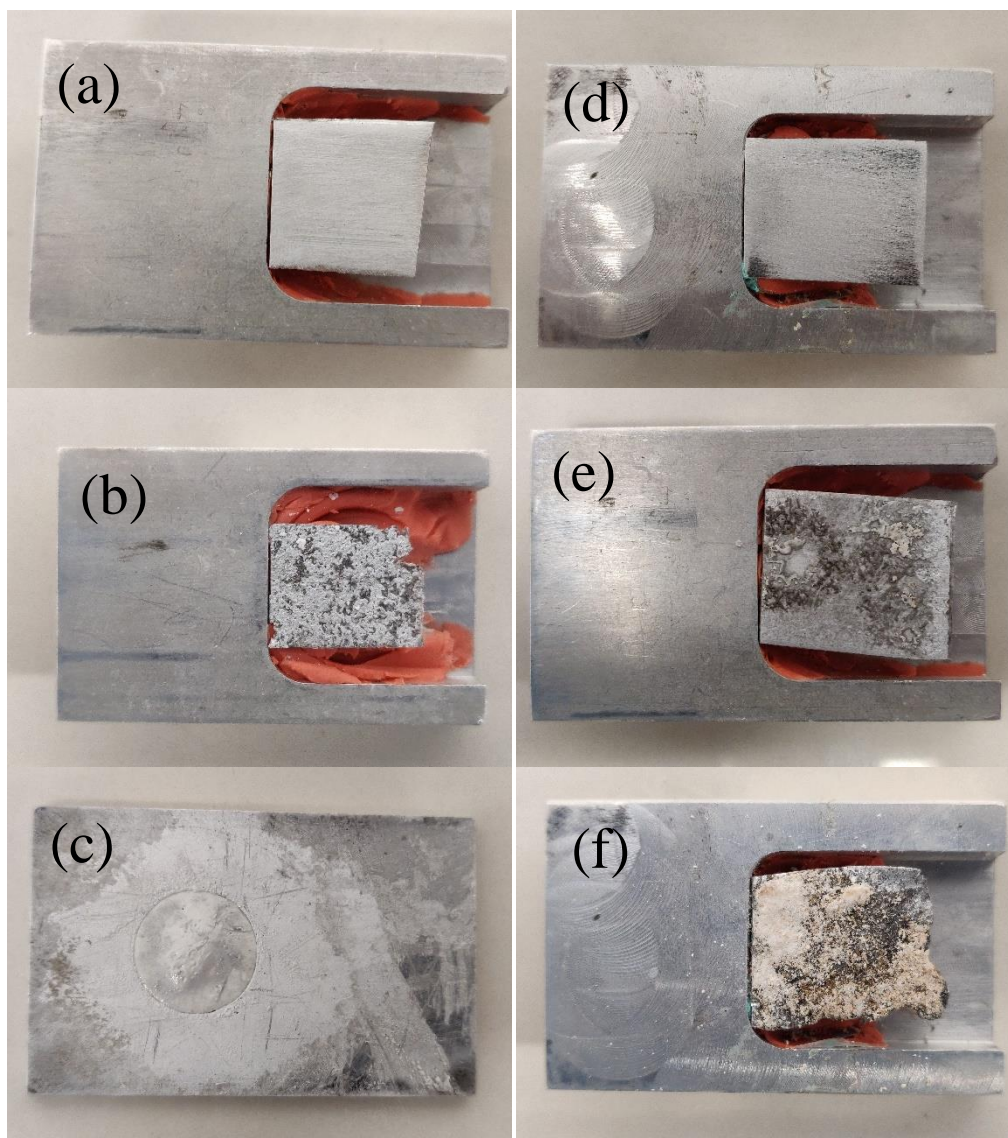
Figure 3.23: XRD specimen for Pure Aluminium (a) before the experiment, (b) two hours after the experiment, and (c) two weeks after the experiment; and Aluminium Alloy 6063 (d) before the experiment, (e) two hours after the experiment, and (f) two weeks after the experiment.

For XRD test, the scanning ranges from $10\,°$ to $90\,°$, with a step size of $2\,°$/min. The time taken to complete scanning one specimen is 40 minutes. The resultant XRD graph from each specimen is analysed using X'Pert HighScore software. This software compares the XRD graph with other closely-matched patterns compiled in the database to identify what the specimen is. The outcome of the experiment is illustrated in section 4.6.

3.8.3   SEM-EDX Specifications

After the XRD test, the specimens are then inspected using SEM-EDX to examine their surface properties. This experiment is conducted using a Hitachi SEM model S-3400N. Samples were taped firmly on each holder as shown in Figure 3.24.
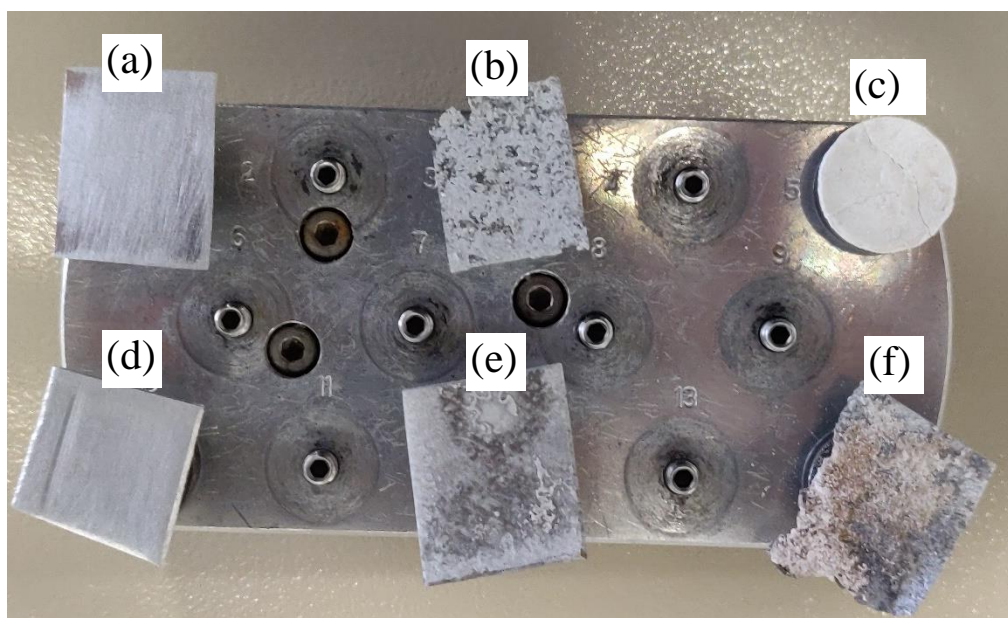
Figure 3.24: SEM-EDX specimen holder with Pure Aluminium (a) before the experiment, (b) two hours after the experiment, and (c) two weeks after the experiment; and Aluminium Alloy 6063 (d) before the experiment, (e) two hours after the experiment, and (f) two weeks after the experiment.

The microstructure investigation is commenced using SEM at 5 different magnification power, which are $50\times$, $500\times$, $700\times$, $1200\times$, and $3500\times$. The image from each magnification power is captured for further analysis. This is to observe the corrosion of anode at different perspectives while finding out the optimal magnification power that can clearly display the surface structure. The material composition for each specimen is scanned and computed using EDX at magnification power of $70\times$. A relatively lower magnification power is chosen because it can cover a wider area of the anode surface to avoid focusing on a specific regime that might be strongly attacked by corrosion or is part of the unreactive regime. The EDX is meant to inspect the overall material composition of the anode to have an overview of the corrosion level.

3.9 Work Plan

Table 3.5 and Table 3.6 show work plan for FYP part 1 and part 2.

Table 3.5: Gantt Chart for Final Year Project Part 1.

No.	Project Activities	W1	W2	W3	W4	W5	W6	W7	W8	W9	W10	W11	W12	W13	W14
M1	Problem identification & Project planning	■	■												
M2	Literature review			■	■	■	■	■	■						
M3	Data gathering						■	■	■	■					
M4	Report writing								■	■	■	■	■	■	
M5	Presentation														■

Table 3.6: Gantt Chart for Final Year Project Part 2.

No.	Project Activities	W1	W2	W3	W4	W5	W6	W7	W8	W9	W10	W11	W12	W13	W14
M1	Material procurement	■													
M2	Prepare the materials at workshop and lab		■												
M3	Build aluminium-air battery, conduct pre-test		■	■											
M4	Conduct experiments, XRD and SEM-EDX analysis				■	■	■	■	■	■					
M5	Data Analysis									■	■	■			
M6	Report writing & presentation											■	■	■	■

3.10 Summary

Firstly, the materials required for constructing the aluminium-air battery are purchased. Pure aluminium and alloy 6063 are cut into desirable sizes at the workshop and the electrolyte, 4M KOH solution is prepared at the chemical lab. After gathering all the required materials, the construction of aluminium-air battery is commenced. The battery prototype is pre-tested to figure out the most suitable material to function as an effective air cathode among the purchased material, which happens to be the set with only coarse steel mesh. It is therefore selected as the standard air cathode layout for aluminium-air battery.

The open-circuit voltage of aluminium-air battery with pure aluminium and alloy 6063 as anodes are identified. Then, the next experiment is to research the effects of different catalysts and anodes on the performance of aluminium-

air battery, which involves graphite felt, graphite powder, pure aluminium and alloy 6063. This experiment is inclusive of 3 tests using potentiostat with ZIVELAB Smart Manager software, which are constant current discharge test, Tafel test, and the capacity test.

Double cathode aluminium-air battery experiment aims to design an aluminium-air battery model that can promote air cathode activity by increasing the reactive area in anode. It is designed using Solidworks. The double cathode aluminium-air battery is tested with constant current discharge and compared with single cathode design that was previously experimented.

On the other hand, the anode samples for XRD and SEM-EDX are prepared. XRD and SEM-EDX analysis are conducted to investigate the surface of aluminium anodes before and after their short-term and long-term exposure to alkaline environment.

CHAPTER 4

RESULTS AND DISCUSSION

4.1   Preliminary Test – Optimal Setup

The pre-test is conducted to select the optimal air cathode material among the purchased materials. Table 4.1 depicts the resultant open-circuit voltage of each distinct prototype with different materials.

Table 4.1: Open-circuit voltage of Aluminium-air Battery with different Air Cathode Building Materials.

	PTFE sheet (0.25mm)	PTFE sheet (1mm)	PTFE sheet (0.25mm), carbon paper	PTFE sheet (1mm), carbon paper
Fine steel mesh	1.270V	1.263V	1.172V	1.169V
Coarse steel mesh	1.398V	1.401V	1.296V	1.302V
	Only steel mesh		With carbon paper	
Fine steel mesh	1.282V		1.274V	
Coarse steel mesh	1.441V		1.436V	

Based on Table 4.1, it can be perceived that coarse steel mesh generally produced a significantly higher open-circuit voltage than fine steel mesh. It is believed that coarse steel mesh can allow more air exchange at the air cathode, thus enhancing the battery performance. The fine steel mesh is 100 mesh screen, which indicates that there will be 100 openings per inch. These fine openings will cause the electrolyte to fill in the openings more easily due to water surface tension and eventually hinder the oxygen flow. This phenomena can reduce the performance of the battery. The hypothesis is supported by Liu *et al.* (2017) as the authors mentioned that the oxygen accessibility will be reduced when the openings of air cathode are penetrated and filled by electrolyte. Coarse steel mesh is a better candidate to be used as the current collector.

Table 4.1 also shows that the addition of PTFE sheet into the air cathode has minimal effect on the battery performance. The open-circuit voltage before and after its integration illustrates minimal differences regardless of the sheet thickness. While the PTFE sheet does not significantly affect the battery output performance, its sole purpose is to contain the electrolyte within aluminium-air

battery. However, it is discovered in the experiment that the separator is capable of fulfilling such feat by absorbing and storing the electrolyte, making the PTFE sheet redundant to be implemented into this battery model.

During the experiment, an electric fan is used to manipulate the air flow around the aluminium-air battery. The air is blown perpendicularly towards the aluminium-air battery prototype but the voltage reading does not change correspondingly. It is inferred that improving the air flow around aluminium-air battery has negligible or no effect on the battery performance.

Pan *et al.* (2019) utilised carbon paper in the air cathode to boost the battery performance. However in our experiment, there is no significant increment in the open-circuit voltage after adding the carbon paper into the prototype. It is suspected that the specification of the carbon paper used in the experiment is not suitable. Since carbon paper has failed to function as an effective catalytic layer, two new catalytic layer candidates are introduced to replace the carbon paper, which are the graphite felt and graphite powder.

The set of materials that resulted in the highest open-circuit voltage is the set with only coarse steel mesh. Hence, the aluminium-air battery model used for further examination will be constructed based on this air cathode setup.

4.2 **Separator Optimisation with Kim's Wipe**

During the experiment, the chemical absorbent paper can perform adequately as a separator. Yet, there are still some flaws noticeable at the graph and the surface of used aluminium anode. Referring to Figure 4.2, the battery model with chemical absorbent paper has produced a graph with fluctuations along the line.
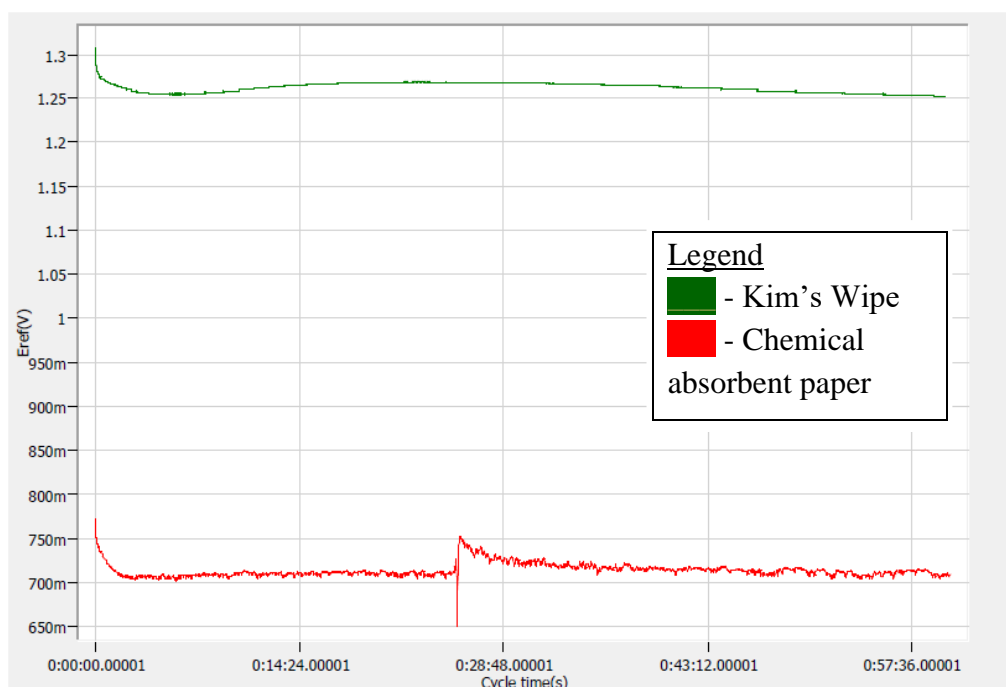
Figure 4.2: Graph Stability Performance of Different Separator.

In addition, the dimple patterns on the chemical absorbent paper have caused the reaction to divert from the area below the dimple spot as the electrolyte can hardly access that area. As a result, numerous spots of un-reacted aluminium can be observed as circled in Figure 4.3. Although the Crisben Company claims their product would have no lint fall even after reaching absorption saturation (section 3.2.1), lint residues of chemical absorbent paper is found to adhere onto aluminium anode, especially the region near the dimple pattern as depicted in Figure 4.1. One possible inference is that electrochemical activity in aluminium-air battery can dissociate the chemical absorbent paper.

Figure 4.3: Used Aluminium Anode with Chemical Absorbent Paper as Separator.

Hence, Kim's Wipe has emerged to be a substitution candidate for the chemical absorbent paper. Kim's Wipe, also known as Kimtech science wipes, is a kind of high quality tissue that is widely used for precise and sensitive tasks such as cleaning lab instruments. It is made out of 100% virgin wood fibre for purity and its water absorbance capacity is 18% stronger than other private label wipers. It also excels in low lint properties so that there will be less accumulation of impurity on aluminium anode (Kimtech Science, n.d.).

The integration of Kim's Wipe as a separator has generated a smoother graph, thus achieving a relatively stable discharge for the battery as illustrated in Figure 4.2. The surface of the used aluminium anode with Kim's Wipe as separator is displayed in Figure 4.4. By comparing Figure 4.3 and Figure 4.4, it can be grasped that the anode reaction with Kim's Wipe is more evenly distributed and there exists less lint residue on the anode as compared to the chemical absorbent paper.

Figure 4.4: Used aluminium anode with Kim's wipe as separator.

During the experiment, another weakness in the chemical absorbent paper is discovered. It is observed that the absorbent paper requires more time than Kim's Wipe to absorb the liquid electrolyte, and there is even leakage from the side because it is not as absorptive as Kim's Wipe. Unlike Kim's Wipe, chemical absorbent paper tends to have unevenly distributed electrolyte, which causes the anode reaction to be focused at the centre as shown in Figure 4.3.

Although this issue can be mitigated by adding more electrolyte to ensure the whole absorbent paper is filled with electrolyte, it proves to be inefficient as more electrolyte is needed to cover the reactive area. In fact, 15ml of electrolyte is used in the chemical absorbent paper battery model to produce the surface in Figure 4.3, while only 8ml of electrolyte is used in the Kim's Wipe to produce the result at Figure 4.4. From these observations, Kim's Wipe is confirmed to replace chemical absorbent paper as separator for the rest of the experiment.

4.3   Open-circuit Voltage Analysis

The open-circuit voltage of the aluminium-air battery in 4M KOH solution is monitored for 2 hours. Figure 4.5 depicts the open-circuit voltage of pure aluminium and alloy 6063 anode aluminium air battery.
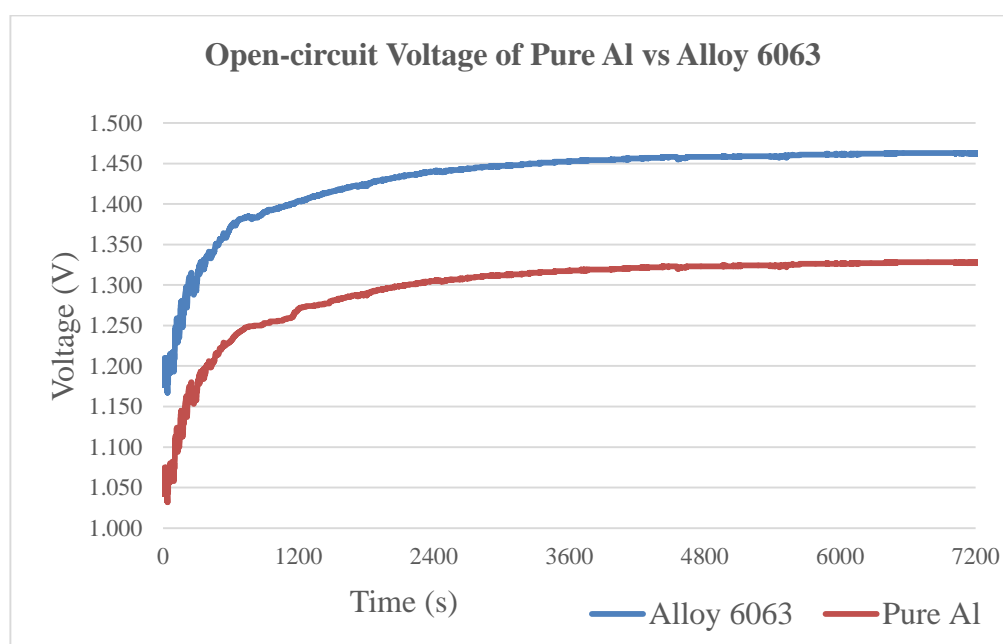
Figure 4.5: Open-circuit voltage of aluminium-air battery with pure aluminium and alloy 6063 as anode.

Open-circuit voltage measures the free potential difference between working and reference electrodes when there is no external current flow. From Figure 4.5 , alloy 6063 has resulted in a higher open-circuit voltage than pure aluminium. The starting open-circuit voltage of pure aluminium is 1.05 V, while alloy 6063 started at 1.16 V. Both anode materials experience a sharp increase at the beginning 20 minutes of the test and eventually slow down and gradually reach a steady voltage value. After 2 hours, pure aluminium achieved 1.326 V and alloy 6063 is 10.3 % higher at 1.461 V, which is still far from theoretical 2.7 V. Neburchilov and Zhang (2016) mentioned that practical aluminium electrode operates at significantly lower potential because aluminium undergoes parasitic corrosion reaction, and the metal is not fully utilised.

The achieved OCV resulted from pure aluminium anode is slightly superior to the aluminium-air battery built by Avoundjian, Galvan and Gomez (2017) using pure aluminium anode, carbon cathode and 1.5M KOH electrolyte that can produce 1.27 V open-circuit voltage. However for alloy 6063, the achieved voltage is not as satisfactory as the aluminium-air battery constructed by Hu *et al.* (2019) that can produce 1.81 V open-circuit voltage in 1 hour. Their battery is made of aluminium alloy, 4M KOH electrolyte, carbon paper catalyst, copper mesh and foam nickel as the cathode electrode.

The underachieving voltage is probably due to lack of effective electrocatalyst for ORR as Neburchilov and Zhang (2016) stated that ORR is one of the limiting factors of metal-air battery in discharging. Therefore, an effective catalyst ought to be invested and the candidates are graphite felt and graphite powder.

4.4　　Effects of Different Catalysts and Anode Materials

4.4.1　　Constant Current Discharge Test

In this test, the discharge characteristic of 6 cm $\times$ 6 cm aluminium anodes are tested with graphite felt and graphite powder, accompanied by a control set without using catalyst. The test ran for 1 hour at 10 mA current discharge.

4.4.1.1　　Control Set (without catalyst)

Figure 4.6 displays the discharge curve of pure aluminium and alloy 6063 control set.
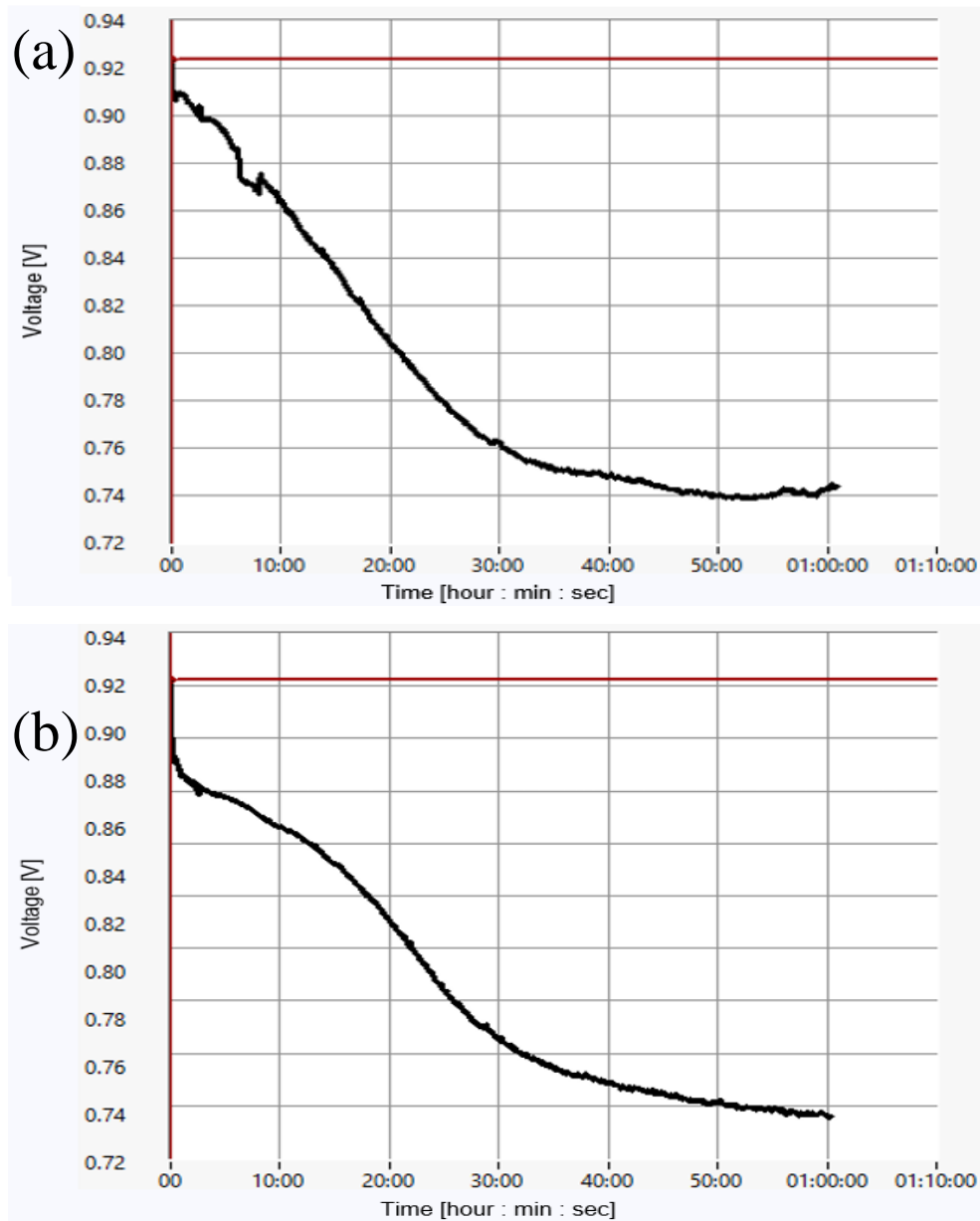
Figure 4.6: Control Set with (a) Pure Aluminium and (b) Alloy 6063.

Pure aluminium begins to discharge at 0.92 V, the discharge is essentially unstable at the beginning and eventually enters an almost linear decrement from the 10 minutes to 30 minutes mark. Alloy 6063 initial discharge voltage is 0.90 V, the discharge is relatively stable as the fluctuations along the graph is less apparent. Unlike pure aluminium, alloy 6063 encounters the voltage drop with increasing gradient from 5 minutes to 30 minutes of discharge. Both anode materials exhibit a similar characteristic such that the voltage decreases significantly for the first 30 minutes and gradually flattens after 30 minutes of discharging, and finally reaching 0.74 V after 1 hour of discharge.

4.4.1.2   Graphite Felt

Next, graphite felt is added as catalytic layer to the aluminium-air battery. The results are illustrated in Figure 4.7.
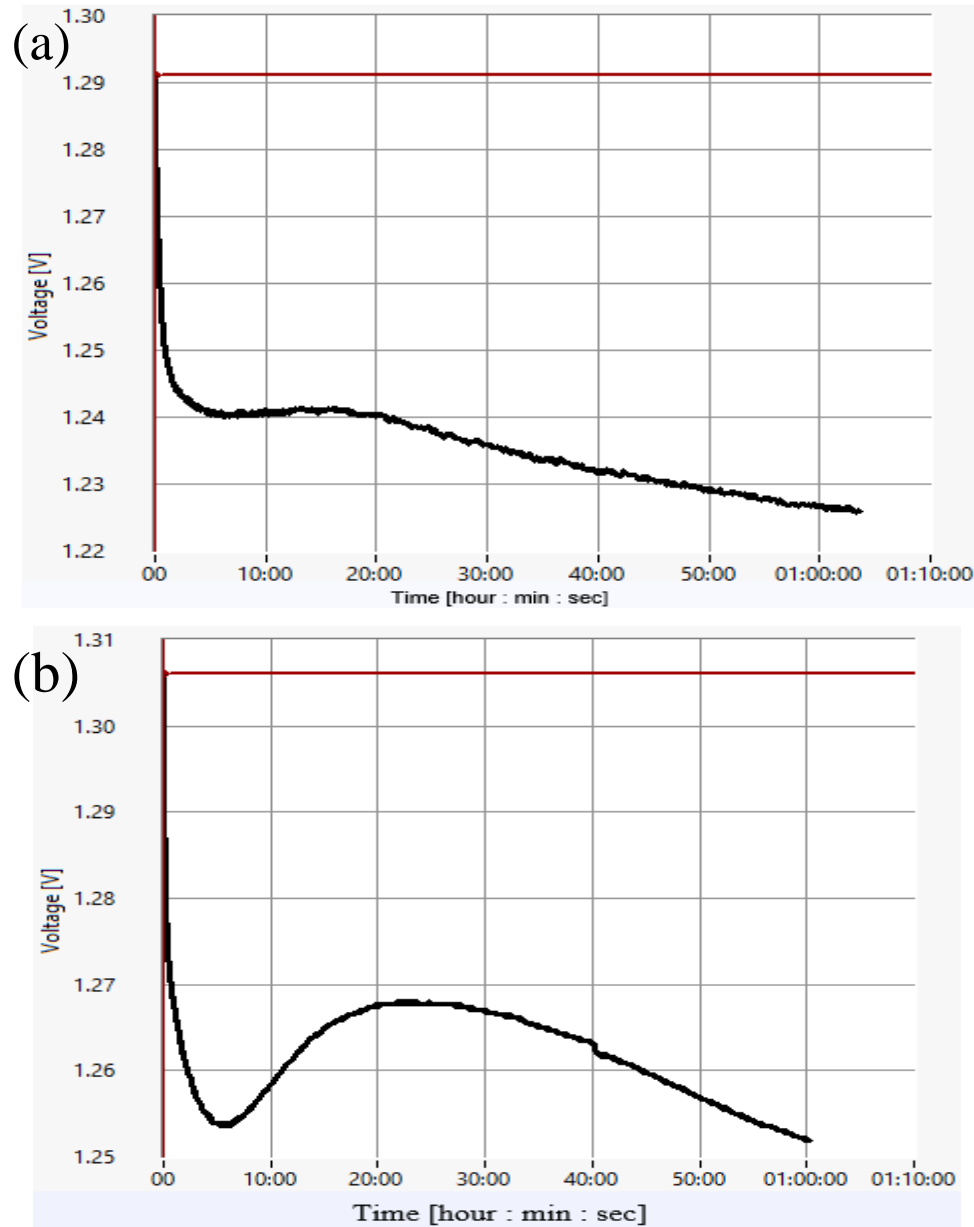
Figure 4.7: Graphite Felt set with (a) Pure aluminium and (b) Alloy 6063.

Referring to Figure 4.7, pure aluminium began the discharge with a dip to 1.24 V and maintained its voltage from 5 minutes to 20 minutes. After that, the voltage enters a linear decrement pattern similar to its control set. The control set came across the linear decrement pattern at approximately 10 minutes mark, while the graphite felt had delayed the occurrence to 20 minutes

after discharging. The linear decrement pattern ends at the 30 minutes mark for the control set while the graphite felt experiment set lasts for the rest of the experiment period after its initiation at 20 minutes. The pure aluminium anode with graphite felt reaches 1.227 V after 1 hour of discharge, which is 0.487 V and 65 % higher than the control set (0.74 V). The graphite felt has improved the initial discharge voltage from 0.92 V by 35 %, reaching 1.24 V.

The starting discharge pattern of alloy 6063 after adding graphite felt is analogous to a damped oscillation system. The voltage of alloy 6063 dipped to 1.255 V after 5 minutes and then surged to a peak of 1.268 V after 25 minutes of discharge. Subsequently, the voltage decreases gradually and reaches 1.253 V after 1 hour of discharge, which is 0.513 V higher than control set (0.74 V), yielding 69 % improvement in final discharge voltage. The voltage drop over the discharge period is minimal at 15 mV with referenced to the peak voltage. The discharge pattern of graphite felt implemented alloy 6063 battery is rather unique as it is the only set with a substantial voltage increase during the discharge process. The graphite felt has successfully improved the initial discharge voltage from 0.9 V by 41 % to 1.268 V. Graphite felt can help to reduce the voltage drop over the discharge period.

4.4.1.3 Graphite Powder

Figure 4.8 depicts the discharge curve of aluminium-air battery that utilises graphite powder as catalysts.

(a)
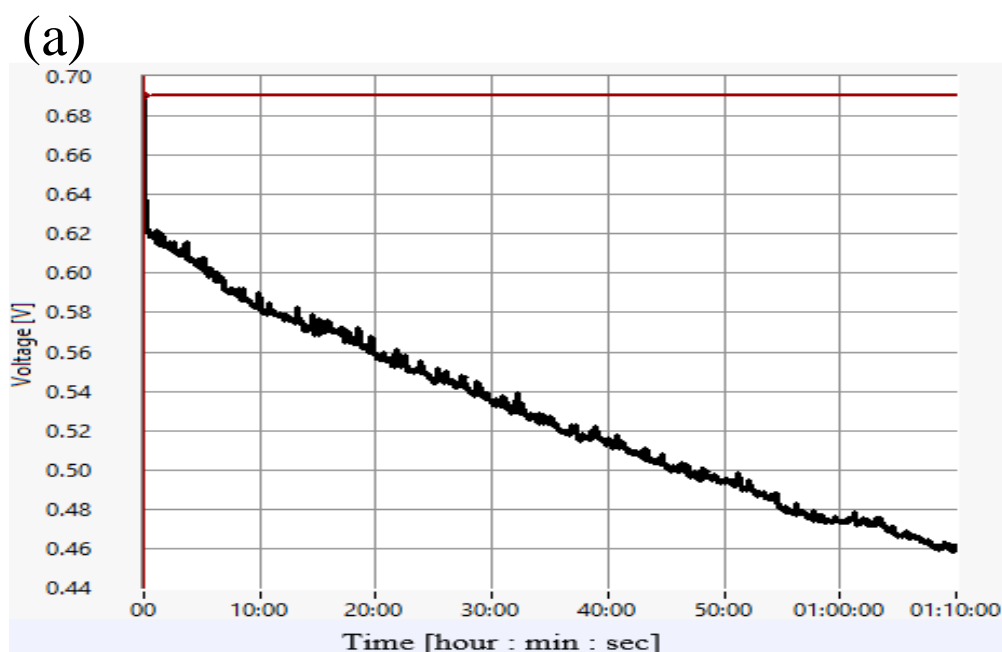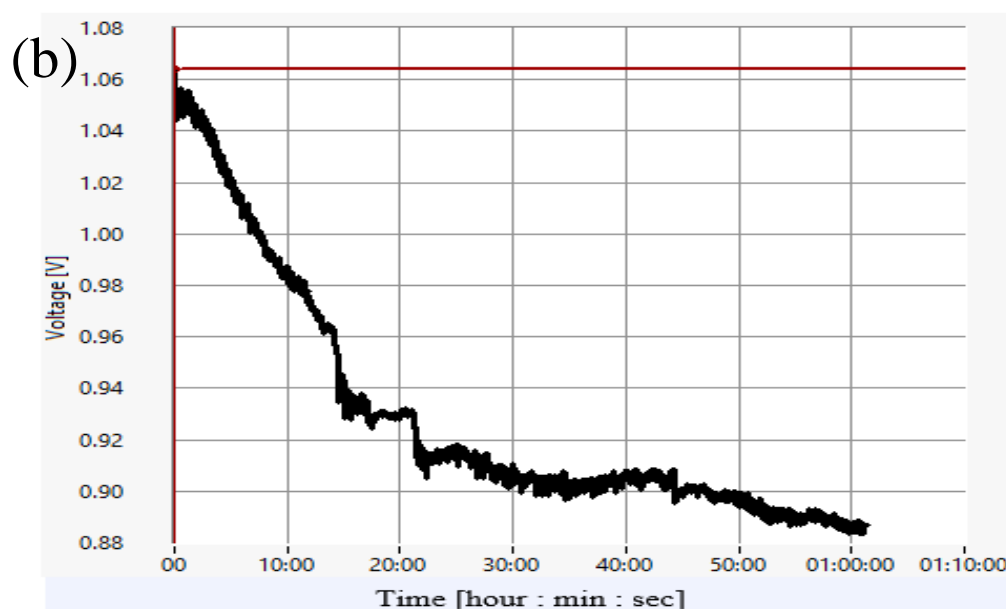
Figure 4.8: Graphite Powder set with (a) Pure Aluminium and (b) Alloy 6063.

The addition of graphite powder to pure aluminium anode battery has led to disastrous results as shown in Figure 4.8. Not only that the discharge becomes less stable due to greater fluctuation in the discharge curve, it also causes the battery to discharge at a lower voltage than the control set. The initial discharge voltage has decreased by 32 % from 0.91 V to 0.62 V and the final discharge voltage has decreased by 35 % from 0.74 V to 0.478 V after adding graphite powder. The discharge decreases with constant gradient from the beginning to the end of test. Such behaviour contradicts what Mckerracher *et al.* (2019) has mentioned, that graphite powder is beneficial in improving the battery discharge performance. The reason for the differences is not clear.

On the other hand, the initial discharge voltage of alloy 6063 has increased 14 % to 1.05 V after adding graphite powder. The final discharge voltage improved 20 % from 0.74 V to 0.89 V after adding graphite powder. Despite the benefit of improved discharge voltage, discharge stability of alloy 6063 is disrupted as the fluctuation remained throughout the graph. Both the aluminium anodes after adding graphite powder are susceptible to heavier voltage fluctuation. It is suspected that the graphite powder is not adequately soluble in the electrolyte as demonstrated in Figure 4.9. This causes detrimental effects on the gaseous exchange process because the openings of steel mesh seems to be obstructed with the mixture of graphite powder and electrolyte.
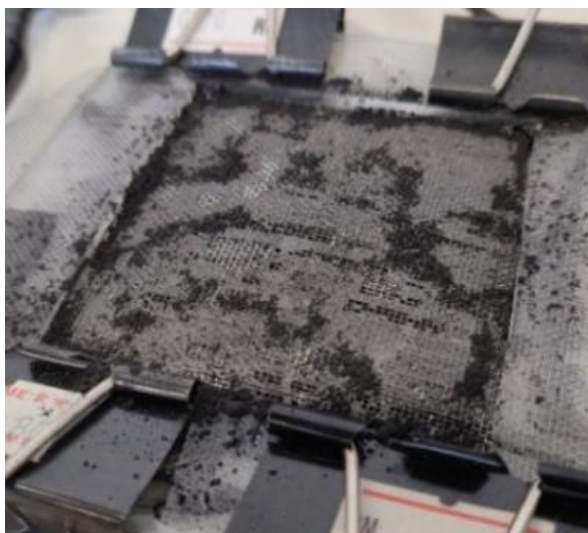
Figure 4.9: Obstructed Steel Mesh Opening after adding Graphite Powder.

4.4.1.4   Discussion – Constant Current Discharge Test

Table 4.2 compiles and records the data for constant current discharge test with different catalysts and anode materials.

Table 4.2: Result Overview for Constant Current Discharge Test.

	Control set		Graphite Felt		Graphite Powder	
	Pure Al	6063	Pure Al	6063	Pure Al	6063
Initial Discharge Voltage	0.920 V	0.900 V	1.240 V (+35 %)	1.268 V (+41 %)	0.620 V (-32 %)	1.05 V (+14 %)
Final Discharge Voltage	0.740 V	0.740 V	1.227 V (+65 %)	1.253 V (+69 %)	0.478 V (-35 %)	0.89 V (+20 %)
Voltage Drop	180 mV	160 mV	13 mV	15 mV	142 mV	160 mV

From this constant current discharge test, it is found that alloy 6063 generally results in higher discharge voltage than pure aluminium. Other than that, it is clear that graphite felt is more superior to graphite powder in terms of improving the discharge voltage and maintaining the discharge stability. Furthermore, aluminium-air battery with graphite felt sustained 13 ~ 15 mV voltage drop with respect to the peak voltage after discharging for 1 hour, which makes it functional as battery. Hence, the following experiments were carried out using graphite felt as the catalyst to further examine the effect of graphite felt on KOH-based aluminium-air battery.

From this experiment, the operating voltage is noticed to decrease rapidly in the early discharging stage and subsequently reaches an approximate constant value. Neburchilov and Zhang (2016) clarified that this occurrence is caused by the battery internal resistance.

Aluminium passivation that occurs on anode surfaces that can affect the discharge patterns in aluminium-air battery. Soler *et al.* (2005) investigated the reaction between aluminium with KOH solution and stated that the decrease in hydrogen evolution rate over time was contributed by aluminium passivation. Aluminium passivation occurs when a thin surface layer of aluminium oxide is formed, which creates a physical barrier to corrosion or further oxidation.

This provided insight that aluminium passivation occurs as a result of chemical reaction between aluminium and KOH solution, which causes the aluminium anode surface to become less reactive as more $Al(OH)_3$ is produced, and the diffusion path for oxygen becomes longer and the reaction is slowed down (Håkansson et al., 2017). It can slow down anode reaction and reduce battery discharge voltage over time. It eventually causes the battery to wear out due to the accumulation of aluminium hydroxide on anode (Pino et al., 2015). The occurrence of aluminium passivation is verified later in EDX analysis.

4.4.2   Tafel Plot
4.4.2.1   Pure Aluminium Results and Calculations

Figure 4.10 expresses the differences in Tafel plot before and after integrating graphite felt into pure aluminium anode aluminium-air battery.
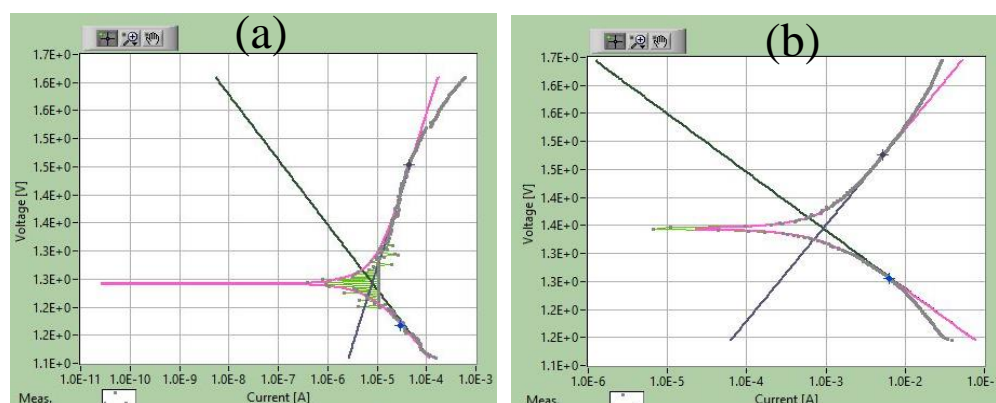
Figure 4.10: Tafel plot of Pure Aluminium anode Battery set (a) before and (b) after adding Graphite Felt catalyst.

Based on Figure 4.10(a), Tafel plot without catalyst demonstrated a relatively noisy curve, especially at the region near E_{corr}. This can be observed as the green lines that connect the preceding and succeeding data points had filled up the near E_{corr} region. There are some discontinuities notable at the anodic slope end at 1×10^{-4} A. After adding graphite felt, the fluctuation in the graph is effectively smoothened as depicted in Figure 4.10(b). With the aid of IVMAN Tafel Analysis feature, the parameters before and after adding graphite felt are obtained as shown in Figure 4.11. The anodic slope is represented by b_a, while the cathodic slope is b_c.

Figure 4.11: Tafel analysis result of Pure Aluminium anode battery set (a) before and (b) after adding Graphite Felt catalyst.

The corrosion current obtained in Figure 4.11 is used to determine the corrosion rate of aluminium anode. The aluminium molecular weight, M is 26.981 u. The number of electrons involved in the electrochemical reaction at aluminium anode is 3, given that 3 electrons are released from the formation of aluminium ions as shown below.

$$Al \rightarrow Al^{3+} + 3e^- \tag{4.9}$$

Given that $E.W. = \dfrac{M}{n}$,

$$E.W. = \frac{26.981\ \text{u}}{3} = 8.94\ \text{u}$$

Equation (4.7) is used to calculate the penetration rate of aluminium anode before and after adding graphite felt. The required parameters and their corresponding values are:

I_{corr} before adding graphite felt	$I_{corr,before}$	$= 8.115\ \mu A$
I_{corr} after adding graphite felt	$I_{corr,after}$	$= 922.369\ \mu A$
Equivalent Weight	$E.W.$	$= 8.94\ \text{u}$
Aluminium density	ρ	$= 2.7\ g/cm^3$
Anode reactive area	A	$= 36\ cm^2 = 0.36\ dm^2$

<u>Penetration rate</u>

$$C.R._{before}\ (mm/year) = 0.003272\ \frac{i_{corr} \times E.W.}{\rho A}$$

$$= 0.003272\ \frac{8.115 \times 8.94}{2.7 \times 36}$$

$$= \mathbf{2.442 \times 10^{-3}\ mm/year}$$

$$C.R._{after}\ (mm/year) = 0.003272\ \frac{i_{corr} \times E.W.}{\rho A}$$

$$= 0.003272\ \frac{922.369 \times 8.94}{2.7 \times 36}$$

$$= \mathbf{0.2776\ mm/year}$$

The percentage change of each measured parameters is calculated using formula:

$$Percentage\ change = \frac{Final\ value - Initial\ value}{Initial\ value} \times 100\ \% \qquad (4.10)$$

$$Percentage\ change\ of\ E_{corr}\ = \frac{1.345 - 1.242}{1.242} \times 100\ \% \qquad = \mathbf{8.3}\ \%$$

$$Percentage\ change\ of\ I_{corr}\ = \frac{922.369 - 8.115}{8.115} \times 100\ \% \qquad = \mathbf{11266}\ \%$$

$$Percentage\ change\ of\ b_a\ = \frac{171 - 276}{276} \times 100\% \qquad = \mathbf{-38}\ \%$$

$$Percentage\ change\ of\ b_c\ = \frac{105 - 116}{116} \times 100\ \% \qquad = \mathbf{-9}\ \%$$

$$Percentage\ change\ of\ C.R.\ = \frac{0.2776 - 2.442 \times 10^{-3}}{2.442 \times 10^{-3}} \times 100\ \% = \mathbf{11262}\ \%$$

$$Percentage\ change\ of\ R_p.\ = \frac{30.5 - 4359}{4359} \times 100\ \% \qquad = \mathbf{-99.3}\ \%$$

The experiment results for pure aluminium anode aluminium-air battery are documented in Table 4.3.

Table 4.3: Effect of Graphite Felt on Pure Aluminium anode Aluminium-air Battery.

Parameters	Before adding graphite felt	After adding graphite felt	Percent change
E_{corr}	1.242 V	1.345 V	8.3 %
I_{corr}	8.115 µA	922.369 µA	11266 %
Anodic slope, b_a	276 mV/decade	171 mV/decade	-38 %
Cathodic slope, b_c	116 mV/decade	105 mV/decade	-9 %
Corrosion rate, C.R.	2.442×10^{-3} mm/year	0.2776 mm/year	11262 %
Polarization resistance, R_p	4359	30.5	-99.3 %

4.4.2.2 Alloy 6063 Results and Calculations

Figure 4.12 compares the differences in Tafel plot before and after integrating graphite felt into alloy 6063 anode aluminium-air battery.
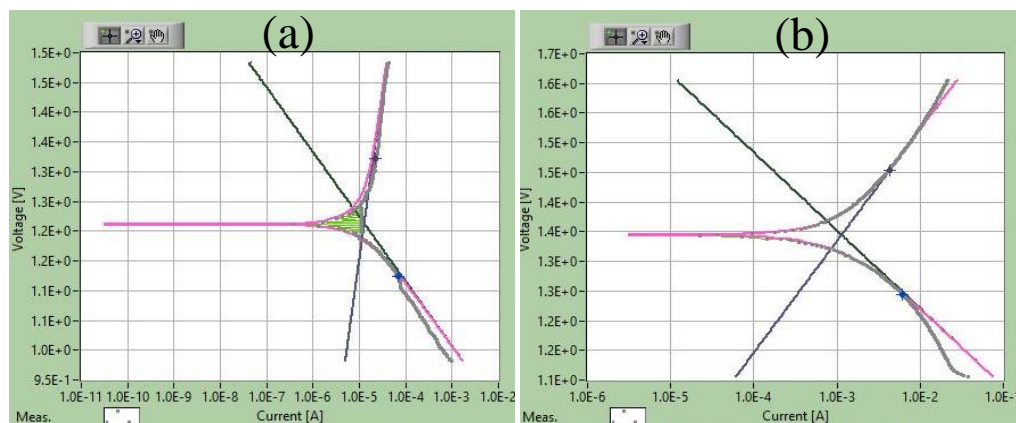

Figure 4.12: Tafel plot of Alloy 6063 anode Battery set (a) before and (b) after adding Graphite Felt catalyst

Referring to Figure 4.12, it can be observed that the Tafel plot of alloy 6063 without catalyst presented an identical trait as the pure aluminium anode without catalyst. They both share the same noisy curve characteristics near the

E_{corr} region. Furthermore, a sudden surge can be perceived at the cathodic slope around 1×10^{-4} A. Adding graphite felt into alloy 6063 anode aluminium-air battery had induced a smoothening effect on the Tafel graph. The other performance parameters before and after adding graphite felt into alloy 6063 anode battery are analysed with IVMAN software and recorded in Figure 4.13.
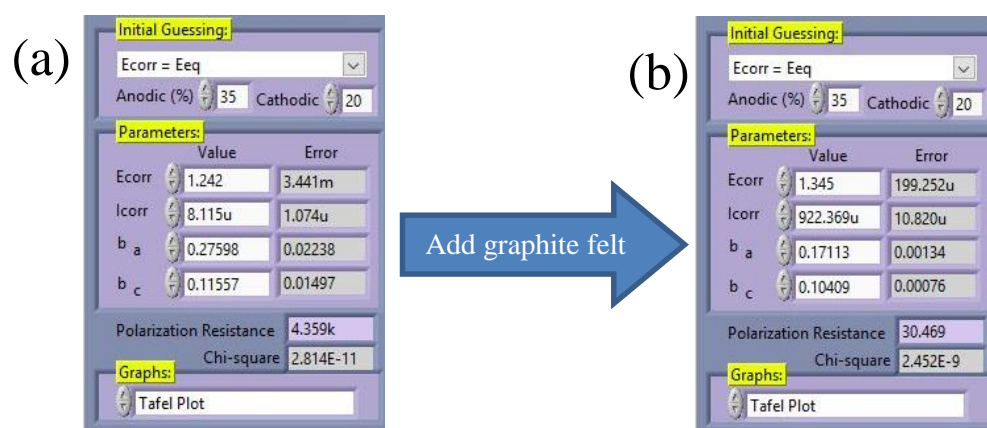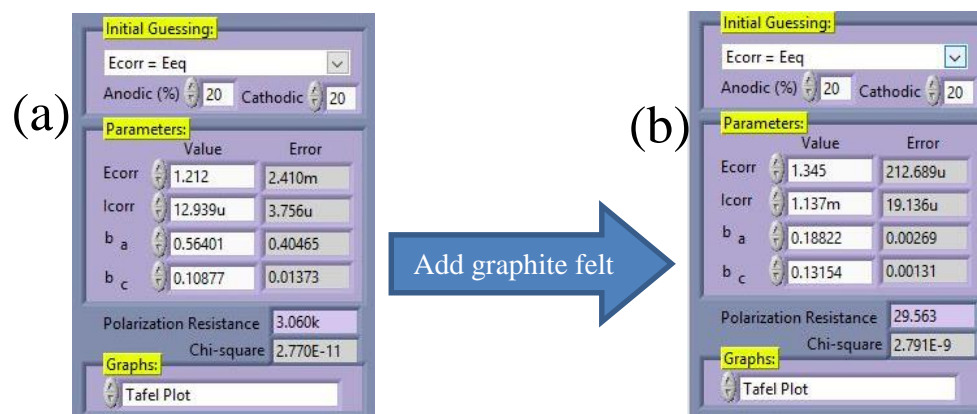

Figure 4.13: Tafel analysis result of Alloy 6063 anode Battery set (a) before and (b) after adding Graphite Felt catalyst.

Akin to the calculation for pure aluminium anode battery set, the alloy 6063 corrosion rate is computed using corrosion current obtained in Figure 4.13. Equation (4.7) is used to calculate the corrosion rate of alloy 6063 anode before and after adding graphite felt. The required parameters are:

I_{corr} before adding graphite felt	$I_{corr,before}$	$= 12.939 \ \mu A$
I_{corr} after adding graphite felt	$I_{corr,after}$	$= 1137 \ \mu A$
Equivalent Weight	$E.W.$	$= 8.94 \ u$
Aluminium density	ρ	$= 2.7 \ g/cm^3$
Anode reactive area	A	$= 36 \ cm^2$

$$C.R._{before} \ (mm/year) = 0.003272 \ \frac{i_{corr} \times E.W.}{\rho A}$$

$$= 0.003272 \ \frac{12.939 \times 8.94}{2.7 \times 36}$$

$$= \mathbf{3.894 \times 10^{-3} \ mm/year}$$

$$C.R._{after}\ (mm/year) = 0.003272\ \frac{i_{corr} \times E.W.}{\rho A}$$

$$= 0.003272\ \frac{1137 \times 8.94}{2.7 \times 36}$$

$$= \boldsymbol{0.3422\ mm/year}$$

The percentage change of each parameter is calculated using equation (4.10).

$Percentage\ change\ of\ E_{corr}\ = \frac{1.345 - 1.212}{1.212} \times 100\ \%\qquad = \boldsymbol{11}\ \%$

$Percentage\ change\ of\ I_{corr}\ = \frac{1137 - 12.939}{12.939} \times 100\ \%\qquad = \boldsymbol{8687}\ \%$

$Percentage\ change\ of\ b_a\qquad = \frac{188 - 564}{564} \times 100\%\qquad = \boldsymbol{-67}\ \%$

$Percentage\ change\ of\ b_c\qquad = \frac{131 - 109}{109} \times 100\ \%\qquad = \boldsymbol{20}\ \%$

$Percentage\ change\ of\ C.R.\ = \frac{342.2 - 3.894}{3.894} \times 100\ \%\qquad = \boldsymbol{8688}\ \%$

$Percentage\ change\ of\ R_p.\qquad = \frac{29.6 - 3060}{3060} \times 100\ \%\qquad = \boldsymbol{-99.0}\ \%$

The experimental results for alloy 6063 anode are documented in Table 4.4.

Table 4.4: Effect of Graphite Felt on Alloy 6063 anode Aluminium-air Battery.

Parameters	Before adding graphite felt	After adding graphite felt	Percent change
E_{corr}	1.212 V	1.345 V	11 %
I_{corr}	12.939 μA	1.137 mA	8687 %
Anodic slope, b_a	564 mV/decade	188 mV/decade	-67 %
Cathodic slope, b_c	109 mV/decade	131 mV/decade	20 %
Corrosion rate, C.R.	3.894×10^{-3} mm/year	0.3422 mm/year	8688 %
Polarization resistance, R_p	3060	29.6	-99 %

4.4.2.3 Discussion – Tafel Plot

The results for the Tafel plot test with pure aluminium anode and alloy 6063 anode are compiled and compared in Table 4.5.

Table 4.5: Result overview of Tafel plot.

Parameters	Before adding graphite felt		After adding graphite felt		Percent change	
	Pure Al	6063	Pure Al	6063	Pure Al	6063
E_{corr}, V	1.242	1.212	1.345	1.345	8.3 %	11 %
I_{corr}, µA	8.115	12.939	922.369	1137	11266 %	8687 %
b_a, mV/dec	276	564	171	188	-38 %	-67 %
b_c, mV/dec	116	109	105	131	-9 %	20 %
C.R., mm/year	2.442×10^{-3}	3.894×10^{-3}	0.2776	0.3422	11262 %	8687 %
R_p, Ω	4359	3060	30.5	29.6	-99.3 %	-99 %

Corrosion potential, E_{corr} also represents the open-circuit voltage of the aluminium anode. From Table 4.5, pure aluminium anode has slightly higher E_{corr} than alloy 6063. By installing the graphite felt, the E_{corr} of pure aluminium increased 8.3 % while alloy 6063 increased 11.3 %. Both of them reach the same OCP value at 1.345 V *vs* SHE. The achieved open-circuit voltage in this experiment is much lower than previous section 4.3 that achieved 1.461 V for alloy 6063 and 1.326 V for pure aluminium without catalyst. Since the Tafel plot takes only 8 minutes, it could be that the aluminium-air battery are still in the sharp increase phase as observed previously in open-circuit voltage analysis in section 4.3, which means that the aluminium-air battery is not performing at its peak steady-state open-circuit voltage.

Additionally, it is found that the stainless steel mesh is corroded after using it for so many times. The stainless steel mesh has turned yellowish at the reactive area, it no longer has its shiny appearances. It is inferred that the corroded current collector has negatively affected the open-circuit voltage of the battery. The hypothesis is verified with a simple test using multimeter. The open-circuit voltage of aluminium-air battery with old stainless steel mesh is measured and compared with the one with new stainless steel mesh. It is found that the new stainless steel mesh has resulted in higher open-circuit voltage

(1.514 V) than used stainless steel mesh (1.348V). One possible inference is that the corroded current collector has higher electrical resistance thus reduces the voltage. However, redo of the experiment with the new stainless steel mesh is forbidden with the university closure due to COVID-19 outbreak.

The corrosion rate for pure aluminium and alloy 6063 before adding graphite felt is 2.442 μm/y and 3.894 μm/y respectively, showing that alloy 6063 corrodes 60% faster than pure aluminium. When the graphite felt is added, the corrosion rate increases 11266 % for pure aluminium and 8687 % for alloy 6063, yielding 0.2776 mm/y and 0.3422 mm/y respectively. Based on a study conducted by Prabhu and Rao (2017), the corrosion rate of alloy 6063 in 0.5M NaOH solution at 20 ℃ is 49.59 mm/y and the corresponding I_{corr} is 4.55 mA/cm^2. Both KOH and NaOH solutions are the most chemically similar of the hydroxides and are almost interchangeable (Chambers, 2012). This experiment used a more concentrated alkaline than the authors, yet the resultant corrosion rate is around 150 times lesser than the result from the authors. The experimental result is suspicious as higher concentration of alkaline should result in greater corrosion rate as concluded by Prabhu and Rao (2017). Therefore, it is suspected that there are some errors when obtaining the I_{corr}.

Xia *et al.* (2020) state that Tafel slope determines the rate of electron transfer during the OER/ORR process. The anodic slope, b_a was initially very high at 276 mV/dec for pure aluminium and 564 mV/dec for alloy 6063. Chu and Savinell (1991) found that the Tafel slope for aluminium dissolution in 5 M KOH electrolyte were 570 mV/decade. Graphite felt had successfully reduced the anodic slope to 171 mV/dec and 188 mV/dec respectively, which indicates that graphite felt is effective for OER catalytic activity. It also means that less overpotential is required to achieve higher current density.

According to Toshev *et al.* (2006), polarization resistance is defined as the resistance of the specimen to oxidation during the application of an external potential. Table 4.5 shows that graphite felt had effectively reduced the polarization resistance up to 99 %, thus allowing oxidation to occur more easily at the anode and eventually improves the battery discharge performance.

Pure aluminium has lower I_{corr} than alloy 6063 before and after adding graphite felt. The calculated corrosion rate based on I_{corr} shows that pure

aluminium is more corrosion resistance than alloy 6063. The compositions of alloy 6063 are shown in Table 4.6.

Table 4.6: Composition of Aluminium Alloy 6063 (Prabhu and Rao, 2017).

Element		Composition (% by weight)
Silicon	Si	0.412
Iron	Fe	0.118
Copper	Cu	0.057
Magnesium	Mg	0.492
Aluminium	Al	Balance

Aluminium alloy 6063 is composed of several elements, mainly Si and Mg. Sukiman *et al.* (2011) states that the addition of silicon and magnesium in 6xxx series aluminium alloys allows the precipitation of Mg_2Si particles beneficial in terms of increasing strength but renders the alloy prone to localised corrosion, while the excess amount of silicon may also lead to intergranular corrosion and stress corrosion cracking. It is also supported by Katsoufis *et al.* (2020) as the authors said that common aluminium alloys corrode faster than pure aluminium due to the presence of Mg_2Si grains that promotes corrosion. In addition, impurities present in alloy 6063 such as Fe and Si is known to accelerate corrosion (Nestoridi, 2008). The result shows that alloy 6063 is 60 % more vulnerable to self-corrosion issue than pure aluminium.

4.4.3 Capacity Test with Reduced Anode Size

In this test, the capacity of the graphite felt integrated aluminium-air battery is tested by allowing aluminium anode with 1.5 cm ×1.5 cm reactive area to fully discharge under constant 10 mA and 20 mA current flow. Hence, the current density for this test is 4.444 mA/cm^2 and 8.889 mA/cm^2. The mass loss after the discharge is measured. The resulting capacity is compared between pure aluminium and alloy 6063 air battery. Figure 4.14 demonstrates the discharge curve of aluminium-air battery with pure aluminium and graphite felt.
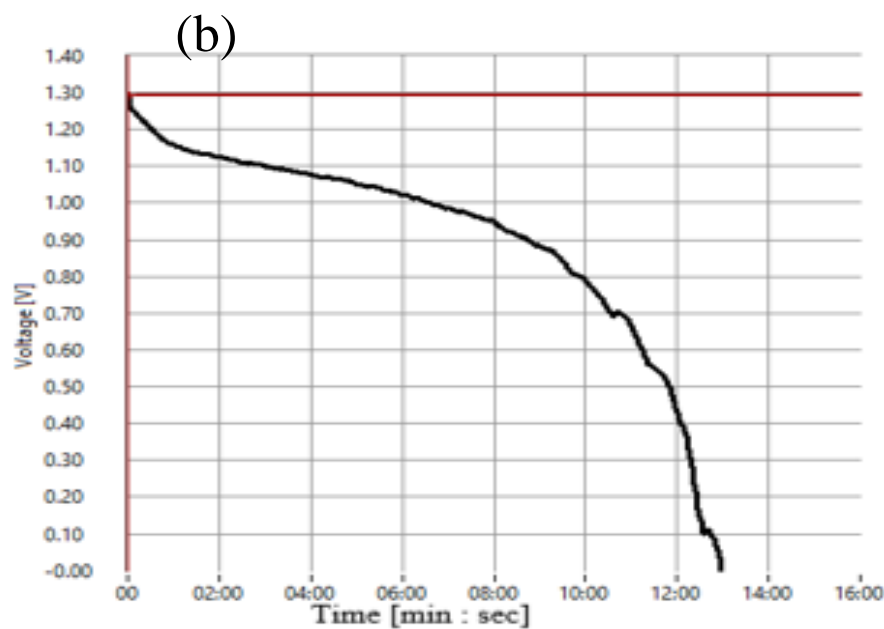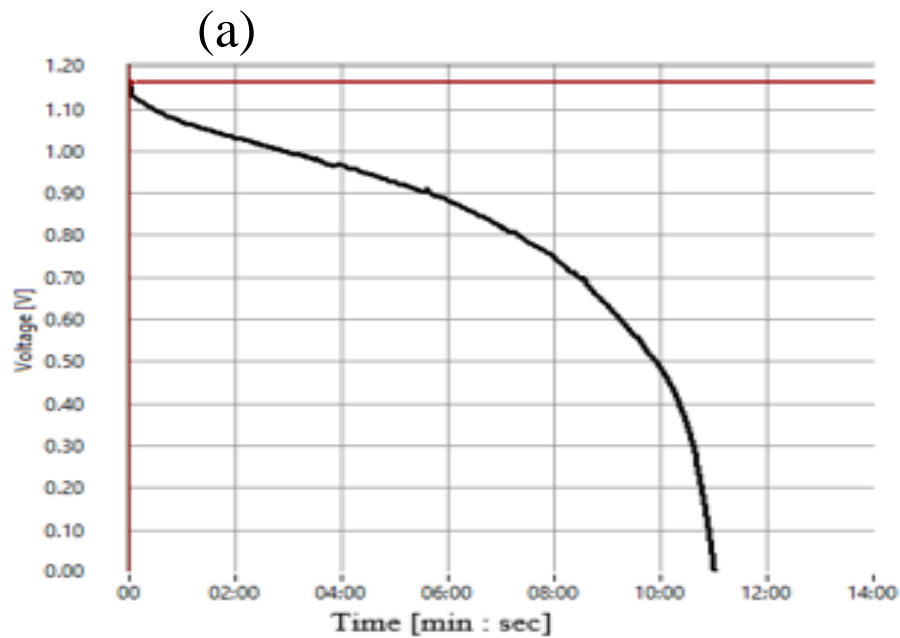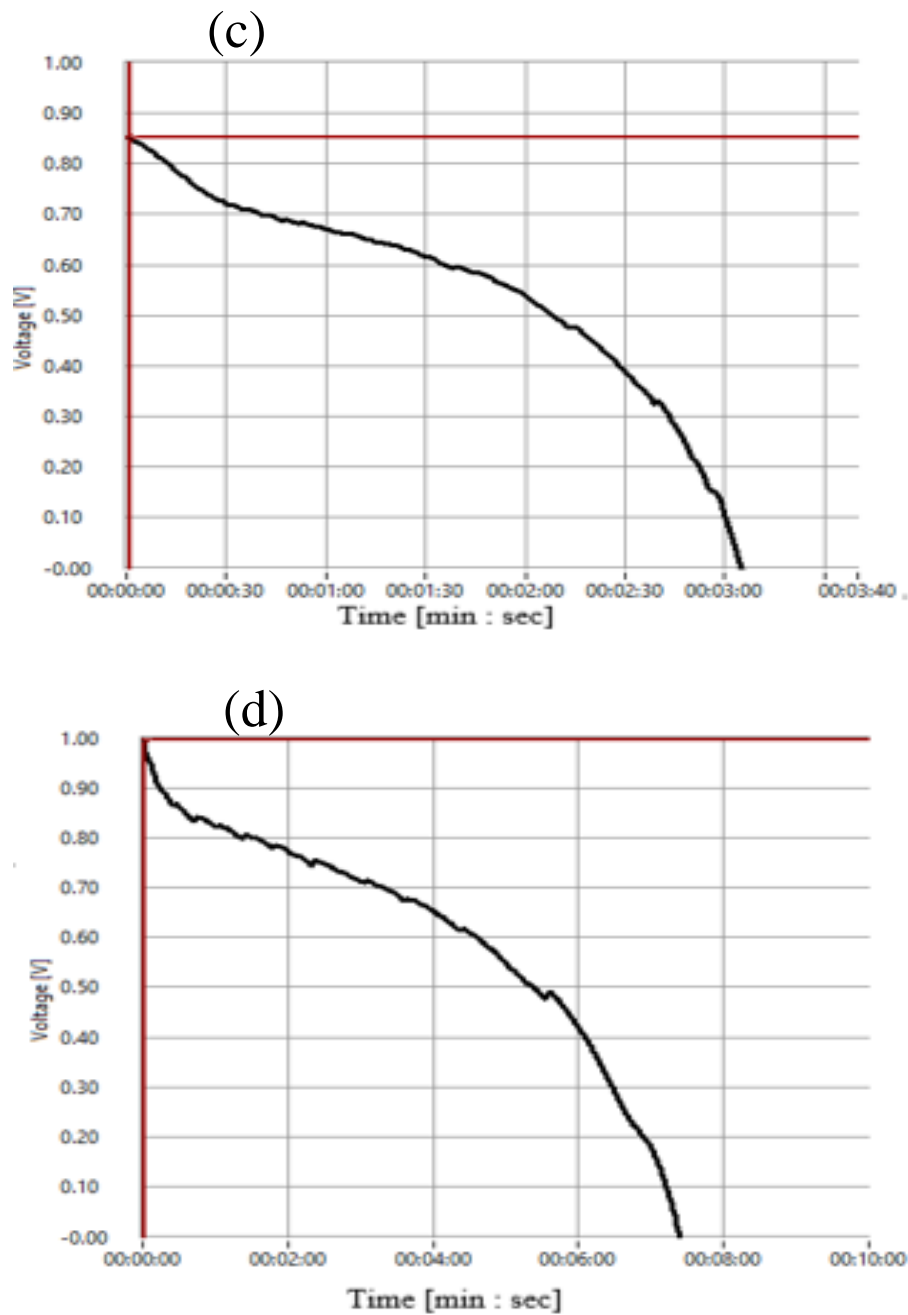
Figure 4.14: Discharge Curve in 4.444 mA/cm² with (a) Pure Aluminium and (b) Alloy 6063; in 8.889 mA/cm² with (c) Pure Aluminium and (d) Alloy 6063.

Table 4.7 recorded all the data collected for this test and the calculation result.

Table 4.7: Result of 1.5 cm $\times$ 1.5 cm anode reactive area test.

	Current density at 4.444 mA/cm^2		Current density at 8.889 mA/cm^2	
	Pure Al	6063	Pure Al	6063
Initial discharge voltage (V)	1.16	1.29	0.85	0.98
Discharge Time	11 m 24 s	12 m 58 s	3 m 4 s	7 m 13 s
Mass Loss (g)	0.016	0.019	0.009	0.014
Capacity (mAh)	1.9	2.161	1.022	2.406
Capacity density (Ah/kg)	118.75	113.74	111.33	**171.86**

The battery capacity is the energy stored in the battery expressed as Amp-hour. The calculations to determine the battery capacity are shown below.

For **4.444 mA/cm^2** (10mA current discharge),

Pure Aluminium

$Capacity = Ampere(A) \times Time(h)$

$$= 0.01\ A \times 11\frac{24}{60} \min\ \times \frac{1hr}{60min}$$

$$= \mathbf{1.9\ mAh}$$

$$Capacity\ density = \frac{Capacity}{Mass}$$

$$= \frac{1.9\ \times 10^{-3} Ah}{0.016 \times 10^{-3}\ kg}$$

$$= \mathbf{118.75\ Ah/kg}$$

Alloy 6063

$Capacity = Ampere(A) \times Time(h)$

$$= 0.01\ A \times 12\frac{58}{60} \min\ \times \frac{1hr}{60min}$$

$$= \mathbf{2.161\ mAh}$$

$$Capacity\ density = \frac{Capacity}{Mass}$$

$$= \frac{2.161 \times 10^{-3} Ah}{0.019 \times 10^{-3}\ kg}$$

$$= \boldsymbol{113.74\ Ah/kg}$$

For **8.889 mA/cm²** (20mA current discharge),

<u>Pure Aluminium</u>

$$Capacity = Ampere(A) \times Time(h)$$

$$= 0.02\ A \times 3\frac{4}{60}\min \times \frac{1hr}{60min}$$

$$= \boldsymbol{1.022\ mAh}$$

$$Capacity\ density = \frac{Capacity}{Mass}$$

$$= \frac{1.022 \times 10^{-3} Ah}{0.009 \times 10^{-3}\ kg}$$

$$= \boldsymbol{111.33\ Ah/kg}$$

<u>Alloy 6063</u>

$$Capacity = Ampere(A) \times Time(h)$$

$$= 0.02\ A \times 7\frac{13}{60}\min \times \frac{1hr}{60min}$$

$$= \boldsymbol{2.406\ mAh}$$

$$Capacity\ density = \frac{Capacity}{Mass}$$

$$= \frac{2.406 \times 10^{-3} Ah}{0.014 \times 10^{-3}\ kg}$$

$$= \boldsymbol{171.86\ Ah/kg}$$

By observing Figure 4.14, it can be perceived that the discharge curve for pure aluminium is relatively smooth while alloy 6063 has minor fluctuations. Alloy 6063 discharge curve has notable voltage increase during the discharge process that is also found in Figure 4.7(b) that shows the discharge curve of similar setup with graphite felt but with larger anode size. All the graphs in

Figure 4.14 encounter sharp voltage drop at the early stage of the discharge due to battery internal resistance as clarified by Neburchilov and Zhang (2016).

From Table 4.7, the initial discharge voltage of alloy 6063 is higher than pure aluminium in both current densities. This observation is consistent with constant current discharge tests that showed alloy 6063 can often deliver higher voltage than pure aluminium. On top of that, alloy 6063 can also last longer than pure aluminium when they are discharging at the same rate. The capacity of alloy 6063 is 14 % greater than pure aluminium at 4.444 mA/cm^2, and 135 % at 8.889 mA/cm^2.

The experiment also realises that the mass loss of alloy 6063 is greater than pure aluminium at both current densities. Hence, the capacity density of alloy 6063 at 4.444 mA/cm^2 is smaller than pure aluminium. It could be a result of greater self-corrosion rate in alloy 6063. At 8.889 mA/cm^2 current density, the capacity density of alloy 6063 is the highest from the test at 171.86 Ah/kg. It is superior to the aluminium-air battery constructed by Martinez *et al.* (2017) using alloy 2024 and air cathode with 0.2 M KOH electrolyte that can achieve 97 Ah/kg at current density of 3.2 mA/cm^2. The authors had invested in alleviating self-corrosion in the anode by using less concentrated alkaline as the electrolyte, which eventually sacrificed other battery performance such as the capacity density.

From the capacity test, the best performing aluminium anode in air battery is alloy 6063 at 8.889 mA/cm^2 current density. The battery is capable of achieving capacity of 2.406 mAh with only 2.25 cm^2 anode size, and has a capacity density of 171.846 Ah/kg.

4.5   Double Cathode Aluminium-air Battery

The reactive area is doubled by involving both sides of the aluminium anode in the reaction. Two air positive cathodes are prepared for each side of the aluminium anode, thus it requires two sets of graphite felt, Kim's wipe, and current collector. The current discharge is set at 10mA and the samples are allowed to run for 1 hour and its outcome is depicted in Figure 4.15. The mass loss of the aluminium anode is measured and recorded in Table 4.8.
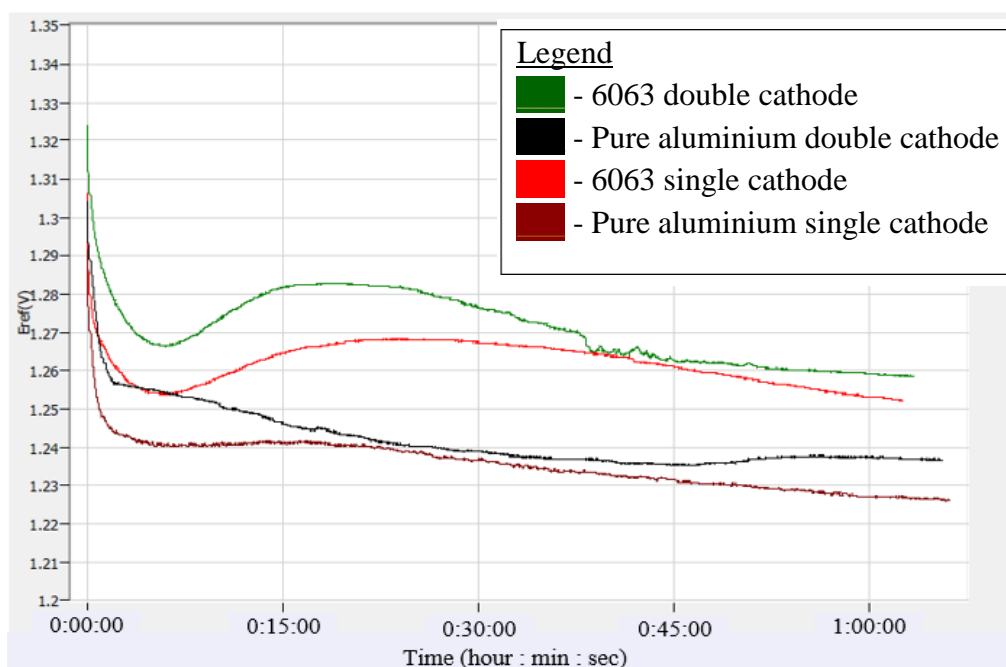
Figure 4.15: Discharge performance of Double Cathode Aluminium-air Battery with Different Anode Material.

Table 4.8: Mass Loss of Aluminium Anode in Single and Double Cathode Design.

Anode Material	Cathode design	Mass before the experiment (g)	Mass after the experiment (g)	Mass loss (g)
Pure Aluminium	Single	1.493	1.429	0.064
	Double	1.408	1.277	0.131
Alloy 6063	Single	11.490	11.405	0.085
	Double	11.374	11.197	0.177

The result proves that double cathode design is capable of improving the discharge performance of aluminium-air battery as the average discharge voltage has increased as compared to the conventional single cathode design. The discharge curve in Figure 4.15 is consistent with the experiment conducted in section 4.4.1.2 as pure aluminium and alloy 6063 exhibited a similar discharge pattern in single cathode and double cathode design.

Referring to Table 4.8, it is noticed that alloy 6063 anode suffers from greater mass loss than pure aluminium. This observation is in good agreement with section 4.4.2.3, which stated that impurities in alloy 6063 are causing greater self-corrosion. In 2020, Katsoufis *et al.* attempted to study the difference of mass loss in pure aluminium and alloy 6061 when immersed in 5M KOH

electrolyte. The authors found that the mass loss due to corrosion in alloy 6061 is 70 % higher than pure aluminium.

In our experiment, the associated mass loss for alloy 6063 is only 33 % and 35% higher than pure aluminium for single cathode design and double cathode design respectively. Since alloy 6061 and 6063 are from the same alloy series, they possess many of the same quality as stated by Clinton Aluminium (2017) because they both employed Mg and Si as alloying elements. Yet, the vast percentage difference in the mass loss from both experiments could be the use of different corrosion measurement method. Katsoufis *et al.* (2020) monitored the production of hydrogen gas and computed the mass loss from that information. Meanwhile in our experiment, the anode weight before and after the discharge are compared. It is realised that this method had disregarded the weight of deposited corrosion products on the anode surface.

Despite having better discharge performance, double cathode design faces greater mass loss as both sides of the aluminium anode are exposed to the alkaline environment that is corrosive to aluminium. Doubled reactive area has caused doubled mass loss over the given discharge period.

The discharge voltage has improved by a small fraction, but the associated mass loss has doubled. This is not desirable for an aluminium-air battery in terms of cost efficiency because the aluminium anode will be consumed twice as fast as the original single cathode design. It is not advised to implement the double cathode design in alkaline electrolyte based aluminium-air battery due to severe self-corrosion.

4.6   Aluminium Anode in Alkaline Environment

4.6.1   Visual Inspection

The physical appearances of pure aluminium and alloy 6063 anodes after 2 hours and 2 weeks of experiment are depicted in Figure 4.16.
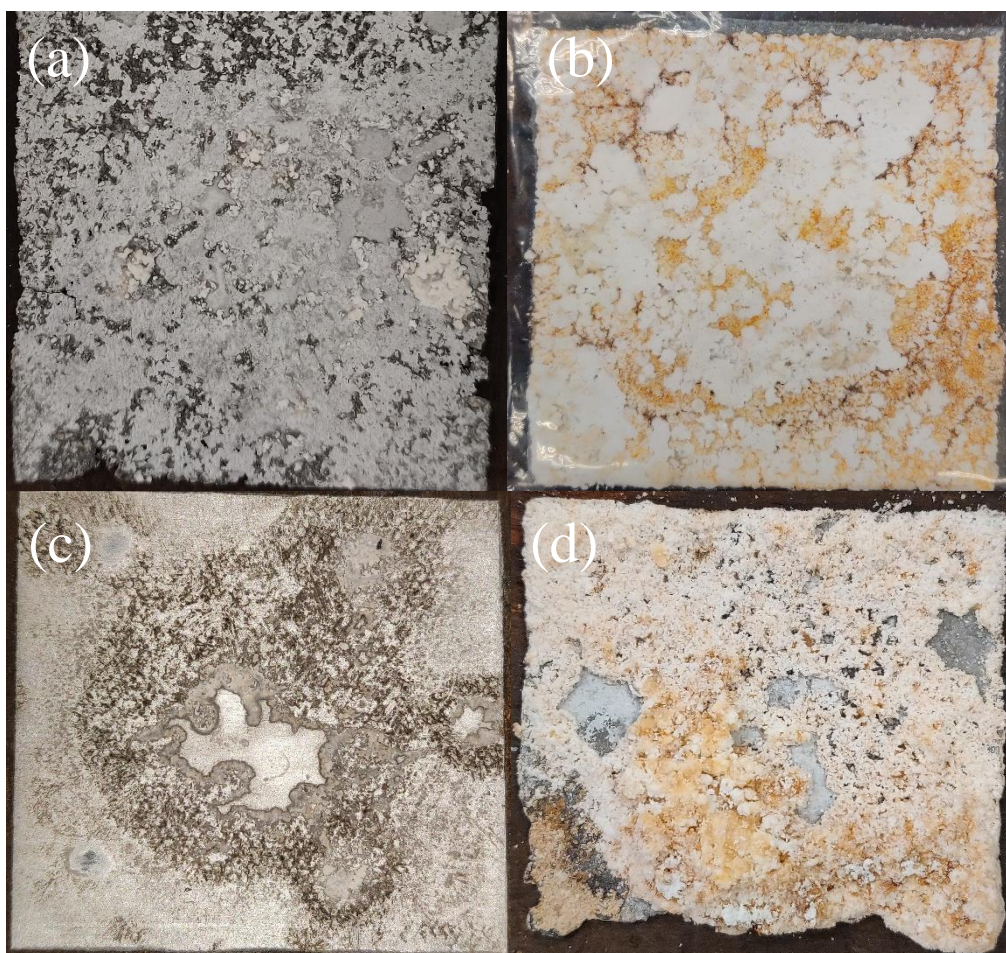
Figure 4.16: Pure Aluminium anode after (a) 2 hours of experiment and (b) 2 weeks of experiment. Alloy 6063 anode after (c) 2 hours of experiment and (d) 2 weeks of experiment.

The self-corrosion behaviour and surface passivation of pure aluminium and alloy 6063 in alkaline environment is investigated. The alkaline used is 4M KOH solution that was used as electrolyte in aluminium-air battery. After two hours of exposure to 4M KOH solution, pure aluminium sheet anode has become more fragile. Flaked-off aluminium pieces from the edges can be found as shown in Figure 4.16(a). There are white substances deposited on the surface, making the surface to be rough. Those surfaces without the white deposits

mostly turned black. After two weeks of exposure, pure aluminium has lost its solid properties and what remains is the gelatinous white and brown precipitate as depicted in Figure 4.16(b). The remaining paste-like substance is very viscous and sticky. There is no sign of pure aluminium sheet metal left. Pure aluminium is fully consumed after two weeks in 4M KOH solution.

Based on Figure 4.16(c) some of the areas in alloy 6063 have turned black and the surface were also rough after two hours of electrolyte exposure, especially at the centre position. The shiny appearance is no longer present. Alloy 6063 that is exposed to 4M KOH solution for two weeks has become more fragile. The alloy at the edge had flaked off as shown in Figure 4.16(d). During its cutting process to prepare for XRD and SEM-EDX analysis, it is noticed that the alloy 6063 had become less rigid and can be cut more easily. There are white and brown deposits on the anode that were soft and can be removed when force is applied. The texture of this deposit is different from the adhesive deposit found on pure aluminium after two weeks. It is in powder form in the case of alloy 6063. Areas with the deposits formation has increased thickness while the area without it has decreased thickness.

During the operation of aluminium-air battery, both pure aluminium and alloy 6063 are observed to release gas bubbles. The gas bubbles emitted are hydrogen gas as a result of parasitic corrosion reaction. Zhou, Bhonge and Cho (2019) explained that the generated bubbles can hinder the access of reactants into the reaction site at the electrode surface, which causes a shielding effect of bubbles that can significantly affect the performance of aluminium-air battery.

4.6.2 Scanning Electron Microscopy (SEM)

Pure aluminium and alloy 6063 anode surface are characterised by SEM as shown in Figure 4.17.
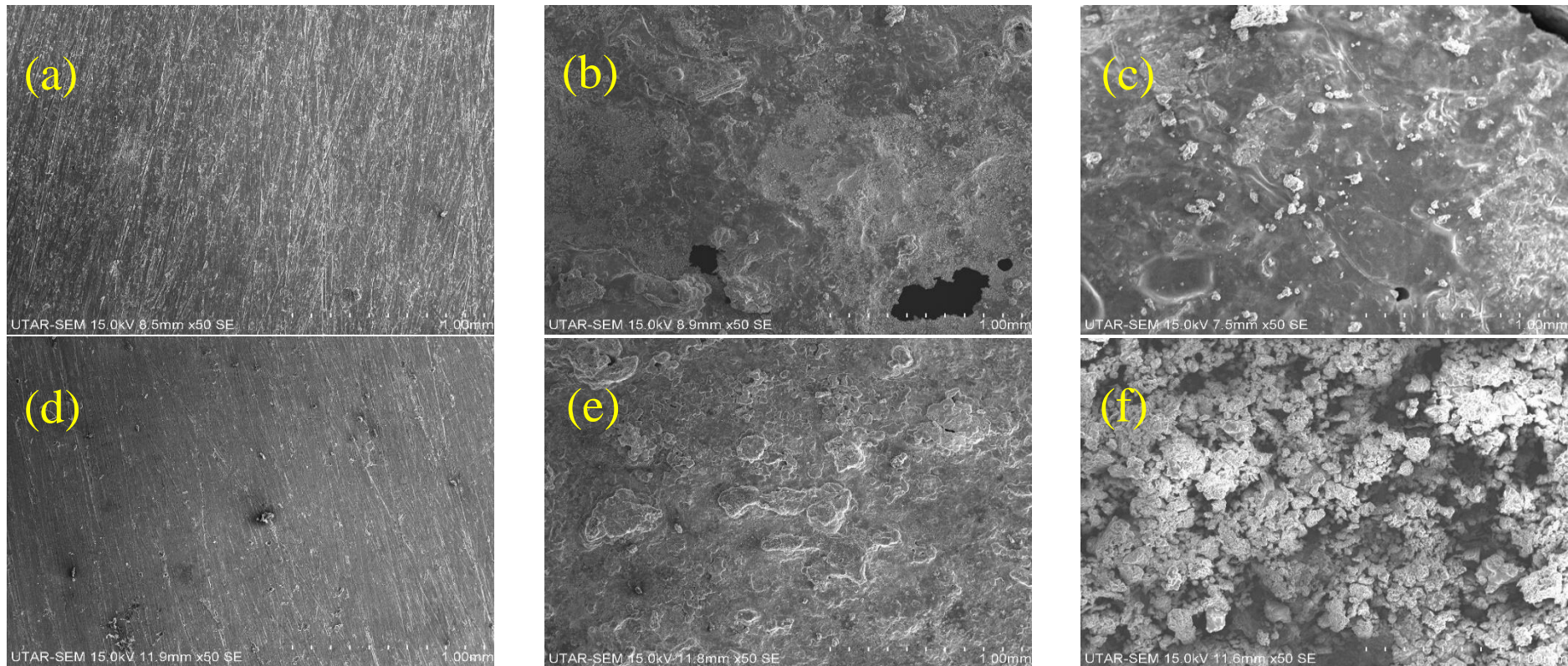
Figure 4.17: SEM images of Pure Aluminium (a) before the experiment, (b) two hours after the experiment, and (c) two weeks after the experiment; Alloy 6063 (d) before the experiment, (e) two hours after the experiment, and (f) two weeks after the experiment.

Before aluminium anode is inserted into the aluminium-air battery, its surface is always cleaned using sandpaper to scrape off the unreactive oxide layer. Figure 4.17 (a) and (d) presents the cleaned surface of pure aluminium and alloy 6063 respectively. The scratch mark from sand paper in pure aluminium is deeper than the alloy 6063 albeit same grade sandpaper is used. This is because alloy 6063 is harder than pure aluminium due to the presence of alloying elements.

After 2 hours of exposure in 4M KOH solution, corrosion activity can be observed from both anodes. The initial surface scratch mark is lost as a result of corrosion and several 'islands' are formed on the surface as depicted in Figure 4.17(b) and (e). In fact, these 'islands' are clusters of aluminium oxide and/or aluminium hydroxide as stated by Nestoridi (2008) and verified later in the EDX and XRD analysis. The black spots in pure aluminium are the consequence of flaked-off aluminium pieces.

By comparing Figure 4.17(b) and (e), it can be noticed that the number of 'islands' in alloy 6063 is higher than pure aluminium, indicating that alloy 6063 has more corrosion hotspots. Katsoufis *et al.* (2020) suggested that aluminium alloys undergo faster corrosion by enhanced activity at grain boundaries. Both pure aluminium and alloy 6063 formed a very thin oxide layer after 2 hours in alkaline environment. The alumina 'islands' are individually investigated by zooming in the image to $500\times$ magnification power and the result is illustrated in Figure 4.18.
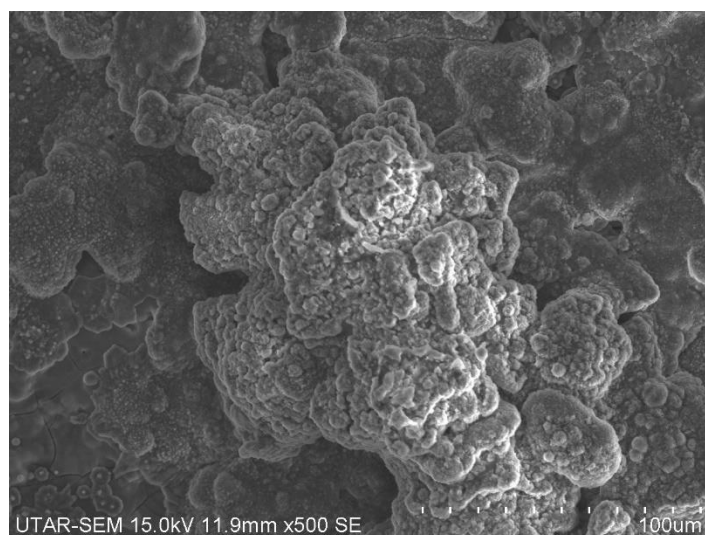
Figure 4.18: Corrosion Hotspot in Alloy 6063 after 2 hours of experiment.

The 'island' is composed of many irregular shaped small fragments, most of them are spherical. These small fragments clumped together disorderly forming a small 'island'. Eventually, these small 'islands' grow bigger and gradually agglomerate with other small 'islands' to become a bigger 'island'. These corrosion products have caused the anode to grow perpendicularly from the surface, causing the anode to become thicker. It is found that the surface condition in Figure 4.18 is analogous with the anode surface condition illustrated by Pino *et al.* (2015) as shown in Figure 4.19. Both the figures show the deposition of aluminium hydroxide as 'islands' on the anode surface.
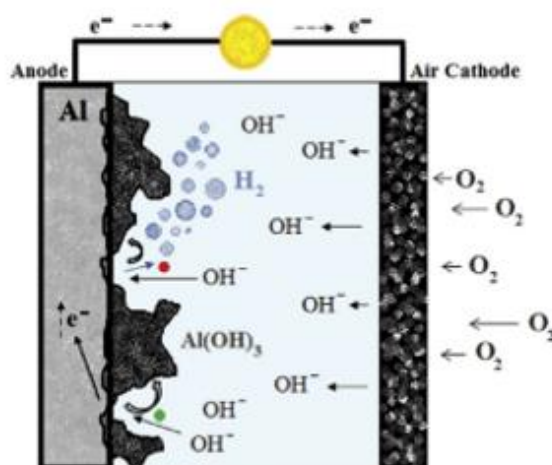
Figure 4.19: Schematic Representation of Anode Surface Condition (Pino et al., 2015).

Figure 4.17(c) shows the pure aluminium surface condition after 2 weeks of alkaline solution exposure. It is found that there is no big 'island' that should be present as the product of the corrosion, and the surface was relatively flat. It is realised that the surface condition was disturbed during the sample preparation process for XRD and SEM-EDX analysis, where the sticky paste-like substance is dried to be in powder form, and then pressed into the specimen holder. By further zooming into the surface up to $700\times$ magnification power, it is found that there are still some residues of the irregularly-shaped small fragments as displayed in Figure 4.20.
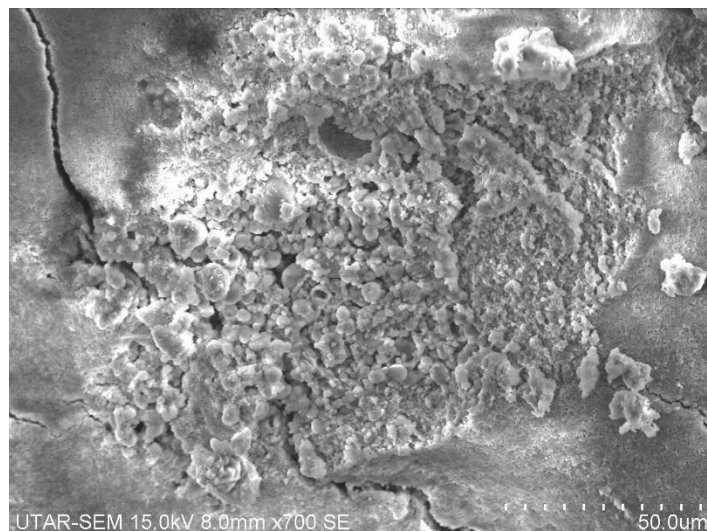
Figure 4.20: Residues of Irregularly-shaped Small Fragments in Pure Aluminium Sample after 2 weeks of experiment.

On the other hand, alloy 6063 after 2 weeks of experiment is demonstrated in Figure 4.17(f). The 'islands' have grown all over the surface, which indicates that the corrosion has affected the whole alloy 6063 plate. Thick and porous films of alumina are formed. By referring to Figure 4.19, it suggested that the aluminium hydroxide layers formed are porous because of the evolution of hydrogen gas. This explains why the deposited white and brown substances are so soft and can be removed easily.

4.6.3   Energy Dispersive X-ray spectroscopy (EDX)

EDX is conducted to identify the composition of pure aluminium and alloy 6063 after different durations in alkaline electrolyte. The magnification power at which the EDX analysis is carried out is $70\times$, this magnification is relatively lower as it is to allow a wider coverage so that an average composition of the specimen can be tested. The atomic percent of different elements are recorded and analysed to probe the changes of pure aluminium surface composition in alkaline environment. Figure 4.21 displays the EDX result of pure aluminium anode in aluminium-air battery and their corresponding SEM images.
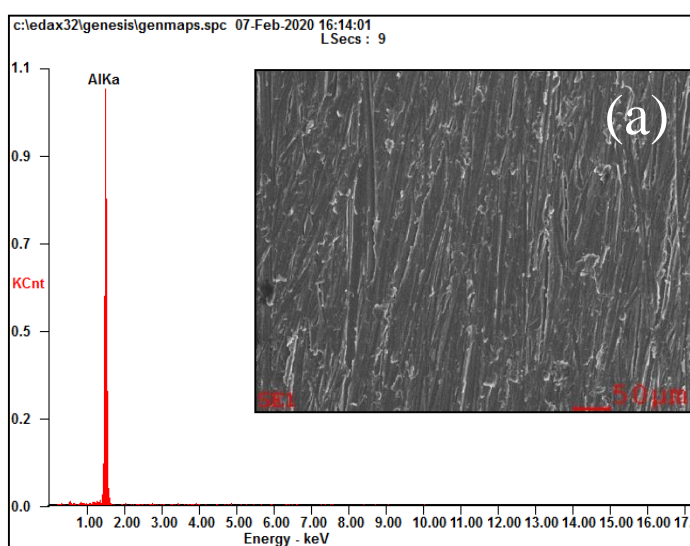
Element	At%
Al	100.00
Matrix	MThin
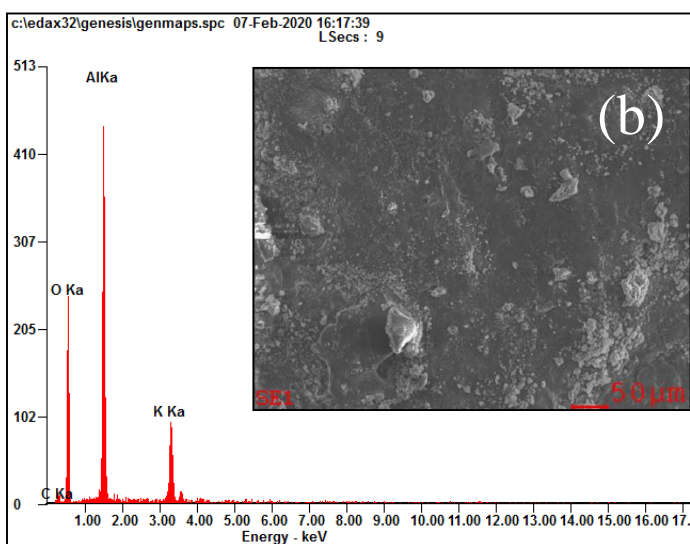
Element	At%
CK	01.58
OK	43.89
AlK	42.11
KK	12.41
Matrix	MThin
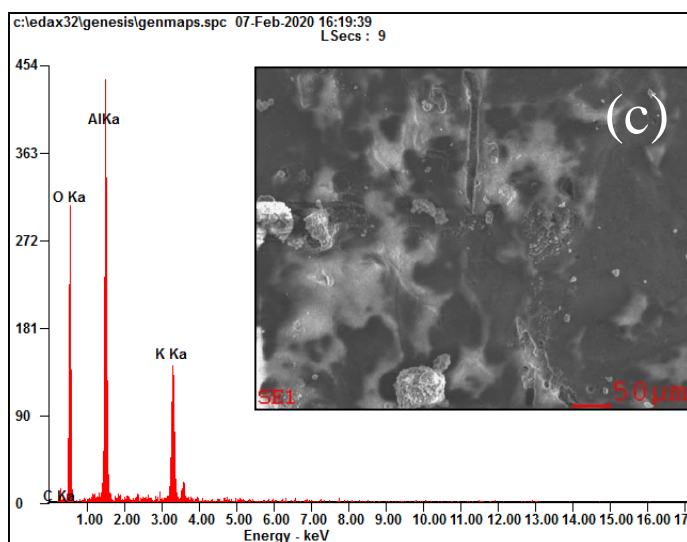
Element	At%
CK	02.88
OK	04.40
AlK	92.19
KK	00.53
Matrix	MThin

Figure 4.21: EDX results of Pure Aluminium sample (a) before the experiment, (b) two hours after the experiment, and (c) two weeks after the experiment.

From Figure 4.21, it can be noticed that the SEM images are displaying the same characteristics as the SEM analysis conducted in previous section. The details regarding composition of pure aluminium will be discussed together with alloy 6063 later. Figure 4.22 shows the EDX result of alloy 6063 anode in aluminium-air battery and their corresponding SEM images, in addition of their elements atomic percentages.
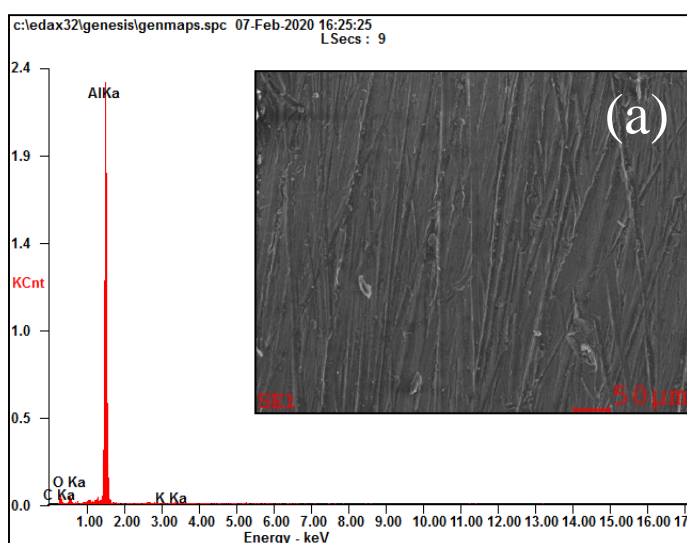
Element	At%
CK	01.13
OK	49.82
AlK	33.58
KK	15.47
Matrix	MThin
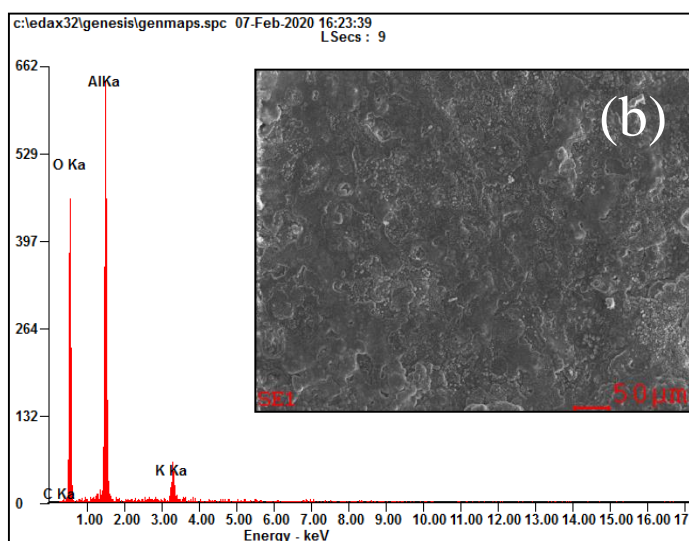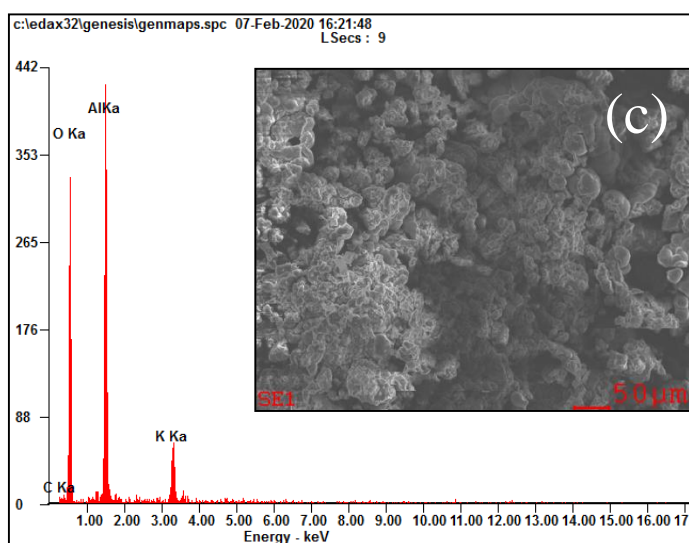
Figure 4.22: EDX results of alloy 6063 sample (a) before the experiment, (b) two hours after the experiment, and (c) two weeks after the experiment.

The relevant elements that pure aluminium and alloy 6063 contain are carbon, oxygen, aluminium, and potassium. The atomic percentage of different elements in pure aluminium and alloy 6063 before and after their exposure in alkaline environment are summarised and tabulated in Table 4.9. The weight percentage results from EDX analysis are not considered as it does not provide insight regarding the chemical reaction between pure aluminium and alloy 6063 with electrolyte.

Table 4.9: Atomic percent of each element found in anode.

Anode Materials	Element	Atomic percent (At %)		
		Before the experiment	After 2 hours of experiment	After 2 weeks of experiment
Pure Aluminium	C	-	01.58	01.13
	O	-	43.89	49.82
	Al	100	42.11	33.58
	K	-	12.41	15.47
Alloy 6063	C	02.88	00.28	01.36
	O	04.40	58.49	58.04
	Al	92.19	37.10	33.68
	K	00.53	04.13	06.93

EDX analysis is conducted to identify the composition of elements present in aluminium anodes. The oxygen content is mainly contributed by the formation of aluminium oxide and aluminium hydroxide. Since this is an aluminium-air battery, pure aluminium and alloy 6063 that function as the anode tends to undergo oxidation, and eventually produce aluminium oxide.

$$4Al + 3O_2 \rightarrow 2Al_2O_3 \qquad (4.11)$$

The formation of aluminium hydroxide in KOH solution is explained by Soler *et al.* (2005). The chemical reaction between aluminium that is amphoteric in nature and the alkaline, potassium hydroxide solution are shown below:

$$2Al + 2KOH + H_2O \rightarrow 2KAl(OH)_4 + 3H_2 \uparrow \qquad (4.12)$$
$$KAl(OH)_4 \rightarrow KOH + Al(OH)_3 \downarrow \qquad (4.13)$$
$$2Al + 6H_2O \rightarrow 2Al(OH)_3 \downarrow + 3H_2 \uparrow \qquad (4.14)$$
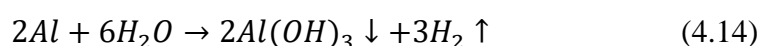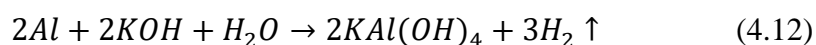
The authors said that the chemical reaction (4.12) between aluminium and potassium hydroxide solution will produce parasitic hydrogen gas and a water soluble salt, known as potassium aluminate, which explains the loss of Al atoms from the anode. From reaction (4.13), it is understood that potassium

aluminate will dissociate into potassium hydroxide and aluminium hydroxide that is spontaneously precipitated from the solution as it is water insoluble. The authors also mentioned that chemical reaction (4.14) is the global reaction of steps (4.12) and (4.13), which means that potassium hydroxide consumed in reaction (4.12) can be regenerated in reaction (4.13). This statement supports the use of KOH solution as electrolyte because KOH is not consumed when functioning as the electrolyte in aluminium-air battery. KOH solution can last very long as the electrolyte because the global reaction consumes only water.

The carbon and potassium contents found in anodes are mostly due to the atmospheric carbonation reaction of KOH solution. According to Hu *et al.* (2019), KOH solution can react with CO_2 in the atmosphere and produces potassium carbonate, K_2CO_3. Since KOH is a strong base and CO_2 is an acidic oxide, both of them react readily to form salt and water through chemical reaction (4.15). As shown in chemical reaction (4.16), the potassium carbonate, K_2CO_3 formed reacts with carbon dioxide again to form potassium hydrogen carbonate, also known as potassium bicarbonate. It is believed that K_2CO_3 and $KHCO_3$ has interfered with the reaction on the anode surface, thus contributing to the element composition on the anode surface.

$$2KOH + CO_2 \rightarrow K_2CO_3 + H_2O \qquad (4.15)$$

$$K_2CO_3 + CO_2 + H_2O \rightarrow 2KHCO_3 \qquad (4.16)$$
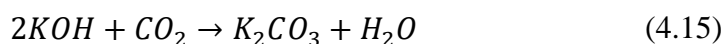
Before their exposure to alkaline solution, pure aluminium surface is made out of 100% Al atoms, and alloy 6063 still remains some of the oxide as shown in Table 4.9. It could be that the scrapping process to remove the oxide layer is not perfect for alloy 6063 due to its strong hardness. This alloy 6063 sample is deemed to be contaminated with 4M KOH solution because it should not contain potassium and carbon elements.

After 2 hours in alkaline environment, the Al atoms have reduced to 42 % for pure aluminium and 37 % for alloy 6063, while the oxygen element is 43.89 % for pure aluminium and 58.49 % for alloy 6063. These data show that more aluminium oxide and hydroxide are formed in alloy 6063 and confirms that alloy 6063 suffers more severe self-corrosion than pure aluminium as mentioned previously.

The number of Al atoms further reduced to 33 % for both pure aluminium and alloy 6063 after 2 weeks in alkaline solution. Meanwhile, the oxygen content for pure aluminium has increased to 49.82 % and the oxygen remained at 58.04 %. The reduced Al atoms and increased O atoms suggest that pure aluminium and alloy 6063 have experienced self-corrosion. Self-corrosion in alloy 6063 is greater than pure aluminium due to faster reduction of Al atoms and increase in O atoms. Table 4.9 also shows that K atoms of pure aluminium are always more than alloy 6063.

It is suggested that the chemical substances present on the anode that are aluminium oxide (Al_2O_3), aluminium hydroxide ($Al(OH)_3$), potassium aluminate ($KAl(OH)_4$), potassium hydroxide (KOH), potassium carbonate (K_2CO_3), and potassium hydrogen carbonate ($KHCO_3$).

4.6.4   X-Ray powder Diffraction crystallography (XRD)

Figure 4.23, Figure 4.24 and Figure 4.25 display the XRD result of pure aluminium before the alkaline exposure experiment, after 2 hours of experiment, and after 2 weeks of experiment respectively.
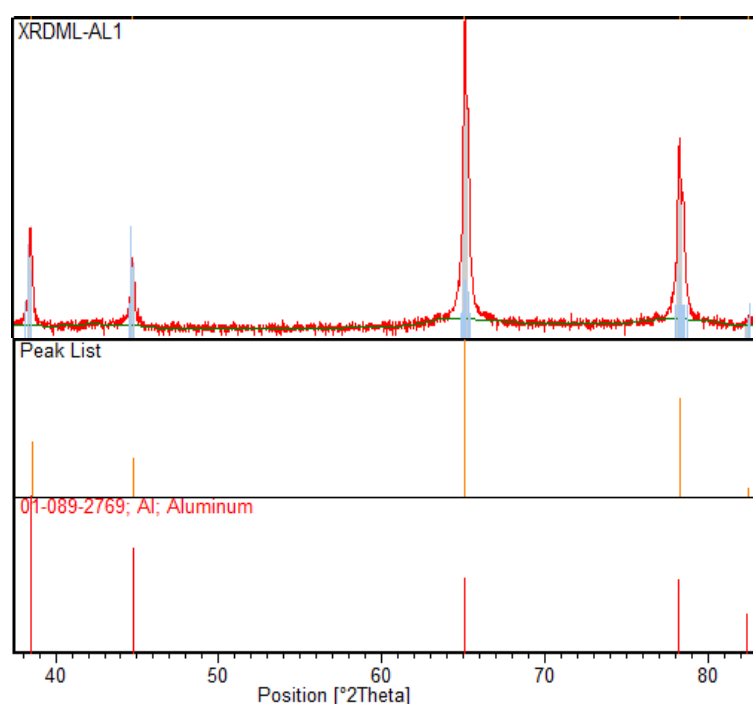
Figure 4.23: XRD result of Pure Aluminium before the experiment.
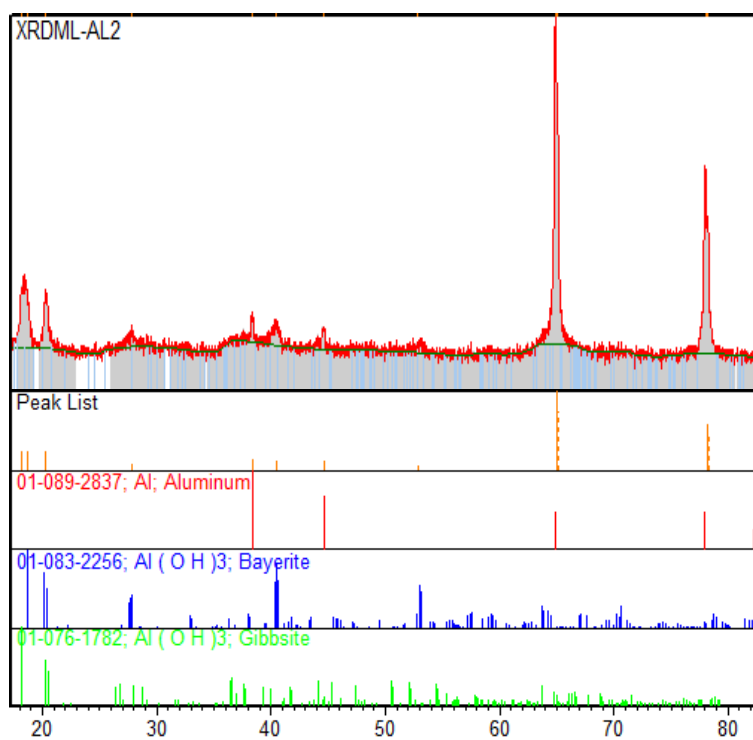
Figure 4.24: XRD result of Pure Aluminium after 2 hours of experiment.
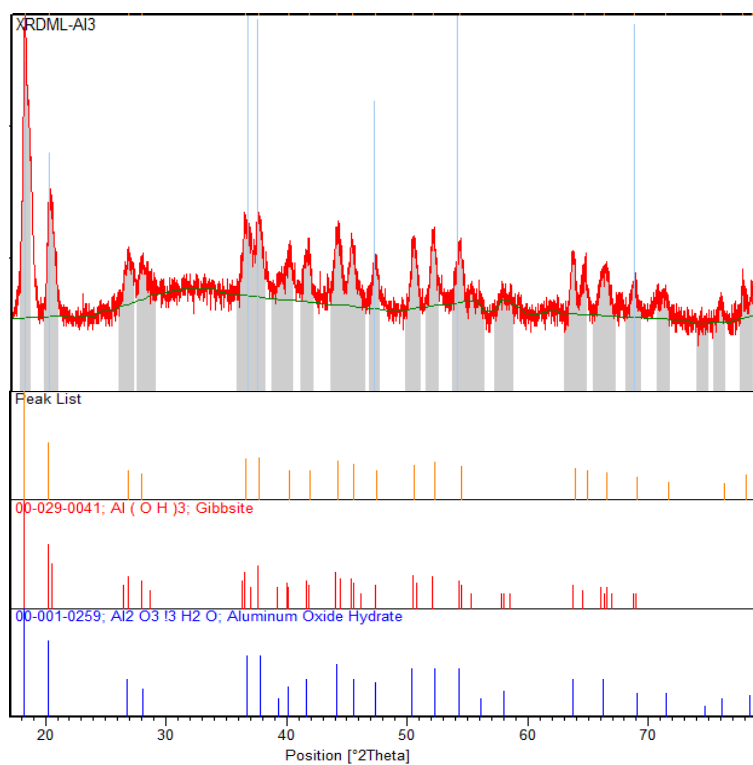
Figure 4.25: XRD result of Pure Aluminium after 2 weeks of experiment.

The XRD results of alloy 6063 before the experiment, 2 hours after the experiment, and 2 weeks after the experiment are presented in Figure 4.26, Figure 4.27, and Figure 4.28 respectively.
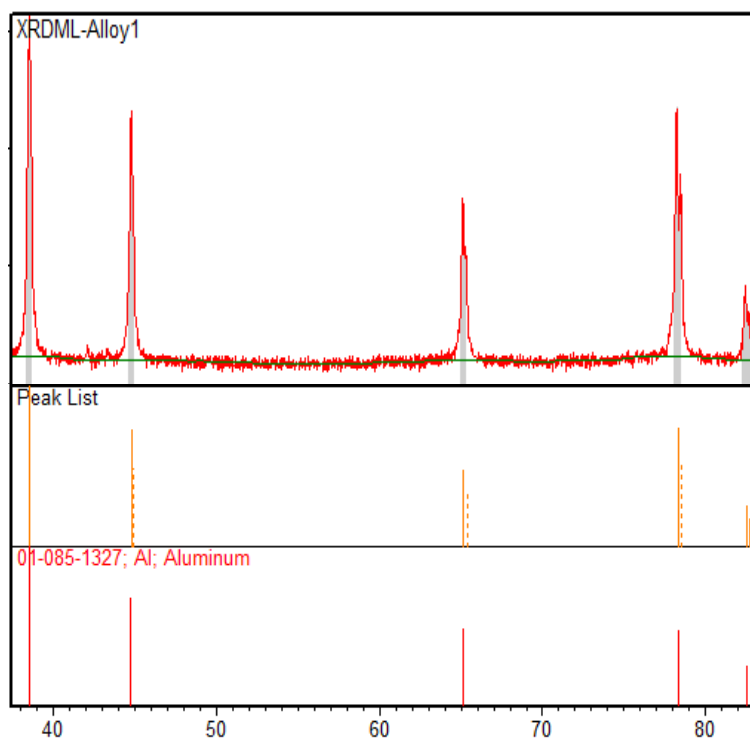
Figure 4.26: XRD result of Alloy 6063 before the experiment.
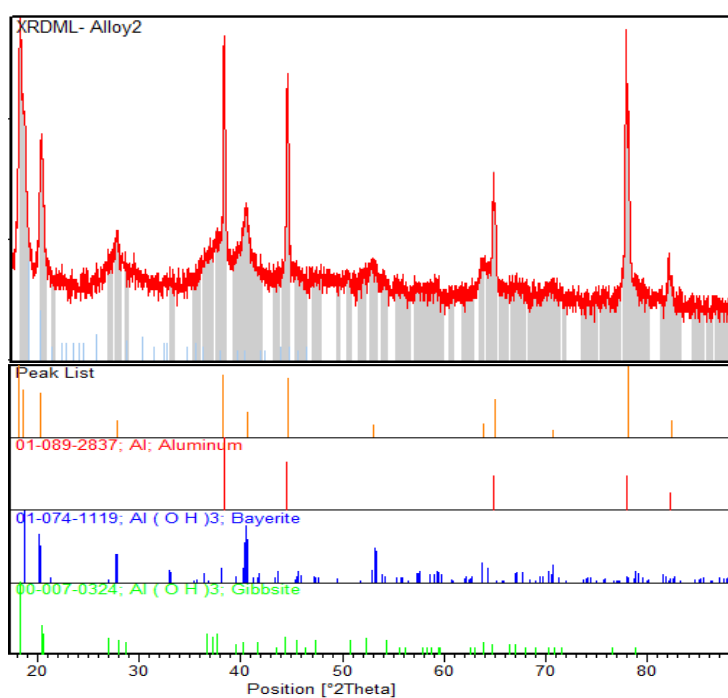
Figure 4.27: XRD result of Alloy 6063 after 2 hours of experiment.
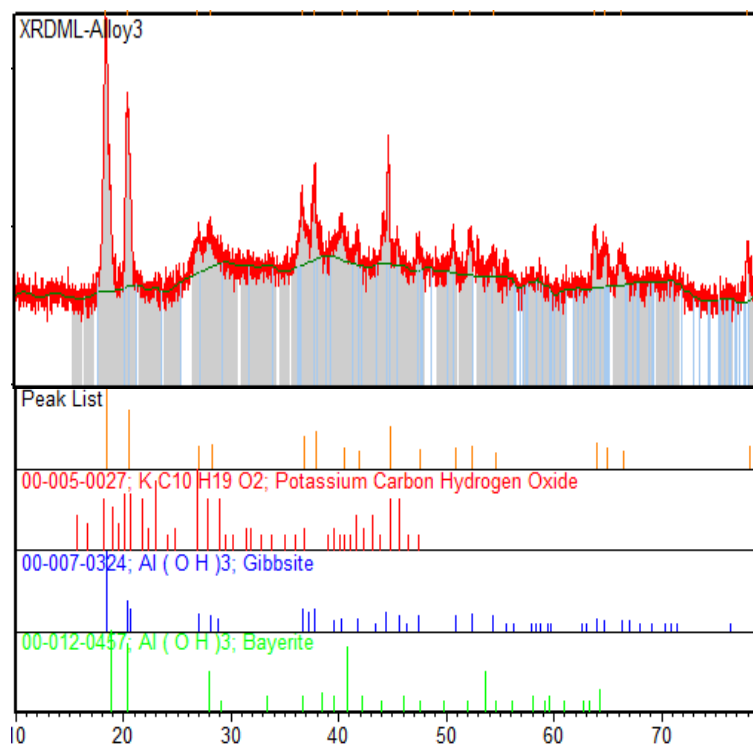
Figure 4.28: XRD result of Alloy 6063 after 2 weeks of experiment.

From the XRD result, it shows that pure aluminium and alloy 6063 is consistent with the SEM-EDX analysis such that only aluminium element is present before they are immersed in KOH solution. After 2 hours of immersion, pure aluminium and alloy 6063 anode is observed to have developed both the polymorphs of aluminium hydroxide, which are Bayerite and Gibbsite. After 2 weeks in alkaline solution, aluminium oxide is still present in pure aluminium and alloy 6063. However in alloy 6063, potassium hydrogen carbonate is found, which is in good agreement with Soler *et al.* (2005) that said potassium hydrogen carbonate is produced from the atmospheric carbonation of alkaline solution.

From the investigation of pure aluminium and alloy 6063 in alkaline environment, it is found that both of the materials are severely corroded after 2 weeks in 4M KOH solution. It is clear that the corrosion rate of both materials are too rapid and it will not work in a aluminium-air battery that immerse and store the anode in alkaline electrolyte because the battery will die due to self-corrosion behaviour of aluminium anode, even if the battery is not in use.

CHAPTER 5

CONCLUSION AND RECOMMENDATIONS

5.1 Conclusions

The electrical characteristics of aluminium-air battery constructed using different anode materials and catalysts under open-circuit and closed-circuit conditions are studied. The electrolyte used is 4M KOH solution throughout the study. The obtained results are concluded as follows:

I. Alloy 6063 as anode has resulted in better electrical characteristic than pure aluminium.

    a. Without catalyst, the open-circuit voltage of alloy 6063 (1.461 V) as anode is 10.3 % higher than pure aluminium (1.326 V).

    b. With and without catalyst, the discharge voltage of alloy 6063 as anode is higher than pure aluminium.

    c. With graphite felt as catalyst, alloy 6063 as anode yielded better battery capacity (171.86 Ah/kg at 8.889mA/cm^2) as compared to pure aluminium (111.33 Ah/kg at 8.889mA/cm^2).

II. In 4M KOH solution, the self-corrosion behaviour of alloy 6063 is more severe than pure aluminium.

    a. Alloy 6063 corrodes 60 % faster than pure aluminium from Tafel plot calculation.

    b. SEM shows that alloy 6063 has more corrosion hotspots than pure aluminium after 2 hours in KOH solution.

    c. EDX shows that after 2 hours in KOH solution, the Al atoms percentage in alloy 6063 (37.1 %) is higher than pure aluminium (42.1 %), while oxygen atom percent in alloy 6063 (58.5 %) is higher than pure aluminium (43.9 %). It concludes that more aluminium hydroxide is formed in alloy 6063 after 2 hours in alkaline solution.

III. Graphite felt is more superior to graphite powder as a catalyst for aluminium-air battery.

a. Graphite felt has improved initial discharge voltage by 35 % and 41 % for pure aluminium and alloy 6063 respectively, while graphite powder has reduced initial discharge voltage by 32 % for pure aluminium and improved by 14 % for alloy 6063.

b. Graphite felt has improved final discharge voltage by 65 % and 69 % for pure aluminium and alloy 6063 respectively, while graphite powder has reduced final discharge voltage by 35 % for pure aluminium and improved by 20 % for alloy 6063.

c. Graphite felt has substantially reduced the voltage drop in pure aluminium and alloy 6063 over an hour of discharge from 180 mV and 160 mV to 13 mV and 15 mV respectively.

This study is the first to implement the double cathode aluminium-air battery design. It is found that this improvised design is capable of improving the discharge performance by a small fraction, but the associated anode weight loss is doubled and is not practical as an aluminium-air battery. One key contribution of this study is the high resolution SEM images of corroded pure aluminium and alloy 6063. It is also found that the corrosion rate of pure aluminium and alloy 6063 are too rapid and it will not work in a aluminium-air battery that immerse and store the anode in alkaline electrolyte because the battery will die due to self-corrosion behaviour of aluminium anode, even if the battery is not in use.

5.2   Recommendations for future work

In this study, the thickness of pure aluminium and alloy 6063 is different and this could be a factor that can affect the results of experiments conducted. If both materials have the same thickness, we can observe the thickness change in the materials after their corrosion in alkaline solution to investigate the penetration rate of the corrosion.

Besides that, stainless steel mesh is found to be contaminated after using several times for the experiments. It is recommended to use material that will not corrode such as the graphite felt as the current collector since it is also an

electric conductor. Walsh *et al.* (2017) also considers that graphite felt is advantageous as an electrode owing to the high permeability and chemically inert properties that make graphite felt resistant to most acids, alkalis and corrosive gases. By doing this, we might also improve the performance of aluminium-air battery as the resistance of stainless steel mesh is eliminated from the battery internal resistance equation.

Before we measure its electrical characteristic, aluminium-air is suggested to be left in open-circuit condition for at least 10 minutes to achieve steady-state. We can also activate the anode by applying a current density of 50 mA/cm^2 as demonstrated by Nestoridi (2008) to create a rougher, more highly pitted surface. This can cause a negative shift in open-circuit potential.

Other than that, it is recommended that corrosion rate to be analysed using hydrogen evolution method as it is widely used by many other researchers, thus it will be easier for comparison. It is not advised to use anode weight loss method to calculate corrosion rate as it neglects the weight of deposited aluminium hydroxide on the anode surface.

The potassium hydroxide, KOH solution will capture carbon dioxide, CO_2 when exposed to the atmosphere, forming carbonate salts that can interfere with the electrochemical reaction in aluminium-air battery. It is advised to keep the KOH solution in a tightly-sealed container or to use freshly-made KOH solution for the experiments.

REFERENCES

Avoundjian, A., Galvan, V. and Gomez, F.A., 2017. An inexpensive paper-based aluminum-air battery. *Micromachines*, 8(7).

Chambers, L., 2012, *Sodium Hydroxide vs. Potassium Hydroxide | eClean Magazine* [Online]. Available at: https://www.ecleanmag.com/sodium-hydroxide-vs-potassium-hydroxide-what-is-the-difference/ [Accessed: 21 April 2020].

Cho, Y.J., Park, I.J., Lee, H.J. and Kim, J.G., 2015. Aluminum anode for aluminum-air battery - Part I: Influence of aluminum purity. *Journal of Power Sources*, 277, pp.370–378. Available at: http://dx.doi.org/10.1016/j.jpowsour.2014.12.026.

Chu, D. and Savinell, R.F., 1991. EXPERIMENTAL DATA ON ALUMINUM IN KOH ELECTROLYTES. *Electrochimica Acta*, 36(10), pp.1631–1638.

Clinton Aluminium, 2017, *6061 Aluminum Vs 6063 In Extrusion Applications | Clinton Aluminum* [Online]. Available at: https://www.clintonaluminum.com/6061-aluminum-vs-6063-in-extrusion-applications/ [Accessed: 21 April 2020].

Edelstein, 2014, *Aluminum-Air Battery Developer Phinergy Partners With Alcoa* [Online]. Available at: https://www.greencarreports.com/news/1090218_aluminum-air-battery-developer-phinergy-partners-with-alcoa [Accessed: 21 April 2020].

Electrical4u, 2019, *Faraday's First and Second Laws of Electrolysis | Electrical4u* [Online]. Available at: https://www.electrical4u.com/faradays-first-and-second-laws-of-electrolysis/ [Accessed: 21 April 2020].

Emmanuel, O., 2018, *Different Types of Batteries and their Applications* [Online]. Available at: https://circuitdigest.com/article/different-types-of-batteries [Accessed: 21 April 2020].

Energy Access Outlook, 2017, *WEO-2017 Special Report: Energy Access Outlook – Analysis - IEA* [Online]. Available at: https://www.iea.org/reports/energy-access-outlook-2017 [Accessed: 21 April 2020].

Fan, L. et al., 2015. The effect of crystal orientation on the aluminum anodes of the aluminum e air batteries in alkaline electrolytes. *Journal of Power Sources*, 299, pp.66–69. Available at: http://dx.doi.org/10.1016/j.jpowsour.2015.08.095.

Goel, P., Dobhal, D. and Sharma, R.C., 2020. Aluminum – air batteries : A

viability review. , 28(October 2019).

Håkansson, E., Hoffman, J., Predecki, P. and Kumosa, M., 2017. The role of corrosion product deposition in galvanic corrosion of aluminum / carbon systems. *Corrosion Science*, 114, pp.10–16. Available at: http://dx.doi.org/10.1016/j.corsci.2016.10.011.

Hu, T. et al., 2019. Experimental research on temperature rise and electric characteristics of aluminum air battery under open-circuit condition for new energy vehicle. *International Journal of Energy Research*, 43(3), pp.1099–1110.

Jingling, M., Jiuba, W., Hongxi, Z. and Quanan, L., 2015. Electrochemical performances of Al-0.5Mg-0.1Sn-0.02In alloy in different solutions for Al-air battery. *Journal of Power Sources*, 293, pp.592–598. Available at: http://dx.doi.org/10.1016/j.jpowsour.2015.05.113.

Katsoufis, P. et al., 2020. Study of some basic operation conditions of an Al-air battery using technical grade commercial aluminum. *Journal of Power Sources*, 450(December 2019), p.227624. Available at: https://doi.org/10.1016/j.jpowsour.2019.227624.

Kimtech Science, *Scientific Products Catalog KIMTECH SCIENCE * KIMWIPES * Wipers KIMTECH SCIENCE * Brand Wipers KIMTECH SCIENCE * KIMWIPES * Wipers*,

Lawson, B., *Lead Acid Batteries* [Online]. Available at: https://www.mpoweruk.com/leadacid.htm [Accessed: 21 April 2020].

Li, Q. and Bjerrum, N.J., 2002. Aluminum as anode for energy storage and conversion: A review. *Journal of Power Sources*, 110(1), pp.1–10.

Liu, J. et al., 2016. Synergistic effects of carboxymethyl cellulose and ZnO as alkaline electrolyte additives for aluminium anodes with a view towards Al-air batteries. *Journal of Power Sources*, 335, pp.1–11. Available at: http://dx.doi.org/10.1016/j.jpowsour.2016.09.060.

Liu, Y. et al., 2017. A comprehensive review on recent progress in aluminum–air batteries. *Green Energy and Environment*, 2(3), pp.246–277. Available at: https://doi.org/10.1016/j.gee.2017.06.006.

Lunarska, E. and Chernyayeva, O., 2006. Effect of corrosion inhibitors on hydrogen uptake by Al from NaOH solution. *International Journal of Hydrogen Energy*, 31(2), pp.285–293.

Martinez, M.P. et al., 2017. *Aluminium-Air Batteries : Study of Commercial Aluminium*. UNIVERSIDAD AUTÓNOMA DE MADRID.

Mckerracher, R.D., Holland, A., Cruden, A. and Wills, R.G.A., 2019. Comparison of carbon materials as cathodes for the aluminium-ion battery. *Carbon*, 144, pp.333–341. Available at: https://doi.org/10.1016/j.carbon.2018.12.021.

Microscopy Australia, 2014, *Introduction | MyScope* [Online]. Available at: https://myscope.training/legacy/xrd/introduction/ [Accessed: 21 April 2020].

Neburchilov, V. and Zhang, J., 2016. Aluminum – Air Batteries. In: *Metal–Air and Metal–Sulfur Batteries: Fundamentals and Applications*. CRC Press, pp. 66–104.

Nestoridi, M., 2008. *The Study of Aluminium Anodes for High Power Density Al-air Batteries with Brine Electrolytes*. UNIVERSITY OF SOUTHAMPTON FACULTY.

Pan, W., Wang, Y., Kwok, H.Y.H. and Leung, D.Y.C., 2019. A low-cost portable cotton-based aluminum-air battery with high specific energy. *Energy Procedia*, 158, pp.179–185. Available at: https://doi.org/10.1016/j.egypro.2019.01.067.

Papalambros, P.Y. and Wilde, D.J., 2018. *Principles and Practice*,

Pino, M. et al., 2016. Carbon treated commercial aluminium alloys as anodes for aluminium-air batteries in sodium chloride electrolyte. *Journal of Power Sources*, 326, pp.296–302.

Pino, M., Chacón, J., Fatás, E. and Ocón, P., 2015. Performance of commercial aluminium alloys as anodes in gelled electrolyte aluminium-air batteries. *Journal of Power Sources*, 299, pp.195–201.

Prabhu, D. and Rao, P., 2017. Corrosion behaviour of 6063 aluminium alloy in acidic and in alkaline media. , pp.2234–2244.

Shapley, P., 2012, *Common Battery Types* [Online]. Available at: http://butane.chem.uiuc.edu/pshapley/GenChem2/C6/3.html [Accessed: 21 April 2020].

Sleight, K., 2011, *Huge Potential from Air-Aluminum Battery Research* [Online]. Available at: https://www.brighthub.com/environment/renewable-energy/articles/117074.aspx [Accessed: 21 April 2020].

Soler, L., Macanás, J., Muñoz, M. and Casado, J., 2005. Hydrogen Generation From Aluminum In A Non-Consumable Potassium Hydroxide Solution Hydrogen Generation From Aluminum In A Non-Consumable Potassium Hydroxide Solution. , (July).

Sukiman, N.L. et al., 2011. Durability and Corrosion of Aluminium and Its Alloys : Overview , Property Space , Techniques and Developments.

Sun, S. et al., 2016. Electrochimica Acta Oxygen reduction reaction catalysts of manganese oxide decorated by silver nanoparticles for aluminum-air batteries. *Electrochimica Acta*, 214, pp.49–55. Available at: http://dx.doi.org/10.1016/j.electacta.2016.07.127.

Sun, Z. et al., 2015. Performance of Al-Air Batteries Based on Al–Ga, Al–In and Al–Sn Alloy Electrodes. *Journal of The Electrochemical Society*, 162(10), pp.A2116–A2122.

Sun, Z. and Lu, H., 2015. Performance of Al-0.5In as Anode for Al–Air Battery in Inhibited Alkaline Solutions. *Journal of The Electrochemical Society*, 162(8), pp.A1617–A1623.

The International Aluminium Institute, 2018, *Mining and Refining – Process* [Online]. Available at: http://bauxite.world-aluminium.org/refining/process/ [Accessed: 21 April 2020].

Thomas National Accelerator Facility, 2020, *Glossary Term - 10 Most Abundant Elements in the Earth's Crust* [Online]. Available at: https://education.jlab.org/glossary/abund_ele.html [Accessed: 21 April 2020].

Toshev, Y. et al., 2006. *Protective coating of zinc and zinc alloys for industrial applications*, Woodhead Publishing Limited.

U.S. Department of Energy, 2019, *All-Electric Vehicles* [Online]. Available at: https://www.fueleconomy.gov/feg/evtech.shtml [Accessed: 21 April 2020].

Walsh, F.C., Nava, L., Ponce, C. and Le, D., 2017. Electrochimica Acta Graphite felt as a versatile electrode material : Properties , reaction environment , performance and applications Lattice Boltzmann method. , 258.

Xia, Z. et al., 2020. Cobalt ion intercalated MnO_2 / C as air cathode catalyst for rechargeable aluminum e air battery. *Journal of Alloys and Compounds*, 824, p.153950. Available at: https://doi.org/10.1016/j.jallcom.2020.153950.

Yang, S. and Knickle, H., 2003. Design and analysis of aluminum/air battery system for electric vehicles. *Journal of Power Sources*, 112(1), pp.162–173.

Zhou, C., Bhonge, K. and Cho, K.T., 2019. Analysis of the effect of hydrogen-evolving side reaction in the aqueous aluminum-air battery. *Electrochimica Acta*, p.135290. Available at: https://doi.org/10.1016/j.electacta.2019.135290.

APPENDICES

APPENDIX A: Procurement website link

Acrylic sheet

- https://www.lazada.com.my/products/acrylic-sheet-3mm-clear-a4-size-i420229043-s610742138.html?ef_id=EAIaIQobChMI77mu-tHp4wIVgTgrCh2j7gyaEAQYASABEgICBvD_BwE:G:s&s_kwcid=AL!3150!3!244160057898!!!u!298495632901!&exlaz=d_1:mm_150050845_51350205_2010350205::12:1032211143!54400014687!!!pla-298495632901!c!298495632901!610742138!131491206&gclid=EAIaIQobChMI77mu-tHp4wIVgTgrCh2j7gyaEAQYASABEgICBvD_BwE

PTFE Teflon sheet

- https://www.lazada.com.my/products/ptfe-teflon-white-sheet-plate-film-thickness-1mm-i411862963-s597012224.html?spm=a2o4k.searchlist.list.3.3bab39467XD82r&search=1

Steel Mesh

- https://www.lazada.com.my/products/free-shipping35x12-100-micron-mesh-stainless-steel-woven-wire-cloth-screen-filter-sheet-new-i18181479-s22372249.html?spm=a2o4k.searchlist.list.5.6ea879a06RdQn8&search=1

Carbon Paper

- https://www.lazada.com.my/products/100-sheets-a4-dark-blue-carbon-hand-copier-stencil-transfer-paper-hectograph-i330835830-s460068813.html?spm=a2o4k.searchlist.list.57.69f414c3kFMUYb&search=1

- https://www.lazada.com.my/products/set-10-sheets-tattoo-carbon-transfer-copier-paper-a4-i316905559-s434232952.html?spm=a2o4k.searchlist.list.75.69f414c306Gc3a&search=1

APPENDIX B: Cell comparison chart

	Lead Acid	NiCad	NiMH	Zinc Air	Aluminium Air	Nickel Iron	Nickel Zinc	Sodium Sulphur
Commercialisation	1881	1956	1990	1997		1901	1920	1960
Cell Voltage	2.0 V	1.2V	1.2V	1.15V	1.5V	1.2V	1.5V	2.1V
Energy by Weight: Wh/Kg	30-40	40-60	30-80	200	220	50	60	110
Specific Power W/Kg	180	150	250 - 1000	80-140	30	100	300	150
Energy by Volume Wh/L	60-75	50-150	140-300	220			100	
Max discharge rate	10C		20C					
Recharge Time	>10 Hours	8 Hours	6 Hours					
Cycle Life Cycles	500 -800	2000	1500	200			600	1000
Self Discharge per month	3% – 4%	20%	30%			20% - 40%	<20%	
Temp Range °C		-40°C to +60°C	-20°C to +60°C					
Preferred Charge Method	Const Voltage	Const Current (- Delta V)	Dt/dt - (- Delta V) and Timer	NA	NA			
Average Energy Cost $/kWh	$150	$400-800	$250	$80		$150-200	$150-200	
Comments	Deteriorates with microcycles	Memory Effect	High self discharge rate Useful power down to 50% DOD	Primary Cell Can not accept Regen loads Uses replacable electrodes	Primary Cell Can not accept Regen loads Needs booster due to low specific power	Corrosion problems	Dendrite growth causes short cycle life	High Temp 350°C Damaged if temp < 200°C Discontinued

Generally energy density depends on whether optimised for capacity or power